NAVAL POSTGRADUATE SCHOOL

MONTEREY, CALIFORNIA

DISSERTATION

PERFORMANCE OF COHERENT AND NONCOHERENT *RAKE* RECEIVERS WITH CONVOLUTIONAL CODING RICEAN FADING AND PULSE-NOISE INTERFERENCE

by

Kyle Kowalske

June 2004

Dissertation Supervisor: Clark Robertson

Approved for public release; distribution is unlimited.

THIS PAGE INTENTIONALLY LEFT BLANK

REPORT DOCUMENTATION PAGE			Form Approved OMB No. 0704-0188
Public reporting burden for this collection of information is estimated to average 1 hour per response, including the time for reviewing instruction, searching existing data sources, gathering and maintaining the data needed, and completing and reviewing the collection of information. Send comments regarding this burden estimate or any other aspect of this collection of information, including suggestions for reducing this burden, to Washington headquarters Services, Directorate for Information Operations and Reports, 1215 Jefferson Davis Highway, Suite 1204, Arlington, VA 22202-4302, and to the Office of Management and Budget, Paperwork Reduction Project (0704-0188) Washington DC 20503.			
1. AGENCY USE ONLY *(Leave blank)*	**2. REPORT DATE** June 2004	**3. REPORT TYPE AND DATES COVERED** Dissertation	
4. TITLE AND SUBTITLE: Performance of Coherent and Noncoherent *RAKE* Receivers with Convolutional Coding and Pulse-Noise Interference		**5. FUNDING NUMBERS**	
6. AUTHOR(S) Kyle Kowalske			
7. PERFORMING ORGANIZATION NAME(S) AND ADDRESS(ES) Naval Postgraduate School Monterey, CA 93943-5000		**8. PERFORMING ORGANIZATION REPORT NUMBER**	
9. SPONSORING / MONITORING AGENCY NAME(S) AND ADDRESS(ES) N/A		**10. SPONSORING / MONITORING AGENCY REPORT NUMBER**	
11. SUPPLEMENTARY NOTES The views expressed in this thesis are those of the author and do not reflect the official policy or position of the Department of Defense or the U.S. Government.			
12a. DISTRIBUTION / AVAILABILITY STATEMENT Approved for public release; distribution is unlimited.		**12b. DISTRIBUTION CODE**	

13. ABSTRACT (maximum 200 words) The performance of coherent and noncoherent *RAKE* receivers over a fading channel in the presence of pulse-noise interference and additive white Gaussian noise is analyzed. Coherent *RAKE* receivers require a pilot tone for coherent demodulation. Using a first order phase-lock-loop to recover a pilot tone with additive white Gaussian noise causes phase distortions at the phase-lock-loop output, which produce an irreducible phase noise error floor for soft decision Viterbi decoding. Both coherent and noncoherent *RAKE* receivers optimized for additive white Gaussian noise perform poorly when pulse-noise interference is present. When soft decision convolutional coding is considered, the performance degrades as the duty cycle of the pulse-noise interference signal decreases. The reverse is true for hard decision Viterbi decoding, since fewer bits experience interference and bit errors with high noise variance cannot dominate the decision statistics. Soft decision *RAKE* receiver optimized for pulse-noise interference and additive white Gaussian noise performed the best for both the coherent and noncoherent *RAKE* receivers. This receiver scales the received signal by the inverse of the variance on a bit-by-bit basis to minimize the effect of pulse-noise interference. The efficacy is demonstrated by analytical results, which reveal that this receiver reduces the probability of bit error down to the irreducible phase noise error floor when pulse-noise interference is present. This demonstrates how important it is to design the receiver for the intended operational environment.

14. SUBJECT TERMS *RAKE*, noncoherent *RAKE*, interference, pulse-noise, phase noise, coding			**15. NUMBER OF PAGES** 105
			16. PRICE CODE
17. SECURITY CLASSIFICATION OF REPORT Unclassified	**18. SECURITY CLASSIFICATION OF THIS PAGE** Unclassified	**19. SECURITY CLASSIFICATION OF ABSTRACT** Unclassified	**20. LIMITATION OF ABSTRACT** UL

NSN 7540-01-280-5500 Standard Form 298 (Rev. 2-89)
Prescribed by ANSI Std. 239-18

THIS PAGE INTENTIONALLY LEFT BLANK

Approved for public release; distribution is unlimited.

PERFORMANCE OF COHERENT AND NONCOHERENT *RAKE* RECEIVERS WITH CONVOLUTIONAL CODING RICEAN FADING AND PULSE-NOISE INTERFERENCE

Kyle E. Kowalske
GS-13, Civilian, Department of Defense
B.S.E.E., Marquette University, 1983

Submitted in partial fulfillment of the
requirements for the degree of

DOCTOR OF PHILOSOPHY IN ELECTRICAL ENGINEERING

from the

NAVAL POSTGRADUATE SCHOOL
June 2004

Author: _____
Kyle E. Kowalske

Approved by:

_____
Clark Robertson
Professor of Electrical &
Computer Engineering
Dissertation Supervisor

_____
Tri T. Ha
Professor of Electrical &
Computer Engineering

_____
Monique Fargues
Assoc. Professor of Electrical
& Computer Engineering

_____
Roberto Cristi
Assoc. Professor of Electrical
& Computer Engineering

_____
Wolfgang Baer
Research Assoc. Professor of Information Science

Approved by: _____
John P. Powers, Chair, Department of Electrical & Computer Engineering

Approved by: _____
Julie Filizetti, Associate Provost for Academic Affairs

THIS PAGE INTENTIONALLY LEFT BLANK

ABSTRACT

The performance of coherent and noncoherent *RAKE* receivers over a fading channel in the presence of pulse-noise interference and additive white Gaussian noise is analyzed. Coherent *RAKE* receivers require a pilot tone for coherent demodulation. When a first order phase-lock-loop is used to recover a pilot tone in the presence of additive white Gaussian noise, phase distortions at the phase-lock-loop output result. These phase distortions produce an irreducible phase noise error floor for soft decision Viterbi decoding. Both coherent and noncoherent *RAKE* receivers optimized for additive white Gaussian noise perform poorly when pulse-noise interference is present. When soft decision convolutional coding is considered, the performance degrades as the duty cycle of the pulse-noise interference signal decreases. The reverse is true for hard decision Viterbi decoding, since fewer bits experience interference and bit errors with high noise variance cannot dominate the decision statistics. The soft decision *RAKE* receiver optimized for pulse-noise interference and additive white Gaussian noise performed the best for both the coherent and noncoherent *RAKE* receivers. This receiver scales the received signal by the inverse of the variance on a bit-by-bit basis to minimize the effect of pulse-noise interference. The efficacy of this technique is demonstrated by analytical results, which reveal that this receiver reduces the probability of bit error down to the irreducible phase noise error floor when pulse-noise interference is present. This demonstrates how important it is to design the receiver for the intended operational environment.

THIS PAGE INTENTIONALLY LEFT BLANK

TABLE OF CONTENTS

THIS PAGE INTENTIONALLY LEFT BLANK

LIST OF FIGURES

THIS PAGE INTENTIONALLY LEFT BLANK

ACKNOWLEDGMENTS

I would like to thank my parents for their support and encouragement. My brother also deserves a special word of thanks for visiting me while I was in Monterey, CA and for buying me a membership for the Monterey Bay Aquarium.

My dissertation supervisor, Prof. R. Clark Robertson did a phenomenal job over a period of three years continuing to provide direction and review my dissertation. I truly enjoyed being a student in his classes and thank him for providing such an interesting dissertation topic. It is very difficult to supervise off campus students and based on the amount of pages he faxed to me with corrections to my dissertation, I probably should also thank the fax machine for not breaking.

Prof. Ha is also an excellent teacher and provided valuable input to this dissertation. His diligent reading found several errors that I thought I had already corrected.

Prof. Fargues also provided valuable comments and corrections. I appreciate the time she spent with me listening to my explanations and pointing out errors. Her comments and suggestions improved the quality of this dissertation.

I would also like to thank Prof. Cristi for his comments and corrections. He found an error in a equation I used from previous published literature. I definitely owe him a cappuccino or two.

Finally I would like to thank Prof. Baer for teaching my computer network class and staying on my committee for three years. His idea to add an appendix to further explain the numerical inversion routines added to the quality of this dissertation.

THIS PAGE INTENTIONALLY LEFT BLANK

EXECUTIVE SUMMARY

The performance of coherent and noncoherent *RAKE* receivers for a signal transmitted over a fading channel in the presence of pulse-noise interference and additive white Gaussian noise is analyzed. Unlike commercial systems, which operate under strict FCC regulations, military communication systems are often required to operate with high levels of noise and interference in addition to frequency-selective fading. Reliable communication over a frequency-selective fading channel can be achieved by either using a *RAKE* receiver or orthogonal frequency-division multiplexing (OFDM). This dissertation analyzes the performance of a *RAKE* receiver with convolutional coding with both hard and soft decision decoding. Coherent *RAKE* receivers require a pilot tone for demodulation. The use of a first order phase-lock-loop to recover a pilot tone with additive white Gaussian noise causes phase distortions at the phase-lock-loop output, which produce an irreducible phase noise error floor for soft decision Viterbi decoding. These phase distortions are negligible when the pilot tone signal-to-noise ratio is 20 dB or greater. If the pilot tone is received with a lower signal-to-noise ratio, reliable communication may not be possible. Analytical results for soft decision Viterbi decoding with a 10-dB pilot tone signal-to-noise ratio predicts a catastrophic 50 percent error rate. This demonstrates how critical it is for a coherent communication system to have a good phase reference.

Commercial *RAKE* receivers, such as the ones used in IS95 cellular phones, are optimized for additive white Gaussian noise. This dissertation demonstrates that both coherent and noncoherent *RAKE* receivers optimized for additive white Gaussian noise perform poorly when pulse-noise interference is present. When soft decision Viterbi decoding is considered, the performance degrades as the duty cycle of the pulse-noise interference signal decreases. The reverse is true for hard decision Viterbi decoding, since fewer bits experience interference and bit errors with high noise variance cannot dominate the decision statistics. Soft decision receivers provide a decision if the received bit is a logical “1” or a logical “0” as well as an estimate of the of the receiver confidence in the bit decision. If the pulse-noise interference causes a bit error and the soft decision receiver gives the bit decision a high confidence estimate, then soft decision Viterbi decoding will produce significant errors. Hard decision Viterbi decoding, on the other hand, provides

some immunity to both pulse-noise interference and phase noise. When the pulse-noise interference had a one percent duty cycle, the coherent *RAKE* receiver with hard decision Viterbi decoding produced an error rate of approximately 10^{-10} or lower when the pilot tone signal-to-noise ratio was 20 dB. If the pilot tone is received with only a 10-dB signal-to-noise ratio, then a coherent *RAKE* receiver with hard decision Viterbi decoding could still provide reliable communication. An error rate of 10^{-6} can be obtained when the ratio of the received signal power-to-pulse-noise interference power is 30 dB or greater.

Noncoherent *RAKE* receivers do not track the phase of the received signal, hence they are not affected by phase noise. Using soft decision Viterbi decoding, the noncoherent *RAKE* receiver can perform below the coherent *RAKE* receiver phase noise error floor when the ratio of the received signal power-to-pulse-noise interference power is large. However, the coherent *RAKE* receiver for small values of received signal power-to-pulse-noise interference power performs significantly better than the noncoherent *RAKE* receiver when the effects of phase noise are negligible. This is especially true when hard decision Viterbi decoding is considered. For a pulse-noise duty cycle of one percent and approximately the same received signal power and pulse-noise interference power, the probability of bit error for a noncoherent *RAKE* receiver with hard decision Viterbi decoding was approximately 10^{-6}. This is four orders of magnitude worse than the coherent *RAKE* receiver with hard decision Viterbi decoding.

A *RAKE* receiver optimized for pulse-noise interference and additive white Gaussian noise performed the best for both the coherent and noncoherent cases. This receiver scales the received signal by the inverse of the variance on a bit-by bit basis to minimize the effect of pulse-noise interference. The efficacy of this technique is demonstrated by analytical results, which reveal that this receiver reduces the probability of bit error down to the irreducible phase noise error floor when pulse-noise interference is present. This demonstrates how important it is to design the receiver for the intended operational environment.

I. INTRODUCTION

Wireless communications over multipath fading channels are increasingly important for modern digital communications systems. This is especially true for military communication systems, which may also have to operate in high levels of noise and interference. There are many examples in modern digital communication systems of wireless transmission over fading channels, such as cellular telephones, wireless local area networks, and the physical layer of a mobile *ad hoc* network, such as a network between two ships. Furthermore, with the demand for even higher data bit rates to support ever more sophisticated data applications, the fading channel is more likely to be frequency-selective. Consequently, modern digital communication systems have to be designed to operate over frequency-selective channels in order to avoid significant degradation in performance.

One technique that can be used to eliminate the degradation that results from a frequency-selective channel is *orthogonal frequency-division multiplexing* (OFDM) where the data bits are transmitted on a number of orthogonal carrier frequencies. OFDM is a special case of multicarrier, as opposed to single carrier, modulation where the use of orthogonal carrier frequencies minimizes overall signal bandwidth. If there are N orthogonal carrier frequencies, then one out of every N data symbols is transmitted on the same carrier frequency, and the symbol rate for an individual carrier is reduced by a factor of N. As a result, the bandwidth required for each carrier is reduced by a factor of N as compared with the bandwidth of the signal when only a single carrier frequency is used. By choosing N large enough, the channel for each carrier can be made frequency-nonselective, or flat, even though the channel is frequency-selective when only a single carrier is used. OFDM essentially works by converting a single signal into multiple signals, where each of the multiple signals is frequency-nonselective over the same channel for which the original single carrier signal is frequency-selective.

Another technique for minimizing the performance degradation caused by frequency-selective channels involves the modification of the receiver rather than the transmitter. One type of receiver designed to demodulate signals that have been transmitted over a frequency-selective channel is the *RAKE* receiver. In this dissertation the perform-

ance of a *RAKE* receiver when the signal is transmitted over a frequency-selective channel is analyzed. Since military systems face even more complicated issues such as interference, the effect of pulse-noise interference as well as additive white Gaussian noise (AWGN) is also analyzed. For coherently detected signals, the effect of phase noise on the system performance is analyzed. A block diagram of the assumed transmitter is shown in Figures 1.1.

Figure 1.1 Transmitter Diagram.

As can be seen in Figure 1.1, the data is assumed to be convolutionally encoded, interleaved and modulated as either a Binary Phase Shift Keying (BPSK) waveform or frequency shift keying (FSK) waveform. The signal is assumed to be transmitted over a slow, frequency-selective fading channel with both pulse-noise interference and AWGN. Without loss of generality, in order to evaluate the effect of channel fading and pulse-noise interference on the data signal alone as well as on both the data signal and the pilot tone, the pilot tone is assumed to be transmitted on a separate, independent frequency from the data waveform carrier frequency.

A block diagram of the receiver is shown in Figure 1.2.

Figure 1.2 Receiver Diagram.

A *RAKE* receiver is used to minimize the effect of the frequency-selective fading channel, and the maximum-likelihood *RAKE* receiver for AWGN and pulse-noise interference is analyzed and compared with a *RAKE* receiver designed for AWGN only. De-interleaving the signal randomizes the errors prior to decoding. Both hard decision and soft decision Viterbi decoding are analyzed. In addition, phase noise effects are also considered for coherent systems.

The effects of phase estimation errors in coherent *RAKE* receivers have been examined in the literature. In [1] and [2] a *RAKE* receiver operating at a low signal-to-noise ratio (SNR) was analyzed. At low SNR the *RAKE* receiver has problems estimating the channel tap weights, and at any given time, each finger will have a different random phase error. A lower bound on the error probability for this case was developed in [1], while in [2] an upper bound on the probability of bit error was derived. Phase noise, however, causes each finger of the *RAKE* receiver to have the same tap weight estimation phase error at any instant in time, since the received pilot tone is used to estimate the tap weight. The effects of phase noise on *RAKE* receivers was first published in [3] by Ziemer, Vojcic, Milstein, and Proakis; however, the analysis did not include convolutional coding or pulse-noise interference. Both commercial and military systems use convolutional coding to improve the bit error rate. Military systems often have to provide reliable communication in the presence of interference, hence it is important to extend the analysis in [3] to include the effect of coding and interference. This dissertation will follow the analytical approach in [3] with the appropriate modifications for pulse-noise interference and convolutional coding. In our work, we assume that a pilot tone is transmitted on a separate frequency and is an integer multiple of two ($2n$) times the carrier frequency of the data signal. The received pilot tone then serves as the input to a phase-lock-loop (PLL) and is translated down to the carrier frequency of the data so it can be used for coherent demodulation, as shown in Figure 1.3.

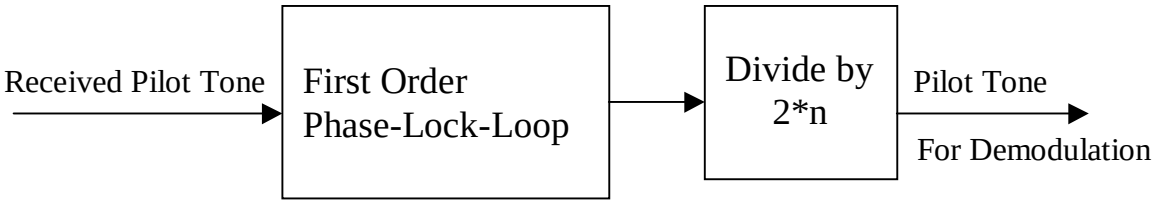

Figure 1.3 Processing Received Pilot Tone.

The analysis is done for various levels of the PLL loop SNR in order to determine how coherent systems perform for different values. It is also assumed that the pilot tone is received with flat fading and either AWGN or AWGN plus a noise-like interference signal that is modeled as additive Gaussian noise. With these assumptions, the effect of pulse-

noise interference with various levels of received signal-to-noise-ratios on the pilot tone can be investigated. The effect of AWGN on a first order phase-locked loop is a Tikonov distributed phase error as shown in [4]. We will show that hard decision Viterbi decoding can perform better than soft decision Viterbi decoding in the presence of Tikonov distributed phase noise.

Commercially available soft decision Viterbi decoders are designed for AWGN channels. In [5] it was shown that these decoders perform poorly in the presence of pulse-noise interference and that hard decision Viterbi decoding performs better when a pulse-noise interference signal is present. Several modifications to improve the performance of soft decision Viterbi decoding have been examined in the literature. In [6] the concept of a noise-normalized receiver was introduced, and simulation results in [7] show that the clipper receiver works slightly better than the noise-normalized receiver. In this dissertation, the performance of a maximum-likelihood *RAKE* receiver optimized for both AWGN and pulse-noise interference is derived, and the resulting performance is compared with those obtained using the *RAKE* receiver designed for AWGN only.

There are various types of channel fading, but in this dissertation frequency-selective, Ricean distributed fading is assumed. Ricean fading has two components, a direct, or line-of-sight, component and a diffuse component. The ratio of the power of the direct to diffuse component will be referred to as K. When $K = 0$ there is no direct signal component, and this is referred to as Rayleigh fading. If $K \to \infty$ then there is no diffuse component, hence no fading, which happens in line-of-sight communications when there is nothing between the transmitter and receiver that can scatter the signal.

Frequency-selective fading implies that different spectral components of the signal are affected differently by the channel. For flat fading channels, all the frequency components of the transmitted signal experience the same amount of fading. It can be shown that the frequency-selective channel can be modeled as an infinitely long tapped delay line with tap spacing $1/W$ where W is the noise-equivalent bandwidth of the base-band signal, and time-varying tap weight coefficients [8]. For a given channel multipath spread, we know that for time delays greater than the multipath spread T_m there is virtually no signal energy. Hence, a very good model for the frequency-selective channel is

obtained by using a tapped delay line with only $L = T_m W$ taps. For the frequency-selective channel where $T_m \gg 1/W$, the time delay $1/W$ between successive taps is sufficient to insure that each of the tap weights are mutually uncorrelated [8]. This model of a frequency-selective channel is shown in Figure 1.4.

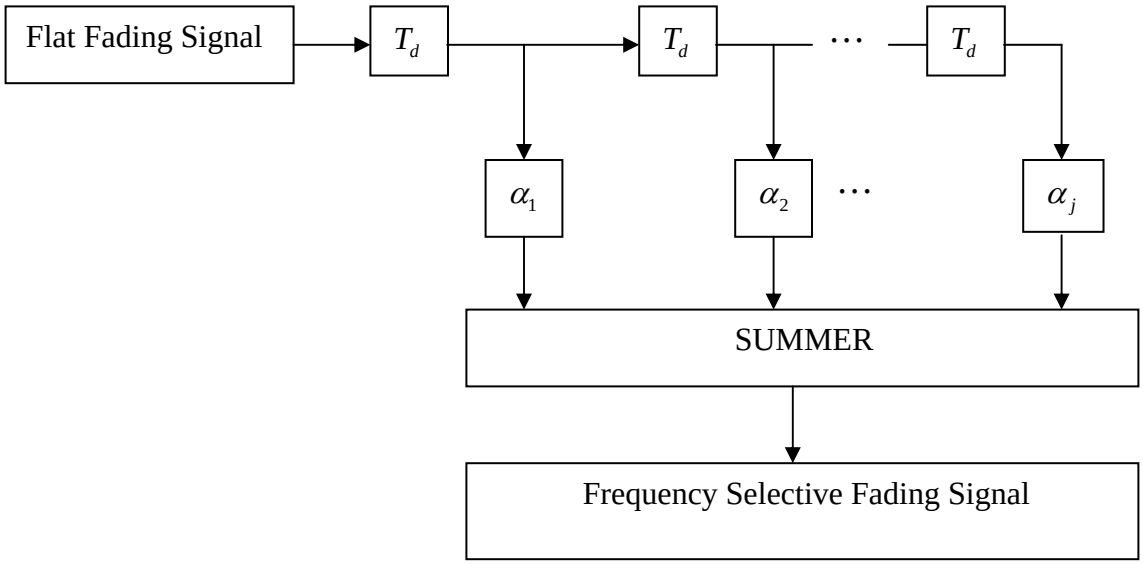

Figure 1.4 Model of the frequency-selective fading channel.

The variables α_1, α_2, and α_L are the channel tap weights that scale the magnitude of the l^{th} signal component by $|\alpha_l|$ and the phase of the l^{th} signal component by $\angle\alpha_l$, and T_d is a fixed time delay. The summer adds the *L* baseband signals together, and the result is a frequency-selective fading signal.

The adjacent bits interfere with each other, as shown in Figure 1.5, when several copies of the transmitted signal are received with different delays. If the three signals shown in Figure 1.5 were added together, the interference between adjacent bits causes intersymbol interference (ISI), which increases the bit error rate. In a coherent *RAKE* receiver the *L* different signals are separated, phase shifted to remove the phase offset imparted by the communication channel, and then coherently added together.

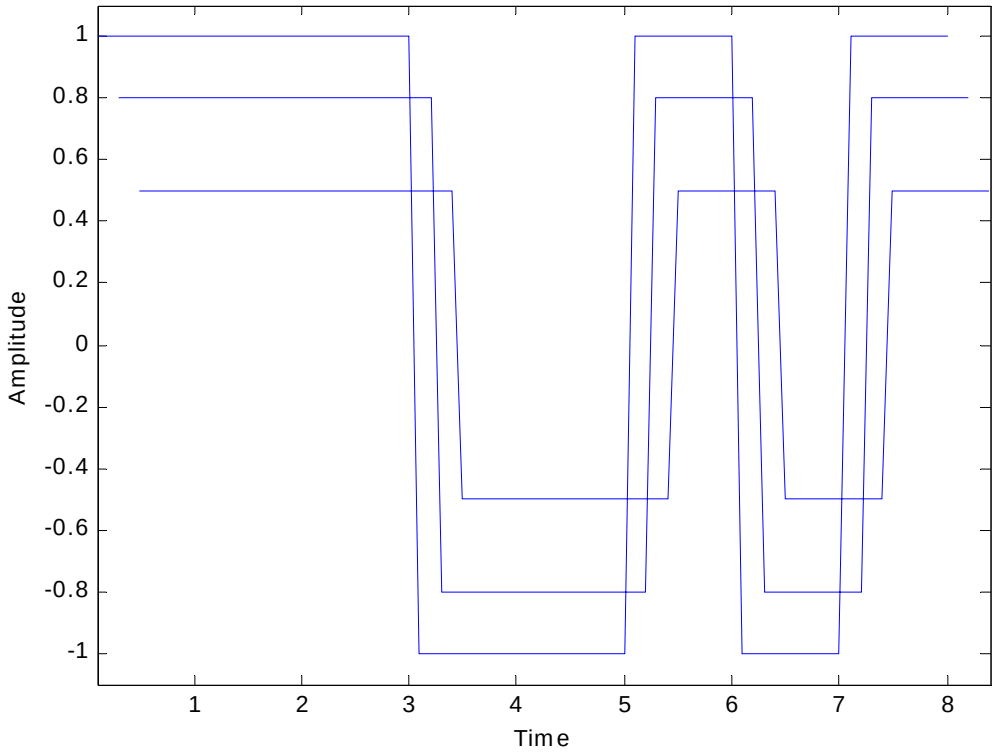

Figure 1.5 Three versions of the same signal with different amplitudes and delays.

This eliminates ISI and increases the received signal-to-noise ratio (SNR). Unfortunately, phase noise degrades the *RAKE* receiver channel tap weight estimation as well as the received signal demodulation. In [3] Ziemer, Vojcic, Milstein, and Proakis did not include both of these effects.

A *RAKE* receiver separates the effective L different received signals in a signal transmitted over a frequency-selective channel by using the correlation properties of direct sequence spread spectrum (DSSS) signals. The correlation function for a DSSS signal is 1 for zero delay, but falls linearly to $-1/N$, where N is the length of the spreading sequence, for delays of one chip or greater. The second generation digital standard for cellular telephones IS95 uses a sequence that has a length of $2^{15}-1$ for the

forward channel spreading. As a result, the correlation is $1/\left(2^{15}-1\right) \approx 0$ for delays greater than a chip. This means that any multipath components arriving with a delay greater than one chip will have zero correlation.

The analysis of the coherent *RAKE* receiver assumes that a pilot tone and the data are transmitted on separate frequencies so that the effects of interference on the carrier and interference on the data can be analyzed separately. The pilot tone is assumed to have a fixed average SNR, which enables the random phase noise effects to be analyzed by fixing the random phase offset and then integrating over the probability density function (pdf) of the phase noise to remove the dependence on the random phase offset. However, this method cannot be used when the pilot tone phase noise is time varying, especially when the pdf for the phase noise depends on the SNR of the pilot tone. Commercial IS95 systems transmit the pilot tone and data on the same frequency, but encode them with separate Walsh functions. The pilot tone is encoded with the all ones Walsh function, which allows the receiver to recover the pilot tone with a lowpass filter. In this case, pulse-noise interference would be able to affect the pilot tone and the data at the same time, which would cause a time-varying phase noise on the received pilot tone, and it would not be possible to derive analytic results. Analytic results presented here are applicable to an IS95-like system with a constant phase noise level. For AWGN channels without phase noise, soft decision Viterbi decoding is better than hard decision Viterbi decoding [5]; however, we will show that hard decision Viterbi decoding is better than soft decision Viterbi decoding when the pilot tone is received with a 10-dB SNR or lower.

For cases of severe fading, a noncoherent *RAKE* receiver is generally used since noncoherent receivers do not need to track the phase of the received signal. This means that noncoherent *RAKE* receivers are not affected by phase noise and do not have to estimate the phase of the channel tap weight. The drawback of using a noncoherent *RAKE* receiver is that the receiver will have noncoherent combining losses when

combining noncoherently detected signals [8]. The performance of a noncoherent *RAKE* receiver in the presence of pulse-noise interference will be compared and contrasted with that of a coherent *RAKE* receiver.

The coherent and noncoherent *RAKE* receivers will be compared using an exponential multipath intensity profile, which is the power of the multipath signal as a function of delay for a given instant of time. The performance of the *RAKE* receiver is best for a uniform multipath intensity profile; however, real world systems seldom operate over channels with uniform multipath intensity profiles. Since an exponential multipath intensity profile is a good approximation for a congested urban area [9], in this dissertation the multipath intensity profile is assumed to be $\exp(-\tau\psi)$, where τ is the delay and ψ is determined by how quickly the power decreases as τ increases. In this work we assume that the first finger of the *RAKE* receiver has a delay $0 < \tau < 1$, the second finger has a delay $1 < \tau < 2$ the third finger has a delay $2 < \tau < 3$, and so on. Both the coherent and the noncoherent *RAKE* receivers will be analyzed with this exponential multipath intensity profile.

In summary, this is the first time that a coherent *RAKE* receiver with phase noise, pulse-noise interference and convolutional coding has been analyzed. While soft decision Viterbi decoding outperforms hard decision Viterbi decoding for AWGN channel with perfect phase synchronization, it is shown that the reverse is true when the pilot tone is received with a 10-dB SNR or lower. A similar result was obtained in [10] where Shamain and Milstein demonstrated that increasing the antenna diversity beyond two actually increased the probability of bit error for a fading channel and a fixed antenna aperture when the loop SNR was 5 dB. In order to get the probability of bit error to continually decreased as the antenna diversity increases, Shamain and Milstein found that a loop SNR of 20 dB was required. In [11,12] performance of a coded, DSSS signal with fading and pulsed-noise interference was analyzed, but these results did not include AWGN and phase noise effects. The maximum likelihood receiver for a coherent *RAKE* receiver with pulse-noise interference is also derived in this dissertation for the first time. Additionally, this is also the first time that a noncoherent BFSK *RAKE* receiver with pulse-noise

interference and convolutional coding has been analyzed. The maximum-likelihood receiver for a noncoherent BFSK *RAKE* receiver with pulse-noise interference is also derived and analyzed.

This chapter described the system investigated, presented the frequency-selective fading channel model and introduced the *RAKE* receiver and imperfect phase synchronization concepts. The system analyzed was compared with IS95-like wireless communication systems. Finally, related research was discussed with an emphasis on the unique contributions from this dissertation.

In the second chapter, the coherent *RAKE* receiver is analyzed. We begin by analyzing the coherent *RAKE* receiver without phase noise and include phase noise effects on demodulation and channel-tap-weight estimation next. Convolutional coding with both hard and soft decision Viterbi decoding is also considered. Ricean fading, pulse-noise interference and AWGN are included in the analysis. In order to optimize the performance, the maximum-likelihood coherent *RAKE* receiver for pulse-noise interference and AWGN is derived and compared with the performance of a coherent *RAKE* receiver optimized only for AWGN.

Chapter III discusses the performance of noncoherent *RAKE* receivers in the presence of pulse-noise interference and AWGN. Once again, convolutional coding with both hard and soft decision Viterbi decoding is included in the analysis. The received signal is assumed to experience Ricean fading, pulse-noise interference and AWGN. The maximum-likelihood receiver for pulse-noise interference and AWGN was derived for the noncoherent *RAKE* receiver and the performance results were compared with a noncoherent *RAKE* receiver designed for only AWGN only. This comparison is of interest because commercial *RAKE* receivers are designed for AWGN only channels.

Next, Chapter IV summarizes the findings and presents recommendations for further research.

THIS PAGE INTENTIONALLY LEFT BLANK

II. COHERENT *RAKE* RECEIVER PERFORMANCE

The received signal obtained after transmission over a frequency-selective multi-path channel as shown in Figure 1.4 is given by

$$r(t) = \mathrm{Re}\left[\tilde{r}(t)e^{j\omega t}\right], \tag{2.1}$$

where ω is the carrier frequency in radians and the complex envelope $\tilde{r}(t)$ is given by

$$\tilde{r}(t) = \sum_{i=1}^{l} \sqrt{2}A_c |\alpha_i| \tilde{c}(t - iT_d) d(t - iT_d) e^{-j(i\omega T_d - \angle\alpha_i)}. \tag{2.2}$$

The signal $r(t)$ can be recovered by a *RAKE* receiver with *k* fingers, as shown in Figure 2.1, where $\sqrt{2}A_c$ is the unfaded carrier amplitude, α_i is the channel tap weight determined by the multipath intensity profile,

$$c(t) = \mathrm{Re}\left[\tilde{c}(t)e^{j\omega t}\right] \tag{2.3}$$

is the locally generated chipping waveform where $\tilde{c}(t)$ is the complex envelope of the

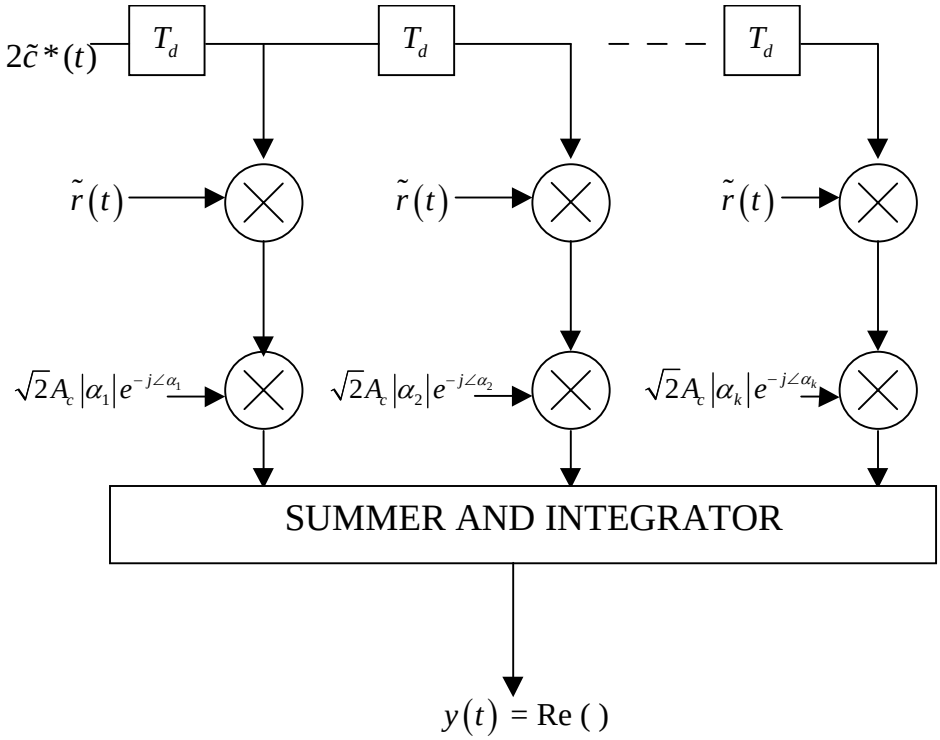

Figure 2.1 Coherent *RAKE* receiver.

chipping waveform, and $d(t)$ is the baseband data waveform which equals s_1 when a binary "1" is transmitted and s_0 when a binary "0" is sent. The channel is assumed to vary slowly compared to the bit period so that α_i can be modeled as a constant during each bit. Each of the *k* components is modeled as a flat fading signal and can have a different fading coefficient α_i, which has a magnitude $|\alpha_i|$ and a phase $\angle\alpha_i$. For this dissertation, the channel tap weights are modeled as Ricean distributed random variables.

The chipping waveform complex envelope $\tilde{c}(t)$, derived from the chipping sequence c_n, is assumed to have a chip rate matched to the *RAKE* finger spacing T_d. The autocorrelation function for the chipping waveform is given by [13]

$$R_{cc}(\tau) = \begin{cases} 1 & \text{if } \tau = 0 \\ \dfrac{-1}{N} & \text{if } 0 < \tau < N, \end{cases} \tag{2.4}$$

which can be approximated by

$$R_{cc}(\tau) = \delta(\tau) \text{ for } -N < \tau < N \tag{2.5}$$

and is periodic with a period of *N*. This approximation is good for DSSS signals with very long PN sequences and for orthogonal sequences. The k^{th} finger of the *RAKE* receiver multiplies the received signal by $2\sqrt{2}A_c|\alpha_k|\tilde{c}^*(t-kT_d)e^{-j(k\omega T_d+\angle\alpha_k)}$. This eliminates the phase difference between the fingers so that each finger can be coherently summed together and integrated over the period of a data bit. The operation of multiplying by a known reference signal and integrating is referred to as a correlation receiver [14]. Since the multipath components of the received signal are delayed by one chip or more, from (2.5) we see that only the multipath component with zero delay compared to the reference signal will correlate with the reference signal and the other multipath components will integrate to zero. The complex envelope of the signal at the output of the *RAKE* receiver is given by

$$\tilde{y}(t) = \frac{1}{T_b}\int_{t-T_b}^{t}\sum_{m=1}^{k} 2\sqrt{2}A_c\left|\alpha_m\right|\tilde{c}^*(\tau - mT_d)e^{-j(m\omega T_d + \angle\alpha_j)} \times \sum_{i=1}^{l}\sqrt{2}A_c\left|\alpha_i\right|\tilde{c}(\tau - iT_d)d(\tau - iT_d)e^{\left[-j(i\omega T_d - \angle\alpha_i)\right]}d\tau, \quad (2.6)$$

and the real baseband output can be found by taking the real part of (2.6). Eliminating the terms that integrate to zero in (2.6), we get

$$y(t) = 2A_c^2 d(t)\sum_{j=1}^{k}\left|\alpha_j\right|^2. \quad (2.7)$$

Hence, the *RAKE* receiver separates the multipath components, removes the phase offset, and then coherently combines them. Since the receiver collects all received signal paths that carry the same information on separate fingers, its action is similar to the way dirt collects between the fingers of a *RAKE* when one *RAKE*s the ground in a garden and thus was named a *RAKE* receiver.

A. TAP WEIGHT ESTIMATION

The channel tap weights α_1, α_2, …, α_l scale both the amplitude and phase of the received signal. Since the channel shifts the phase by $\angle\alpha_l$, the *RAKE* receiver must shift the phase on each finger by $-\angle\alpha_l$ for coherent combining. A block diagram illustrating the technique for estimating the channel tap weights is shown in Figure 2.2. First, the received signal is mixed with a locally generated chipping waveform that is both chip and sequence synchronized with the received signal. Mathematically, the output of the first mixer on the k^{th} finger can be written

$$\tilde{y}_1(t) = 2\sqrt{2}A_c\sum_{i=1}^{l}\left|\alpha_i\right|\tilde{c}^*(t - kT_d - T_b)\tilde{c}(t - iT_d - T_b)d(t - iT_d - T_b)e^{-j(i\omega T_d + \omega T_b - \angle\alpha_i)}e^{-j\omega(kT_d + T_b)}. \quad (2.8)$$

The above result is delayed by one bit to allow for demodulation and then multiplied by the previous bit decision. At the output of the second mixer, we have

$$\tilde{y}_2(t) = 2\sqrt{2}A_c\sum_{i=1}^{l}\left|\alpha_i\right|\tilde{c}^*(t - kT_d - T_b)\tilde{c}(t - iT_d - T_b)d^2(t - kT_d - T_b)e^{-j(i\omega T_d + \omega T_b - \angle\alpha_i)}e^{-j\omega(iT_d + T_b)}. \quad (2.9)$$

The lowpass filter then removes the high frequency terms, and from (2.5) the output of the lowpass filter is zero when $i \neq k$. Since $\tilde{c}^*(t - kT_d - T_b)\tilde{c}(t - kT_d - T_b) = 1$, the complex output of the k^{th} finger is

$$\tilde{y}(t) = 2\sqrt{2}A_c|\alpha_k|d^2(t - kT_d - T_b)e^{j\angle\alpha_k}. \quad (2.10)$$

Since BPSK signaling is used, $d(t)$ is either +1 or −1, and $d^2(t)$ is always +1. Thus, (2.10) can be simplified to

$$y(t) = 2\sqrt{2}A_c|\alpha_k|e^{j\angle\alpha_k}. \quad (2.11)$$

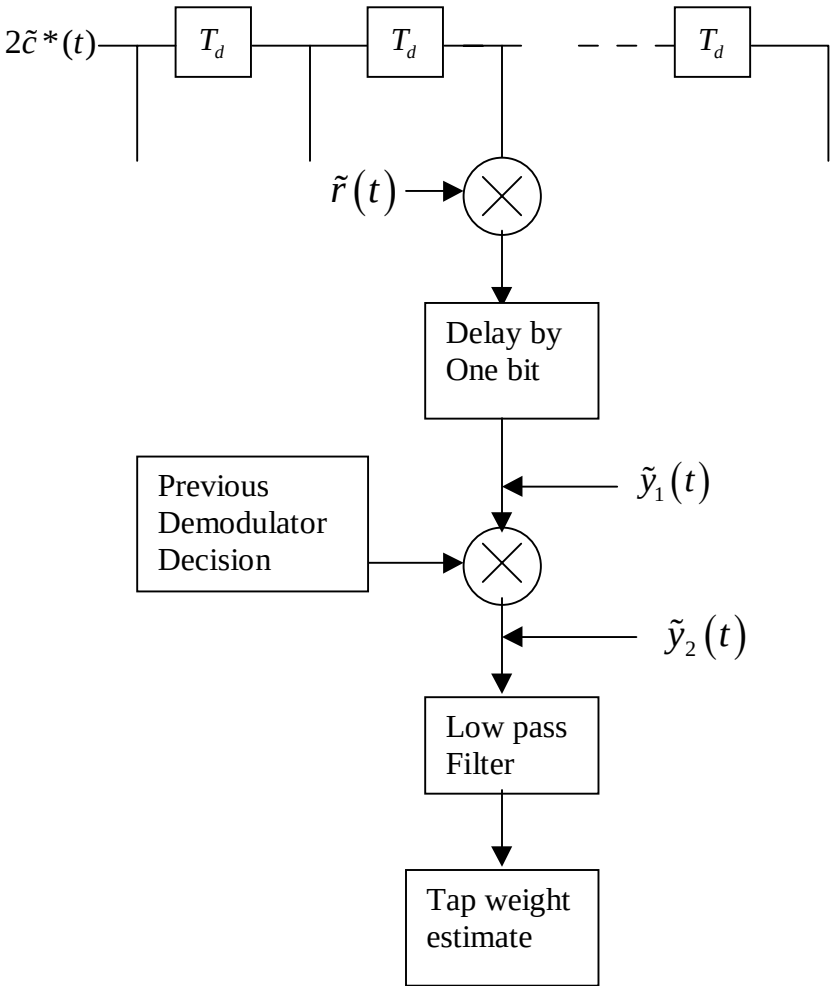

Figure 2.2 Tap Weight Estimator for a Coherent *RAKE* Receiver.

From (2.11) we see that the tap weight estimator provides estimates of both the magnitude of the channel tap weight $|\alpha_k|$ as well as the phase shift $\angle\alpha_k$ and scales these estimates by $\sqrt{2}A_c$, the unfaded carrier amplitude.

B. PHASE NOISE MODEL

Conventional IS95 wireless communication systems can recover the pilot tone on the forward channel by using a low pass filter. This process introduces AWGN which mixes with the AWGN on the data signal and produces multiplicative noise when the recovered pilot tone (plus AWGN) is used to demodulate the data bits. In order to remove the noise from the pilot tone, we can pass the received pilot tone through a bank of matched filters which are matched to different frequencies. The frequency of the pilot tone can then be estimated by interpolating between the two filters with the highest output. This previous step eliminates noise on the pilot tone but can produce a slight frequency offset in the synthesized pilot tone, and frequency offsets in the pilot tone degrade the data demodulation. Finally, we can use a phase-locked loop to track the pilot tone; however, signal fading and AWGN cause phase noise at the phase-locked loop output.

Phase noise is the random phase variation of the carrier and causes the carrier to deviate from a perfect cosine wave. It is shown in [4] that a received signal and AWGN applied to the input of a first order phase-locked loop causes Tikonov distributed phase noise which is a function of the loop SNR. The pdf for the Tikonov distributed phase error is [4]

$$P(\phi \mid \beta) \approx \frac{\exp(\beta\cos(\phi))}{2\pi I_0(\beta)}, \tag{2.12}$$

where β is the loop SNR, which can be affected by channel fading, and I_0 is the modified Bessel function of the first kind and order zero. A plot of the Tikonov pdf for various values of loop SNR is shown in Figure 2.3. The solid line shows the Tikonov pdf

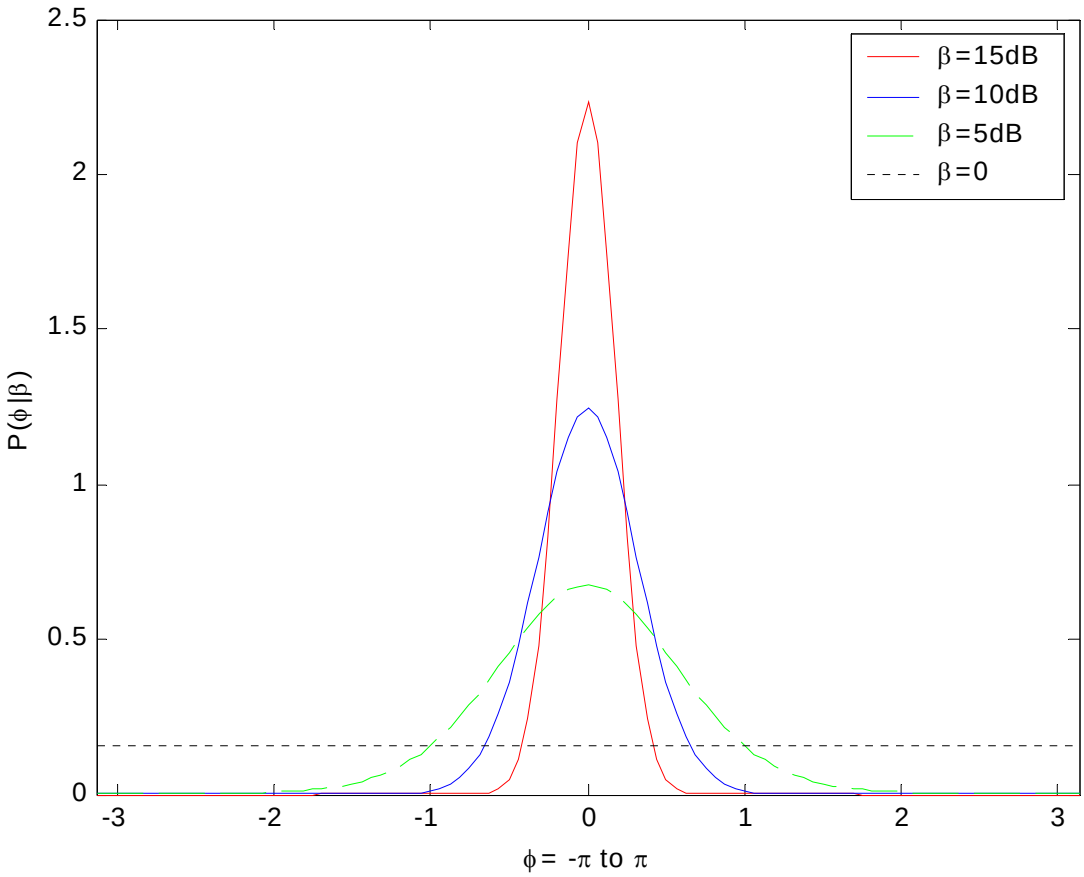

Figure 2.3 $P(\phi \mid \beta)$ vs. ϕ for Tikonov phase noise.

for a loop SNR of 15 dB, and is similar to a Gaussian pdf. The trace with large dashes is for a loop SNR of 10 dB, which also looks like a Gaussian pdf. The trace with small dashes is for a loop SNR of 5 dB, and the probability of large phase offsets increases for this level of loop SNR. Recall that there is no signal present when the loop SNR is zero $(-\infty \text{ dB})$, and we expect the phase error from the phase-locked loop to be uniformly distributed from $-\pi$ to π as shown in Figure 2.3.

C. EFFECT OF PHASE AND FREQUENCY OFFSETS ON BPSK SIGNALS

The next step is to analyze how phase noise affects the received signal. Figure 2.4 shows a BPSK receiver with an unknown frequency offset $\Delta\omega$ and phase offset ϕ in the

local oscillator where the output $P(T)$ is assumed to be sampled every T seconds. The output can then be written as:

$$P(T) = \frac{2\sqrt{2}A_c}{T}\int_0^T \sin(\omega_0 t)\sin\left[(\omega_0 + \Delta\omega)t + \phi\right]dt. \tag{2.13}$$

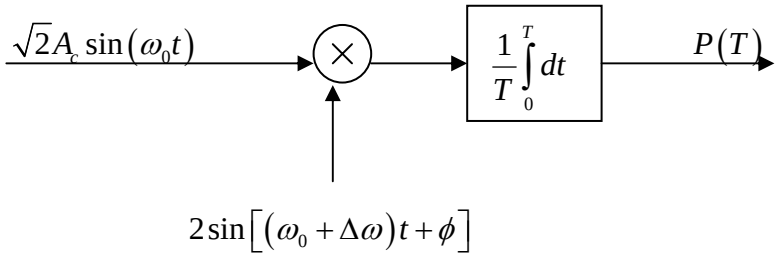

Figure 2.4 BPSK receiver with unknown frequency and phase offset.

Substituting the identity

$$\sin(a)\sin(b) = \frac{1}{2}\left[\cos(a-b) - \cos(a+b)\right] \tag{2.14}$$

into (2.13), we obtain

$$P(T) = \frac{\sqrt{2}A_c}{T}\int_0^T \cos\left[(\Delta\omega)t + \phi\right] - \cos\left[(2\omega_0 + \Delta\omega)t + \phi\right]dt. \tag{2.15}$$

Equation (2.15) has a high frequency term at twice the carrier frequency and a baseband component. Since every complete cycle of the high frequency term will integrate to zero, the high frequency component will either integrate to zero or a very small number if there is not an integral number of cycles over the bit period. Hence, the double frequency term is negligible and only the baseband term will be present at the output of the integrator. Using the identity

$$\cos(a+b) = \cos(a)\cos(b) - \sin(a)\sin(b) \tag{2.16}$$

in (2.15), we get

$$P(T) = \frac{\sqrt{2}A_c}{T}\left[\int_0^T \cos\left[(\Delta\omega)t\right]\cos(\phi)dt - \int_0^T \sin\left[(\Delta\omega)t\right]\sin(\phi)\,dt\right], \tag{2.17}$$

which can be integrated to produce

$$P(T) = \sqrt{2}A_c \cos(\phi)\frac{\sin(\Delta\omega T)}{\Delta\omega T} + \frac{\sqrt{2}A_c \sin(\phi)}{\Delta\omega T}\left[\cos(\Delta\omega T) - 1\right]. \quad (2.18)$$

At this point we will limit our discussion by only considering the phase-locked loop tracking problem, which has no frequency offset but unwanted phase noise due to the pilot tone being received with AWGN. Setting $\Delta\omega$ to zero in (2.18), we get the result

$$P(T) = \sqrt{2}A_C \cos(\phi). \quad (2.19)$$

Hence, the effect of an unknown phase error at the BPSK receiver is to reduce the amplitude of the carrier by the cosine of the phase error.

D. EFFECT OF PHASE NOISE ON CHANNEL TAP WEIGHT ESTIMATION

Not only does phase noise affect the data demodulation in a *RAKE* receiver, it also degrades the *RAKE* receiver channel tap weight estimation. We begin with the tap weight estimator shown in Figure 2.2 to include a random phase offset ϕ as shown in Figure 2.5. For a signal transmitted over a frequency-selective, multipath channel, the complex envelope of the received signal can be written as shown in (2.2). In this case, however, the local oscillator in the receiver is slightly out of phase with the received signal, so the locally generated chipping sequence includes a random carrier phase offset ϕ. We can write the complex envelope of the locally generated chipping sequence on the k^{th} finger as

$$\tilde{l}(t) = \tilde{c}^*(t - kT_d)e^{-j(\omega kT_d - \phi)}. \quad (2.20)$$

Multiplying (2.20) by the complex envelope of the received signal (2.2), we get

$$\tilde{y}_1(t) = 2\sqrt{2}A_c \sum_{i=1}^{l} |\alpha_i| \tilde{c}^*(t - kT_d)\tilde{c}(t - iT_d)d(t - iT_d)e^{-j(i\omega T_d - \angle\alpha_k)}e^{-j(\omega kT_d - \phi)}. \quad (2.21)$$

The above result is delayed by one bit to allow for demodulation and then multiplied by the previous bit decision. At the output of the second mixer, we have

$$\tilde{y}_2(t) = 2\sqrt{2}A_c \sum_{i=1}^{l} |\alpha_i| \tilde{c}^*(t - kT_d)\tilde{c}(t - iT_d)d(t - kT_d)\,d(t - iT_d)e^{-j(i\omega T_d - \angle\alpha_k)}e^{-j(\omega iT_d - \phi)}. \quad (2.22)$$

The lowpass filter then removes the high frequency terms, and from (2.5) the output of the lowpass filter is zero when $i \neq k$. Again, since that $\tilde{c}^*(t-kT_d)\tilde{c}(t-kT_d)=1$, the complex output of the k^{th} finger is

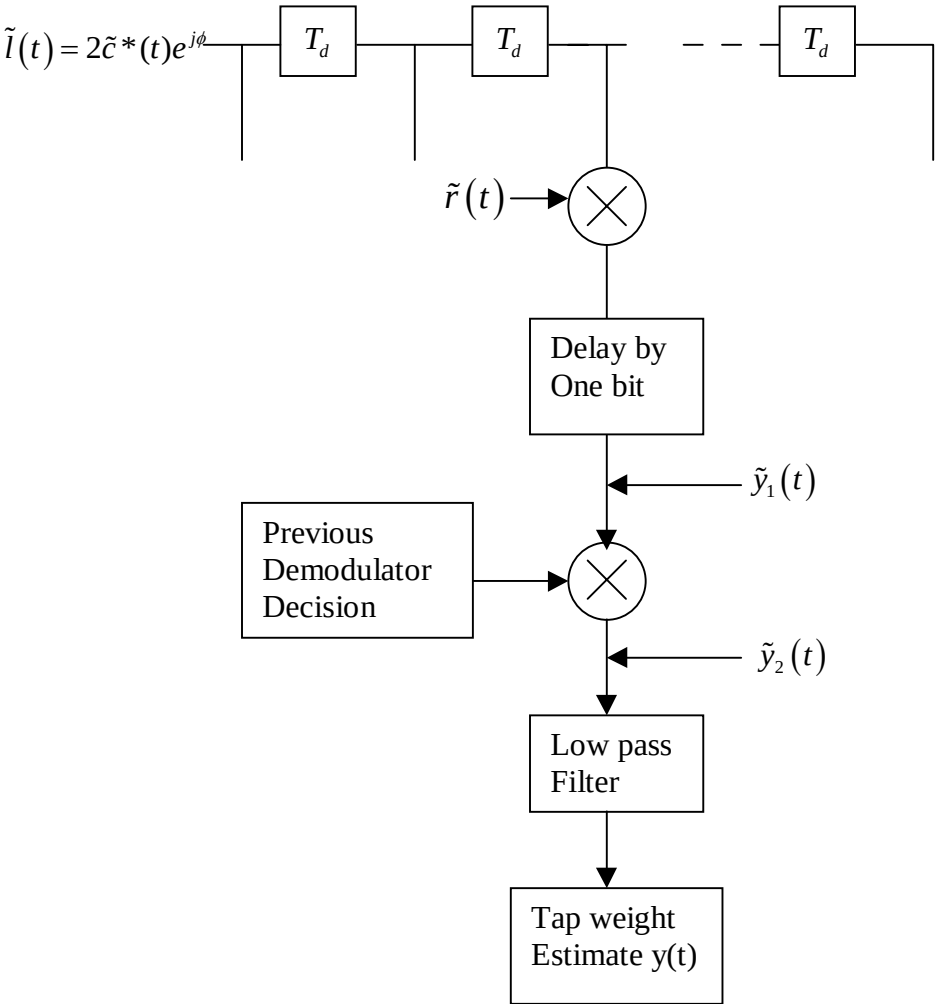

Figure 2.5 Channel Tap Weight Estimator with Phase Noise ϕ.

$$\tilde{y}(t)=2\sqrt{2}A_c|\alpha_k|d^2(t-kT_d)e^{j(\angle\alpha_k+\phi)}. \tag{2.23}$$

Since BPSK signaling is used, $d(t)$ is either $+1$ or -1, and $d^2(t)$ is always $+1$. Thus, (2.23) can be simplified to

$$\tilde{y}(t)=2\sqrt{2}A_c|\alpha_k|e^{j(\angle\alpha_k+\phi)}, \tag{2.24}$$

which differs from the tap weight estimate without phase noise only by the $e^{-j\phi}$ term. It is interesting to note that phase noise affects both the tap weight estimate and the signal demodulation and, to this author's knowledge, no other research has examined the effects of both simultaneously.

E. PULSE-NOISE INTERFERENCE

In addition to phase noise, interference is also considered. The interference signal is modeled as AWGN. Two separate interference scenarios are analyzed since the transmitter is assumed to send a pilot tone on a separate frequency than the data. First, interference of only the data signal frequency is analyzed. Second, interference of the pilot tone is analyzed. When the pilot tone experiences interference, all the data bits are affected by increased phase noise due to the interference since the pilot tone is used to synchronize the receiver local oscillator in order to demodulate the data signal.

Pulsing the interference signal is also investigated. Specifically, if the interference power spectral density is N_j and the duty cycle is ρ, then the interference power is $N_j / \rho T_b$ where T_b is the bit duration. This assures a constant average power interference signal regardless of ρ. Pulsing can be an effective interference strategy because of the increased power when interference is present. Since the probability of bit error is given by $P_b = \rho$ (error rate with pulse-noise interference) + $(1-\rho)$(error rate with AWGN), assuming the probability of bit error is small when only AWGN is present, the overall probability of error is approximately 5×10^{-3} if the interference can cause a 50 percent probability of error when it is on and if the interference duty cycle (ρ) is one percent.

F. MAXIMUM-LIKELIHOOD RECEIVER FOR CHANNELS WITH GAUSSIAN NOISE, PULSE INTERFERENCE, AND DIVERSITY

The maximum-likelihood receiver for a BPSK signal with d independent diversity receptions, of which i have pulse-noise interference, is derived in this section. The received signal is designated $y_m(t)$ where m takes values between 1 and d to represent each of the d different diversity receptions. The interference waveform is modeled as additive Gaussian noise with variance σ_0^2 when only AWGN is present and with variance $\sigma_0^2 + \sigma_j^2$ when interference is present. We begin with a general analysis that is

valid for diversity in space, frequency and time. Assuming that the diversity receptions are independent, we obtain the joint pdf for the "0" bit when i diversity receptions experience interference and $d-i$ diversity receptions have only AWGN as

$$f_0(y) = \int_{t-T}^{t} \left(\frac{1}{2\pi\sigma_0^2}\right)^{\frac{d-i}{2}} \exp\left[\frac{-1}{2\sigma_0^2}\sum_{m=1}^{d-i}\left(y_m(\tau)-s_0(\tau)\right)^2\right] \times \left(\frac{1}{2\pi(\sigma_0^2+\sigma_j^2)}\right)^{\frac{i}{2}} \exp\left[\frac{-1}{2(\sigma_0^2+\sigma_j^2)}\sum_{m=d-i+1}^{d}\left(y_m(\tau)-s_0(\tau)\right)^2\right] d\tau, \tag{2.25}$$

and the joint pdf for the "1" bit is given by

$$f_1(y) = \int_{t-T}^{t} \left(\frac{1}{2\pi\sigma_0^2}\right)^{\frac{d-i}{2}} \exp\left[\frac{-1}{2\sigma_0^2}\sum_{m=1}^{d-i}\left(y_m(\tau)-s_1(\tau)\right)^2\right] \times \left(\frac{1}{2\pi(\sigma_0^2+\sigma_j^2)}\right)^{\frac{i}{2}} \exp\left[\frac{-1}{2(\sigma_0^2+\sigma_j^2)}\sum_{m=d-i+1}^{d}\left(y_m(\tau)-s_1(\tau)\right)^2\right] d\tau. \tag{2.26}$$

Forming the likelihood ratio [15], we obtain

$$\frac{f_1(y)}{f_0(y)} \underset{s_0}{\overset{s_1}{\gtrless}} 1. \tag{2.27}$$

If the likelihood ratio is greater than 1, the receiver decides bit "1" was sent, and, if the likelihood ratio is less than 1, the receiver decides bit "0" was sent. Substituting (2.25) and (2.26) into (2.27) and simplifying, we get

$$\int_{t-T}^{t} \exp\left[\frac{-1}{2\sigma_0^2}\sum_{m=1}^{d-i}\left(2y_m(\tau)s_0(\tau)-2y_m(\tau)s_1(\tau)-s_0^2(\tau)+s_1^2(\tau)\right)\right] \times \exp\left[\frac{-1}{2\left(\sigma_0^2+\sigma_j^2\right)}\sum_{m=d-i+1}^{d}\left(2y_m(\tau)s_0(\tau)-2y_m(\tau)s_1(\tau)-s_0^2(\tau)+s_1^2(\tau)\right)\right] d\tau \underset{s_0}{\overset{s_1}{\gtrless}} 1. \tag{2.28}$$

Taking the natural log of both sides and rearranging terms, we obtain

$$\frac{-1}{\sigma_0^2}\sum_{m=1}^{d-i}\int_{t-T}^{t}\left(y_m(\tau)s_0(\tau)-y_m(\tau)s_1(\tau)\right)d\tau + \frac{-1}{\sigma_0^2+\sigma_j^2}\sum_{m=d-i+1}^{d}\int_{t-T}^{t}\left(y_m(\tau)s_0(\tau)-y_m(\tau)s_1(\tau)\right)d\tau \underset{s_0}{\overset{s_1}{\gtrless}} \frac{-1}{2\sigma_0^2}\sum_{m=1}^{d-i}\int_{t-T}^{t}\left(s_0^2(\tau)-s_1^2(\tau)\right)d\tau + \frac{-1}{2\left(\sigma_0^2+\sigma_j^2\right)}\sum_{m=d-i+1}^{d}\int_{t-T}^{t}\left(s_0^2(\tau)-s_1^2(\tau)\right)d\tau. \tag{2.29}$$

For BPSK signals, note that $s_0(t) = -s_1(t)$ so

$$s_0^2(t) - s_1^2(t) = 0. \tag{2.30}$$

Substituting (2.30) into (2.29), we get the final form for the log likelihood ratio for a coherent *RAKE* receiver with AWGN and pulse-noise interference:

$$\frac{1}{\sigma_0^2}\sum_{m=1}^{d-i}\int_{t-T}^{t}\left(y_m(\tau)s_0(\tau) - y_m(\tau)s_1(\tau)\right)d\tau + \frac{1}{\sigma_0^2+\sigma_j^2}\sum_{m=d-i+1}^{d}\int_{t-T}^{t}\left(y_m(\tau)s_0(\tau) - y_m(\tau)s_1(\tau)\right)\underset{s_0}{\overset{s_1}{\gtrless}}0. \tag{2.31}$$

An implementation of the maximum-likelihood receiver is shown in Figure 2.6, where $1/\sigma^2$ represents the inverse of the received signal variance, which is equal to $1/\sigma_0^2$ when AWGN is present and $1/\left(\sigma_0^2+\sigma_j^2\right)$

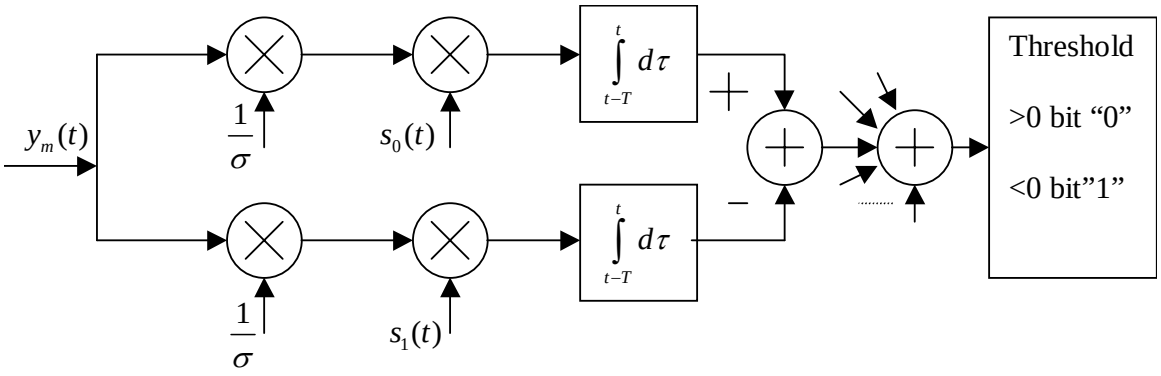

Figure 2.6 Maximum-Likelihood Receiver for Diversity Receptions of Baseband BPSK Signals with Pulse Interference.

when the pulse-noise interference is present. The receiver structure shown in Figure 2.6 can be simplified for BPSK signals. Since $s_0 = -s_1$, the result from correlating with s_0 is the negative of the result from correlating with s_1, which means that only one correlator is necessary. A diagram of the maximum likelihood *RAKE* receiver for AWGN and pulse-noise interference is shown in Figure 2.7, where $1/\sigma^2$ represents the inverse of the variance, equal to $1/\sigma_0^2$ when only AWGN is present and $1/\left(\sigma_0^2+\sigma_j^2\right)$ when the pulse-noise interference is present.

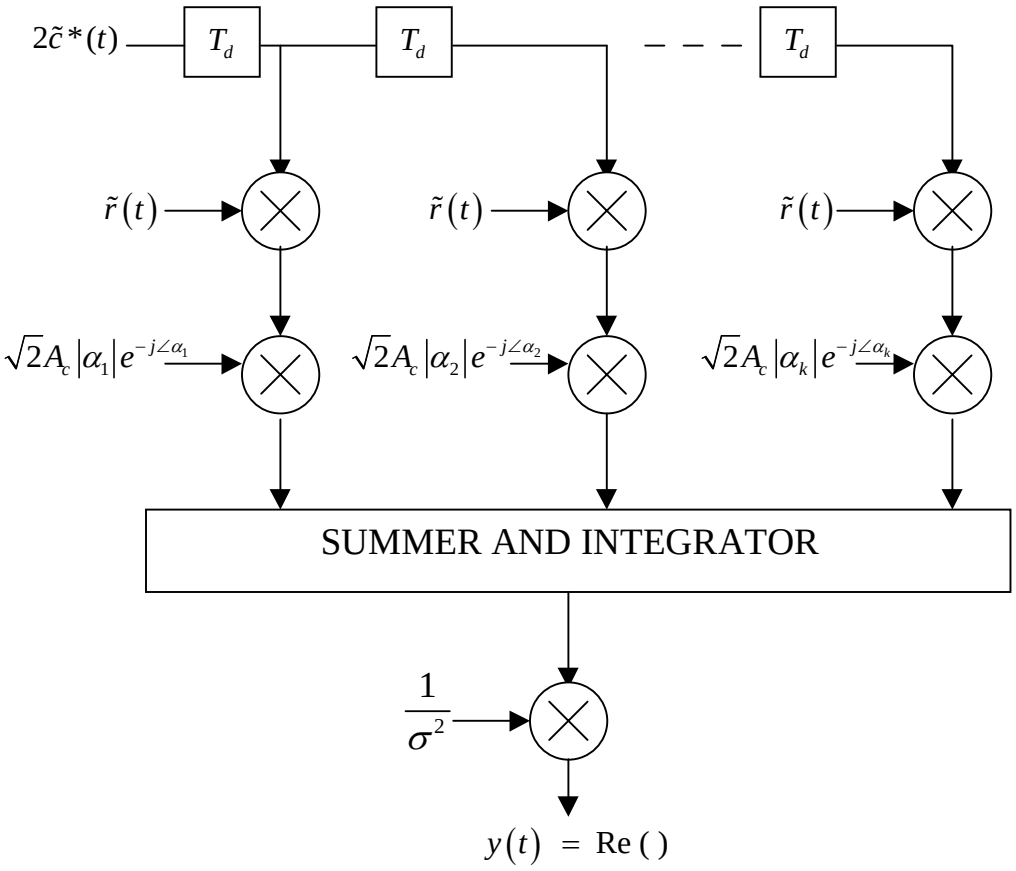

Figure 2.7 Maximum-Likelihood Coherent *RAKE* Receiver for AWGN and Pulse-Noise Interference.

This *RAKE* receiver is similar to the one shown in Figure 2.1, except that the output is multiplied by the inverse of the total variance, not just the inverse of the variance due to AWGN. The multiplication by the inverse of the variance complicates the *RAKE* receiver because the variance must be computed for every bit, which also requires additional circuitry to compute the variance.

G. MEAN AND VARIANCE OF COHERENT *RAKE* RECEIVERS

We stated earlier that pulse-noise interference causes a time-varying variance which we now investigate further. Additionally, we present the method of analysis for coherent *RAKE* receivers with pulse-noise interference and convolutional coding. First, we begin by assuming that the received signal can be modeled as a Gaussian random variable with a conditional mean of $\sqrt{2}A_c|\alpha_k|$, where $|\alpha_k|$ is the random Ricean faded tap

weight, and a variance of σ_r^2. Since $|\alpha_k|$ is modeled as a random variable, we obtain the conditional probability of bit error and then average over the pdf of the random variable $|\alpha_k|$ to get an average probability of bit error. The first mixer in Figure 2.1 multiplies the received signal by the chipping sequence, which removes the spreading but does not change the probability distribution of the received signal. The second mixer in Figure 2.1 multiplies the down-converted received signal by $\sqrt{2}A_c|\alpha_k|e^{-j\angle\alpha_k}$. This scales the signal by $\sqrt{2}A_c|\alpha_k|$ and phase shifts the multipath components by $\angle\alpha_k$ for coherent combining. Hence, the output from the second mixer in Figure 2.1 is a Gaussian random variable with mean $2A_c^2|\alpha_k|^2$ and variance $2\sigma^2A_c^2|\alpha_k|^2$. The coherent *RAKE* receiver in Figure 2.1 then sums together the j fingers. This is the point where pulse interference complicates the analysis. If only AWGN is present, then the mean at the output of the coherent *RAKE* receiver can be written as

$$m = 2A_c^2\sum_{j=1}^{l}|\alpha_k|^2, \tag{2.32}$$

and the variance at the output of the *RAKE* receiver is

$$\sigma_r^2 = 2\sigma^2A_c^2\sum_{j=1}^{l}|\alpha_k|^2, \tag{2.33}$$

where $\sigma^2 = \sigma_0^2$ when only AWGN is present and $\sigma^2 = \sigma_0^2 + \sigma_j^2$ when the pulse-noise interference is present. We require

$$\sum_{k=1}^{l}|\alpha_k|^2 = 1. \tag{2.34}$$

The BPSK bit error rate probability for the *RAKE* receiver is given by

$$P_b\left(\frac{m}{\sigma_r}\right) = \Pr(y>0\,|\,0)\Pr(0) + \Pr(y<0\,|\,1)\Pr(1), \tag{2.35}$$

where *y* is the random variable that represents the *RAKE* output. Due to the symmetry of both the receiver and the noise, when *y* is modeled as a conditional Gaussian random variable, (2.35) can be evaluated to obtain the conditional probability of bit error [17]

$$P_b\left(\frac{m}{\sigma_r}\right) = Q\left(\sqrt{\frac{(m)^2}{\sigma_r^2}}\right). \tag{2.36}$$

Substituting (2.32) and (2.33) into (2.36), we get

$$P_b\left(\frac{m}{\sigma_r}\right) = Q\left(\sqrt{\frac{\left(2A_c^2\sum_{k=1}^{l}|\alpha_k|^2\right)^2}{2A_c^2\sigma^2\sum_{k=1}^{l}|\alpha_k|^2}}\right). \tag{2.37}$$

Equation (2.37) can be simplified to obtain

$$P_b\left(\frac{m}{\sigma_r}\right) = Q\left(\sqrt{\frac{\left(2A_c^2\sum_{j=1}^{l}|\alpha_k|^2\right)}{\sigma^2}}\right). \tag{2.38}$$

By defining

$$\gamma_b = \frac{A_c^2\sum_{j=1}^{l}|\alpha_k|^2}{\sigma^2}, \tag{2.39}$$

the probability of bit error conditioned on γ_b can be written

$$P_b(\gamma_b) = Q\left(\sqrt{2\gamma_b}\right). \tag{2.40}$$

This is equation (14.3-2) on page 817 of [9], which shows how to remove the dependence on γ_b for the case of Rayleigh distributed fading.

Pulse interference complicates the analysis since the interference can be on for only a fraction of a bit, in which case each finger would have a different variance. In this case (2.33) has to be written as

$$\sigma_r^2 = 2A_c^2\sum_{k=1}^{l}\sigma_k^2|\alpha_k|^2 \tag{2.41}$$

where σ_k^2 is σ_0^2 when only Gaussian noise is present and $\sigma_0^2+\sigma_j^2$ when the pulse-noise interference is present. To prevent this problem, we assume that each bit will either experience interference for the full bit period or no interference. Since we are not consider-

ing cases where a fraction of a bit experiences interference, (2.36) is valid, with the additional consideration that P_b is conditional on whether or not the bit experiences interference.

The analytic approach taken here is to obtain the pdf at the output of each finger of the *RAKE* receiver and convolve them together to get the pdf for the random variable that represents the sum of the *RAKE* finger outputs. We perform the analysis assuming that a bit "0" was transmitted. The probability of bit error is then determined by integrating the pdf of the random variable that represents the output of the *RAKE* receiver from 0 to ∞. The convolutions are performed by taking the two-sided Laplace transform of each finger's pdf, multiplying the resulting Laplace transforms together, and then taking the inverse Laplace transform, which when integrated from 0 to ∞ gives the probability of bit error.

H. ANALYSIS OF A COHERENT *RAKE* RECEIVER WITH PHASE NOISE AND RICEAN FADING

In Figure 2.1 the coherent *RAKE* receiver shown does not include phase noise. We have already seen that phase noise causes a random phase error ϕ between the locally generated chipping sequence and the received signal and that the complex baseband signal is multiplied by $e^{j\phi}$. The received signal shown in Figure 2.8 now includes the AWGN $n(t) = \mathrm{Re}\left[\tilde{n}(t)e^{j\omega t}\right]$ where:

$$\tilde{r}(t) = \tilde{n}(t) + \sum_{i=0}^{l} \sqrt{2} A_c \alpha_i \tilde{c}(t - iT_d) d(t - iT_d) e^{-j\omega i T_d}. \tag{2.42}$$

Recall that multiplying the received signal by a chipping sequence does not affect the Gaussian noise, so at the output of the first mixer we get

$$\tilde{y}_1(t) = \tilde{n}(t) + 2\sqrt{2} A_c \sum_{i=0}^{l} |\alpha_i| \tilde{c}^*(t - kT_d) \tilde{c}(t - iT_d) d(t - iT_d) e^{-j(i\omega T_d - \angle\alpha_k)} e^{-j(\omega k T_d - \phi)}. \tag{2.43}$$

which then is multiplied by the channel tap weight $\sqrt{2} A_c |\alpha_k| e^{j(\phi + \angle\alpha_k)}$, summed with the output of the other fingers, and integrated. The real baseband output is then found by taking the real part of the integrator output

$$y(t) = 2A_c^2 \cos(2\phi)\, d(t) \sum_{j=1}^{k} |\alpha_j|^2 + n(t). \tag{2.44}$$

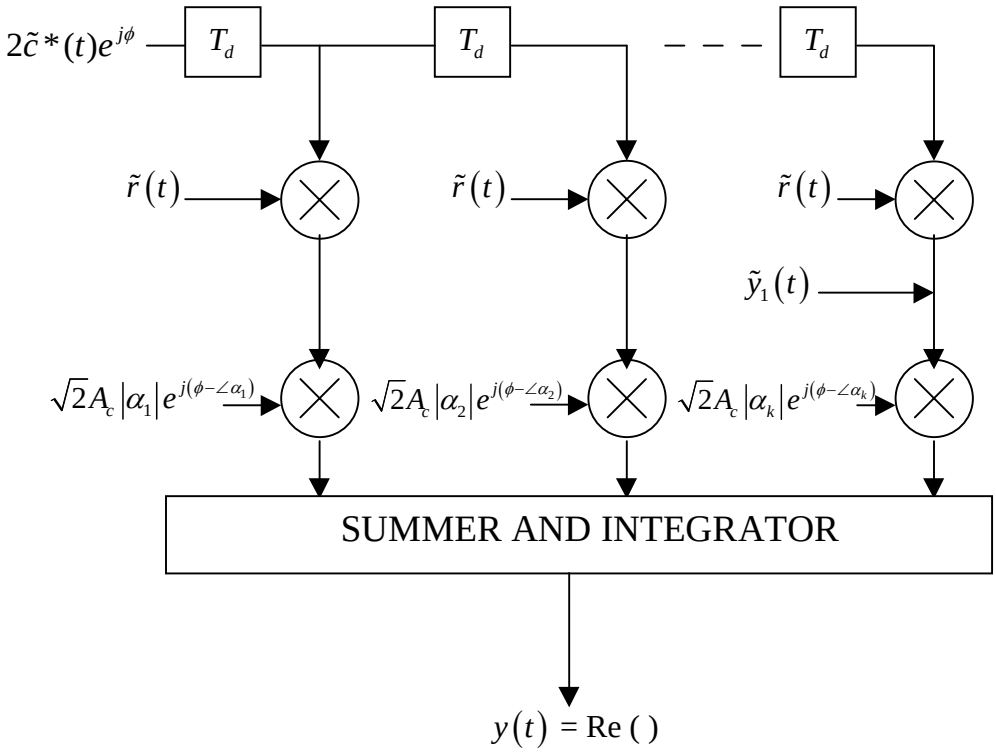

Figure 2.8 Coherent *RAKE* Receiver with Phase Noise.

Since $|\alpha_k|$ is Ricean distributed, then the multiplication by the Ricean faded tap weight estimate produces an output at the k^{th} finger proportional to $\gamma_k = |\alpha_k|^2$, which has a non-central chi-squared distribution [17]

$$f_{\Gamma_k}(\gamma_k) = \begin{cases} \frac{1}{2\sigma_k^2}\exp\left[-\left(\frac{\gamma_k}{2\sigma_k^2}+K\right)\right] I_0\left(\sqrt{\frac{2K\gamma_k}{\sigma_k^2}}\right) & \gamma_k \geq 0 \\ 0 & \gamma_k < 0. \end{cases} \tag{2.45}$$

The ratio of direct-to-diffuse power is K and the diffuse power is $2\sigma_k^2$. The two-sided Laplace transform for a Gaussian random variable with a mean of m and a variance σ^2 is equal to [3]

$$\Phi(s) = \exp\left(sm + \frac{1}{2}s^2\sigma^2\right). \tag{2.46}$$

Equation (2.44) is the output for the summation of all the *RAKE* finger outputs. The mean value at the output of the k^{th} finger is

$$m = 2A_c^2 \cos(2\phi)\gamma_k, \tag{2.47}$$

and the variance is

$$\sigma_r^2 = 2A_c^2 \cos(2\phi)\gamma_k \sigma^2, \tag{2.48}$$

where $\sigma^2 = \sigma_0^2$ when only AWGN is present and $\sigma^2 = \sigma_0^2 + \sigma_j^2$ when the pulse interference is present. From (2.47) and (2.48) we see that both the mean and the variance at the k^{th} finger output are dependent on the noncentral chi-squared distributed γ_k as well as the Tikonov distributed ϕ. Substituting (2.47) and (2.48) into (2.46), we get

$$\Phi_k(s \mid \gamma_k, \phi) = \exp\left[-2A_c^2\gamma_k \cos(2\phi)\left(s - \frac{s^2\sigma^2}{2}\right)\right]. \tag{2.49}$$

We now remove the dependence on γ_k by integrating over the chi-squared distribution function. We rewrite (2.49) as

$$\Phi_k(s \mid \gamma_k, \phi) = \exp[-\beta\gamma_k], \tag{2.50}$$

where

$$\beta = 2A_c^2 \cos(2\phi)\left(s - \frac{s^2\sigma^2}{2}\right). \tag{2.51}$$

Using (2.45) and (2.50), we obtain

$$\Phi_k(s \mid \phi) = \int_0^\infty \exp(-\beta\gamma_k)\frac{1}{2\sigma_k^2}\exp\left[-\left(\frac{\gamma_k}{2\sigma_k^2} + K\right)\right] I_0\left(\sqrt{\frac{2K\gamma_k}{\sigma_k^2}}\right) d\gamma_k, \tag{2.52}$$

which can be written

$$\Phi_k(s \mid \phi) = \exp(-K)\int_0^\infty \frac{1}{2\sigma_k^2}\exp\left[-\left(\beta\gamma_k + \frac{\gamma_k}{2\sigma_k^2}\right)\right] I_0\left(\sqrt{\frac{2K\gamma_k}{\sigma_k^2}}\right) d\gamma_k. \tag{2.53}$$

Equation (2.53) can be evaluated using the identity (6.643.4) from [18]

$$\int_0^\infty x^{n+\frac{1}{2}v} e^{-\alpha x} J_v\left(2\beta\sqrt{x}\right) dx = n!\beta^v e^{-\frac{\beta^2}{\alpha}} \alpha^{-n-v-1} L_n^v\left(\frac{\beta^2}{\alpha}\right), \tag{2.54}$$

where $L_n^v(x)$ is the Lagerre polynomial. The Bessel function of the first kind and order zero J_0 is related to the modified Bessel function of the first kind and order zero I_0 by $I_0(x) = J_0(jx)$ [18] where $j = \sqrt{-1}$. From (2.53) we see that $n = v = 0$, hence we can use the relationship [18]

$$L_0^0(x) = 1. \tag{2.55}$$

Therefore, we obtain the Laplace transform of the pdf at the output of the k^{th} finger as

$$\Phi_k(s \mid \phi) = \frac{1}{2\sigma_k^2 \beta + 1} \exp\left(\frac{-2K\beta\sigma_k^2}{2\beta\sigma_k^2 + 1}\right), \tag{2.56}$$

where β is defined in (2.51) and $2\sigma_k^2$ is the diffuse power in each finger. The *RAKE* receiver adds the outputs of the fingers together, so the Laplace transform of the pdf of the random variable that represents the output of the *RAKE* receiver can be written

$$\Phi(s \mid \phi) = \prod_{k=1}^{l} \left[\Phi_k(s \mid \phi)\right]. \tag{2.57}$$

To remove the dependence on ϕ we must still average over the pdf of ϕ:

$$\Phi(s) = \int \Phi(s \mid \phi) f_\Phi(\phi)\, d\phi. \tag{2.58}$$

Equation (2.58) must be evaluated numerically.

The probability of bit error is the integral from 0 to ∞ of the inverse Laplace transform of $\Phi(s)$. The inverse Laplace transform and the subsequent integration can be done recursively using the Gauss-Chebyshev quadrature method. Defining *Y* as the random variable at the output of the *RAKE* receiver with a pdf given by the inverse Laplace transform of $\Phi(s)$ we have [3]

$$P(Y > 0) = \frac{1}{n} \sum_{k=1}^{n/2} \mathrm{Re}\left[\Phi(s = c + jc\tau_k)\right] + \tau_k \,\mathrm{Im}\left[\Phi(s = c + jc\tau_k)\right] + E, \tag{2.59}$$

where

$$\tau_k = \tan\left[(2k-1)\pi / 2n\right], \tag{2.60}$$

c is a constant chosen to make the algorithm converge quickly and E is an error term that approaches 0 as n gets large. Extremely low bit error rates require larger values of

n. Values of n between 200 and 800 were used. Methods for choosing the parameter c are discussed in [19], and examples of MATLAB code to implement (2.59) are given in Appendix A.

1. Addition of Pulse Interference

The preceding analysis does not include the effect of pulse-noise interference, but it can be easily modified to do so. It is assumed that the variance of the received noise is σ_0^2 when only AWGN is present and $\sigma_0^2 + \sigma_j^2$ when the pulse interference is present. The only term in the preceding analysis that depends on the variance of the received signal is β. We now define

$$\delta_1 = 2A_c^2 \cos(2\phi)\left(s - \frac{s^2\sigma_0^2}{2}\right), \tag{2.61}$$

and

$$\delta_2 = 2A_c^2 \cos(2\phi)\left(s - \frac{s^2\left(\sigma_0^2 + \sigma_j^2\right)}{2}\right). \tag{2.62}$$

When the received signal has only AWGN, we simply substitute $\beta = \delta_1$ into (2.56) and when the interference signal is present we substitute $\beta = \delta_2$ into (2.56), leading to

$$\Phi(s \mid \phi) = \left(\prod_{i=1}^{l} \Phi(s \mid \phi, \beta = \delta_1)\right), \tag{2.63}$$

when only AWGN is present and

$$\Phi(s \mid \phi) = \left(\prod_{i=1}^{l} \Phi(s \mid \phi, \beta = \delta_2)\right) \tag{2.64}$$

when all the fingers experience interference. It should be mentioned that (2.63) and (2.64) are conditional on ϕ and must be numerically integrated over the Tikonov pdf to remove the conditioning on ϕ as shown in (2.58).

2. Maximum-Likelihood *RAKE* Receiver for AWGN and Pulse-Noise Interference

The maximum-likelihood *RAKE* receiver for AWGN and pulse-noise interference shown in Figure 2.7 has an additional mixer that multiplies the received signal by the in-

verse of the variance. Since it is assumed that the bit either completely experiences interference or no interference, this receiver multiplies the received signal by $1/\sigma_0^2$ when only AWGN is present and by $1/\left(\sigma_0^2+\sigma_j^2\right)$ when the pulse-noise interference is present. Multiplying by the inverse of the variance affects both the mean and the variance of the signal at the output of the *RAKE* finger. In this case, the mean is given by (2.47) divided by σ^2

$$\overline{m_{ml}} = \frac{2A_c^2}{\sigma^2}\cos\left(2\phi\right)\gamma_k \tag{2.65}$$

and the variance is given by (2.48) divided by σ^4

$$\sigma_{ml}^2 = \overline{m_{ml}}, \tag{2.66}$$

where σ^2 is σ_0^2 when only Gaussian noise is present and $\sigma_0^2+\sigma_j^2$ when the pulse-noise interference is present. The variance of a *RAKE* receiver designed for AWGN channels is proportional to the variance of the received signal as shown in (2.48). For the maximum-likelihood *RAKE* receiver designed for AWGN and pulse-noise interference, both the mean and variance are proportional to the inverse of the variance. This means that a high powered interference signal will tend to drive the *RAKE* receiver output toward zero, as opposed to the *RAKE* receiver designed only for AWGN where a high powered interference signal will drive the output towards infinity. The analysis for this maximum-likelihood *RAKE* receiver is the same as the previous analysis except that in this case

$$\delta_3 = \frac{2A_c^2}{\sigma_0^2}\cos\left(2\phi\right)\left(1-\frac{s\sigma_0^2}{2}\right)s \tag{2.67}$$

when only AWGN is present and

$$\delta_4 = \frac{2A_c^2}{\left(\sigma_0^2+\sigma_j^2\right)}\cos\left(2\phi\right)\left(1-\frac{s\left(\sigma_0^2+\sigma_j^2\right)}{2}\right)s \tag{2.68}$$

when the interference signal is present. Once again we get

$$\Phi\left(s\,|\,\phi,\beta=\delta_3\right) = \left(\prod_{i=1}^{l}\Phi_i\left(s\,|\,\phi,\beta=\delta_3\right)\right) \tag{2.69}$$

when only AWGN is present and

$$\Phi\left(s \mid \phi, \beta = \delta_4\right) = \left(\prod_{i=1}^{l} \Phi_i\left(s \mid \phi, \beta = \delta_4\right) \right) \tag{2.70}$$

when all the fingers experience interference. The result is numerically integrated over the Tikonov pdf to remove the dependence on ϕ as shown in (2.58).

3. Hard Decision Decoding

The previous analysis computed the uncoded bit error rate. Commercial wireless standards such as IS95 use a convolutional code to improve the bit error ratio. In this section we analyze the performance of a convolutionally encoded signal transmitted over a Ricean distributed, frequency-selective fading channel with pulse-noise interference and hard decision Viterbi decoding.

The probability of bit error P_b is upper bounded by [9]

$$P_b < \sum_{d=d_{free}}^{\infty} B_d P_d, \tag{2.71}$$

where B_d is the total number of nonzero information bits in all weight d paths, P_d is the probability of selecting a code sequence that is a Hamming distance d away from the correct code sequence, and d_{free} is the minimum weight path in the convolutional code state diagram that diverges from and remerges with the all-zero state [20]. For hard decision Viterbi decoding, P_d is given by [9]

$$P_d = \sum_{i=\frac{d+1}{2}}^{d} \binom{d}{i} \cdot p^i \cdot (1-p)^{d-i} \tag{2.72}$$

when d is odd and

$$P_d = \frac{1}{2} \cdot \binom{d}{\frac{d}{2}} \cdot p^{\frac{d}{2}} \cdot (1-p)^{\frac{d}{2}} + \sum_{i=\frac{d}{2}+1}^{d} \binom{d}{i} \cdot p^i \cdot (1-p)^{d-i} \tag{2.73}$$

when d is even. In (2.72) and (2.73), to calculate p we must integrate

$$\Phi\left(s \mid \phi\right) = \rho\left(\Phi_i\left(s \mid \phi, \beta = \delta_1\right)\right) + \left(1-\rho\right)\left(\Phi_i\left(s \mid \phi, \beta = \delta_2\right)\right) \tag{2.74}$$

over the Tikonov pdf, numerically invert the Laplace transform, and integrate the result from 0 to ∞. In (2.74) ρ is the duty cycle of the interference, δ_1 is defined in (2.61) and δ_2 is defined in (2.62). Figure 2.9 shows the probability of bit error for a three finger *RAKE* receiver with rate ½, constraint length 9 convolutional coding and hard hard decision Viterbi decoding where $E_b/N_0 = 15\,\text{dB}$, the pilot tone has a 20-dB loop SNR, the ratio of direct-to-diffuse power is 10 dB, and the interference signal has a one percent duty cycle ($\rho = 0.01$), a 10% duty cycle ($\rho = 0.1$), and a 100% duty cycle ($\rho = 1$). For a

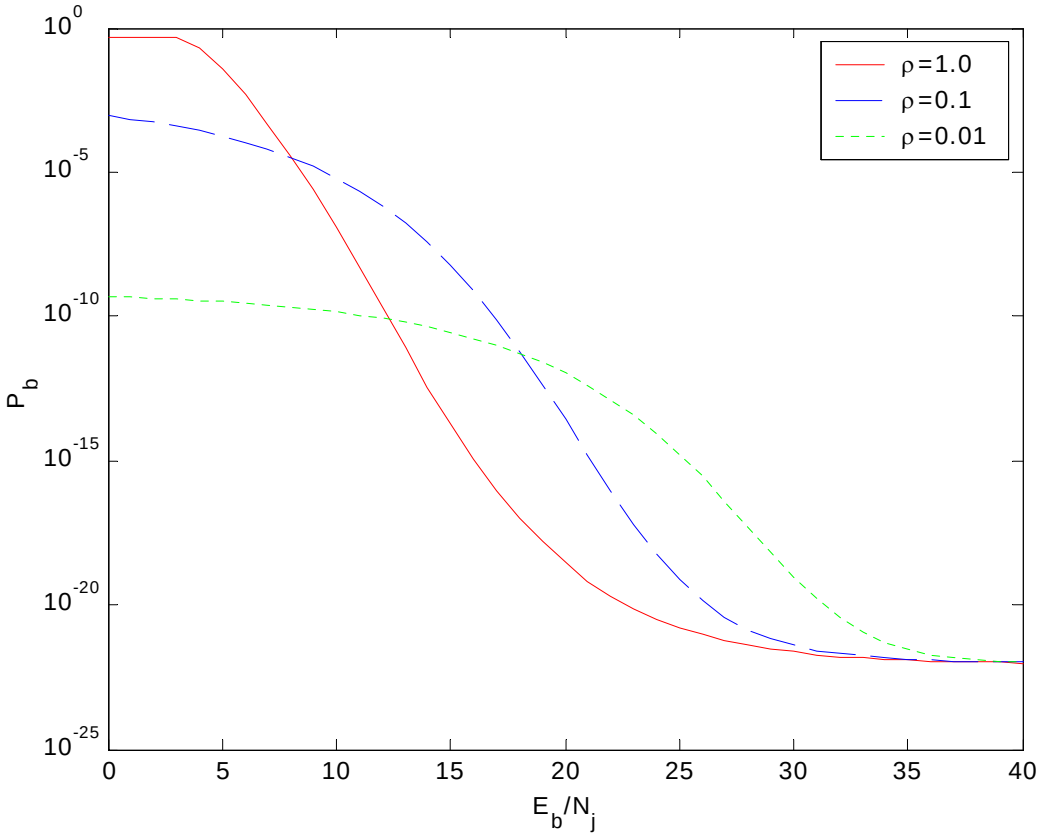

Figure 2.9 Coherent *RAKE* Receiver with Hard Decision Viterbi Decoding.

rate ½, constraint length 9 convolutional code the first nonzero three terms of the series in (2.71) are $33P_{12} + 281P_{14} + 2179P_{16}$. An exponential multipath intensity profile (MIP) is assumed where each finger has 10 dB less signal energy than the previous finger. We see from Figure 2.9, that the interference should be on all the time if it has approximately the

same power as the received signal when hard decision Viterbi decoding is used. When the interference has less power than the received signal, then pulsing the interference signal is the best strategy. It is interesting to note that the error rate is extremely low for all values of E_b/N_j when the interference duty cycle is 0.01. We will show that pulsing the interference signal is much more effective against soft decision Viterbi decoding.

For the case of the maximum-likelihood *RAKE* receiver designed for AWGN and pulse-noise interference, the probability of making an error *p* can be calculated by integrating

$$\Phi(s\,|\,\phi) = \rho\left(\Phi(s\,|\,\phi, \delta = \delta_3)\right) + (1-\rho)\left(\Phi(s\,|\,\phi, \delta = \delta_4)\right) \tag{2.75}$$

over the Tikonov pdf as shown in (2.58), numerically inverting the Laplace transform and integrating the result from 0 to ∞. The results for hard decision Viterbi decoding using the maximum-likelihood *RAKE* receiver designed for AWGN and pulse-noise interference were the same as the *RAKE* receiver designed for AWGN. This can be explained by noting that, for the *RAKE* receiver designed for AWGN, the interference signal causes the variance of the received signal to be very large when the interference signal is on, which in turn can lead to a 50 percent error rate. The maximum-likelihood *RAKE* receiver designed for AWGN and pulse-noise interference causes the mean and variance to tend towards zero when the interference signal is present. Since hard decision Viterbi decoding makes decisions on a bit-by-bit basis, a received signal with a mean and variance of zero will cause a 50 percent error rate. Hence, we should not expect any improvement from the maximum-likelihood *RAKE* receiver designed for AWGN and pulse-noise interference when hard decision Viterbi decoding is used.

4. Soft Decision Viterbi Decoding

For soft decision Viterbi decoding, P_d can be written as [9]

$$P_d = \sum_{i=0}^{d} \binom{d}{i} \rho^i (1-\rho)^{d-i} P_d(i), \tag{2.76}$$

where ρ is the duty cycle of the pulse-noise interference, and $P_d(i)$ is the probability of selecting a code word a Hamming distance *d* from the correct code word, given that *i* of the *d* receptions experience interference. To calculate $P_d(i)$ we must integrate

$$\Phi(s\,|\,\phi)=\left(\prod_{k=1}^{l}\Phi_k(s\,|\,\phi,\beta=\delta_1)\right)^{i}\times\left(\prod_{k=1}^{l}\Phi_k(s\,|\,\phi,\beta=\delta_2)\right)^{d-i} \tag{2.77}$$

over the Tikonov pdf to eliminate the dependence on ϕ as shown in (2.58), numerically invert the Laplace transform, and integrate the result from 0 to ∞. As can be seen from (2.77), this must be done $d+l$ times. We will use the same rate ½, constraint length 9 convolutional code where the first three terms of (2.71) are $33P_{12}+281P_{14}+2179P_{16}$, which are sufficient to calculate the probability of bit error. Even though the B_d terms are increasing, the P_d terms in (2.71) go to zero much faster. An exponential MIP is assumed where each finger has 10 dB less signal energy than the previous finger. Figure 2.10 shows results obtained for a three finger *RAKE* with soft decision Viterbi decoding where $E_b/N_0=15\,\text{dB}$, the pilot tone has a 20-dB loop SNR, a ratio of direct-to-diffuse power of 10 dB, and a interference signal that has a one percent duty cycle ($\rho=0.01$), a ten percent duty cycle ($\rho=0.1$), and a 100 percent duty cycle ($\rho=1$). The case where the interference signal is on all the time was also simulated for low values of E_b/N_j since the union bound given by (2.71) is know to be loose for low SNR. Recall that the signal input to the *RAKE* receiver is assumed to be a Gaussian random variable with a Ricean distributed mean. Multiplication by a Ricean distributed tap weight estimate produces a noncentral chi-squared mean value [21]. The Matlab statistics toolbox has a noncentral chi-squared random variable generator. These samples must be multiplied by $\cos(2\phi)$ where ϕ is a Tikonov distributed random variable. A Tikonov random variable generator was developed specially for this simulation. The mean value is then multiplied by -1 to simulate all-zeros being transmitted. This eliminates the need to convolutionally encode the data since an all zero file input to a convolutional encoder will produce an all-zero output file. The variance of the received Gaussian random variable is $\sigma_0^2+\sigma_j^2$. Since the mean and variance are known, the received Gaussian random variable can now be simulated using the Matlab *randn* command. Each finger was simulated separately and summed together. The resultant signal was then quantized and convolutionally decoded using the Matlab communications toolbox. Any data bit ones at the decoder output represent a bit

error, so the bit error rate was computed by summing the values in the convolutional decoder output file and then dividing by the total number of bits simulated. Monte-Carlo simulations were conducted for each point where an asterisk is shown in Figure 2.10. A line between simulated values has been added to help the eye follow the progression between simulated points. Since the error rate varied slightly between simulations, three simulation were run at each point, and the median value was plotted in Figure 2.10. Due to the computational complexity, only error rates with analytical values above 10^{-5} were simulated. These simulation results are found to be within 1 dB of the analytical results, which shows that using only the first three terms of the union bound provides an accurate estimate of the system performance.

We see that for soft decision Viterbi decoding, pulsing the interference signal degrades the performance much more than it does for hard decision Viterbi decoding. Soft decision Viterbi decoding uses soft decision receiver outputs with confidence estimates and, if any incorrect decisions have a large confidence value, then soft decision decoder performance significantly degrades. Essentially, the soft decision Viterbi decoding algorithm attempts to combine several soft decision outputs together in order to decode the received data. The maximum-likelihood receiver weights the soft decision outputs by the inverse of the variance, which we derived in Section F, to avoid placing high confidence values on bits with interference. Unfortunately, conventional *RAKE* receivers do not perform this function. By modeling the soft decision receiver output as a Gaussian random variable and noting that the sum of independent Gaussian random variables is a Gaussian random variable where the mean is the sum of the means and the variance is the sum of the variances [15], it is easy to see that any bits that experience interference will dramatically increase the bit error ratio unless the signal power is greater than the interference power.

For the case of the maximum-likelihood *RAKE* receiver designed for AWGN and pulse-noise interference, the mean and variance of the signal on each *RAKE* finger both approach zero when a large interference signal is present. This means that soft decision Viterbi decoding will perform much better in the presence of pulse-noise interference

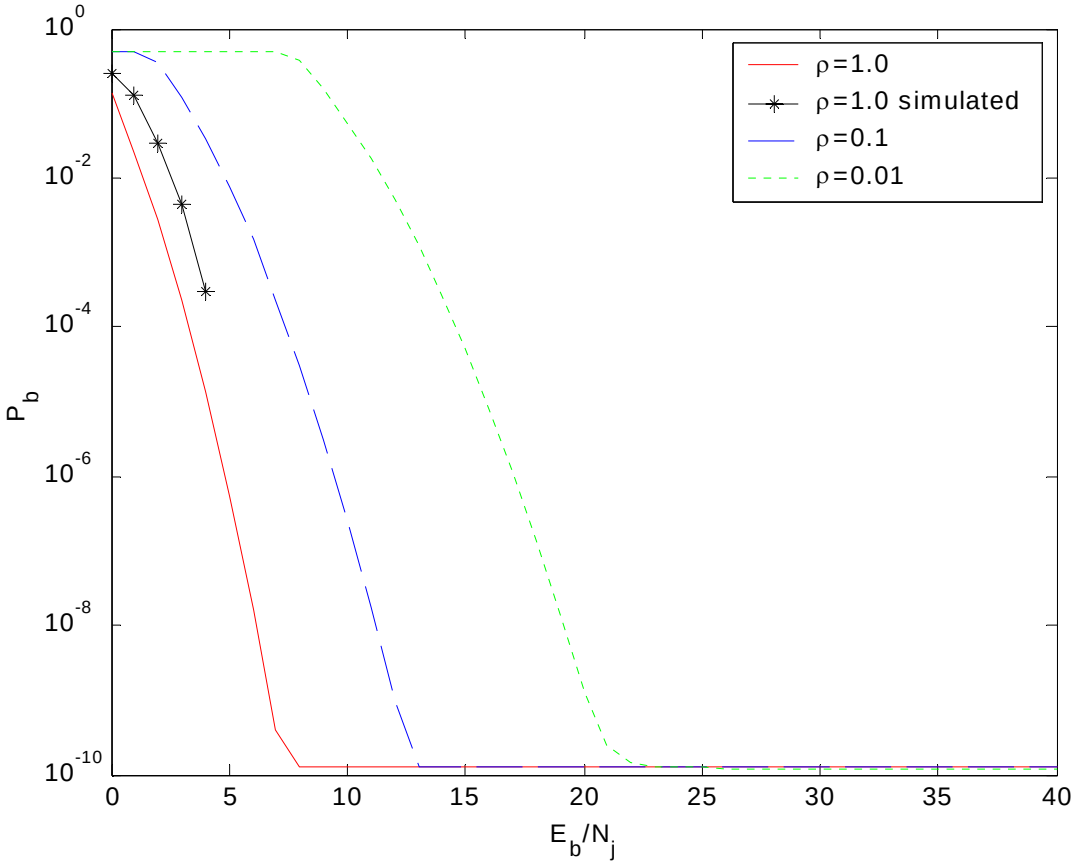

Figure 2.10 Coherent *RAKE* Receiver with Soft Decision Viterbi Decoding.

since this *RAKE* receiver does not allow the bits with interference to dominate the decoding decision. Results for a three-finger maximum-likelihood *RAKE* receiver designed for AWGN and pulse-noise interference with soft decision Viterbi decoding where $E_b/N_0 = 15\,\text{dB}$, the pilot tone has a 20-dB loop SNR, a ratio of direct-to-diffuse power of 10 dB, and a interference signal with a one percent duty cycle $(\rho = 0.01)$, a ten percent duty cycle $(\rho = 0.1)$ and a 100 percent duty cycle $(\rho = 1.0)$ are shown in Figure 2.11. As expected, Figure 2.11 shows that the maximum-likelihood *RAKE* receiver designed for AWGN and pulse-noise interference mitigates the effect of pulse-noise interference.

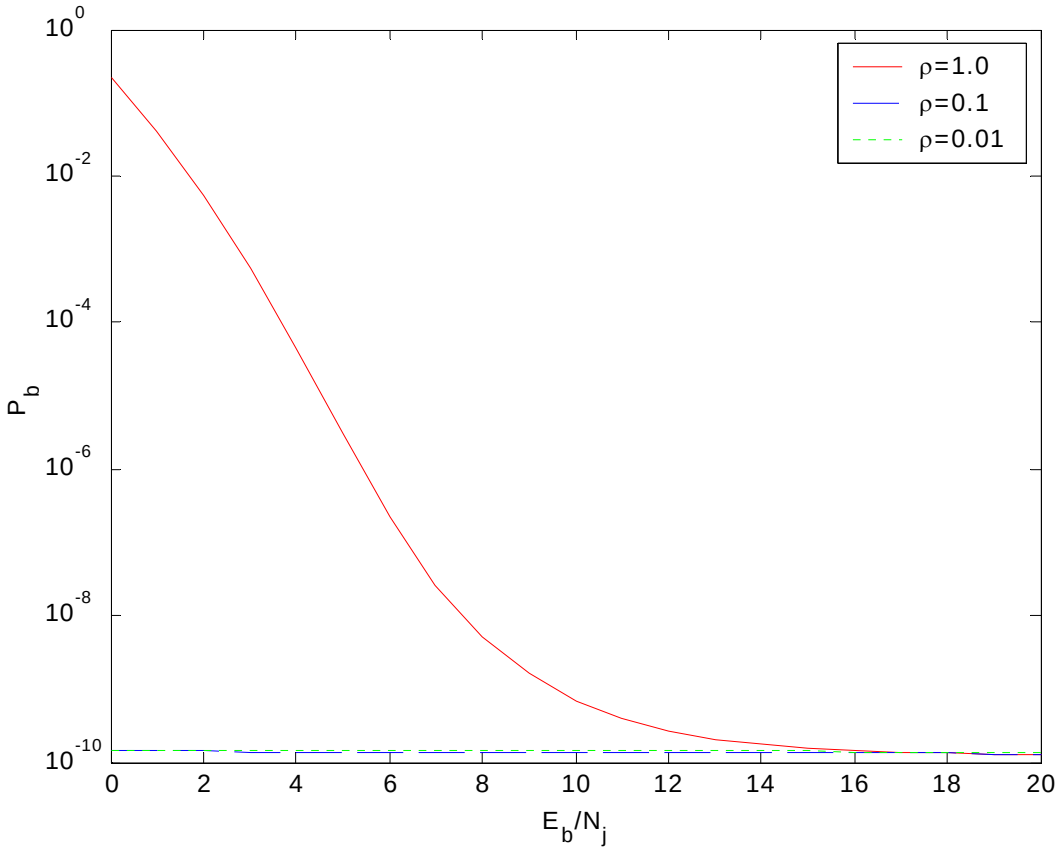

Figure 2.11 Maximum-Likelihood *RAKE* Receiver for AWGN and Pulse-Noise Interference with Soft decision Viterbi decoding.

When the interference signal is on all the time, the performance of the maximum-likelihood *RAKE* receiver designed for AWGN and pulse-noise interference is the same as the conventional *RAKE* receiver.

5. Optimal Finger Spacing

Since we assumed an exponential multipath intensity profile where the SNR for each finger was 10 dB below the previous finger, it may be possible to obtain better performance by trying to reduce the difference in the signal power on each finger. Diversity performance improves when we decrease the finger spacing to reduce the difference in finger SNR; however, if we limit the *RAKE* to three fingers then the total received power decreases as we decrease the finger spacing. In Figure 2.12 we show an example of the multipath intensity profile as a function of delay with two different possible *RAKE* finger spacing. In the one case the first finger collects 90 percent of the received power, the sec-

ond nine percent, and the third 0.9 percent; while in the other case, the first finger collects 53.54 percent of the received power, the second collects 24.87 percent, and the third finger collects 11.56 percent. The second case provides better diversity performance since the received power on the three fingers are closer together, but it only collects about 90 percent of the received signal power as opposed to the first case which collects 99.9 percent of the received signal power.

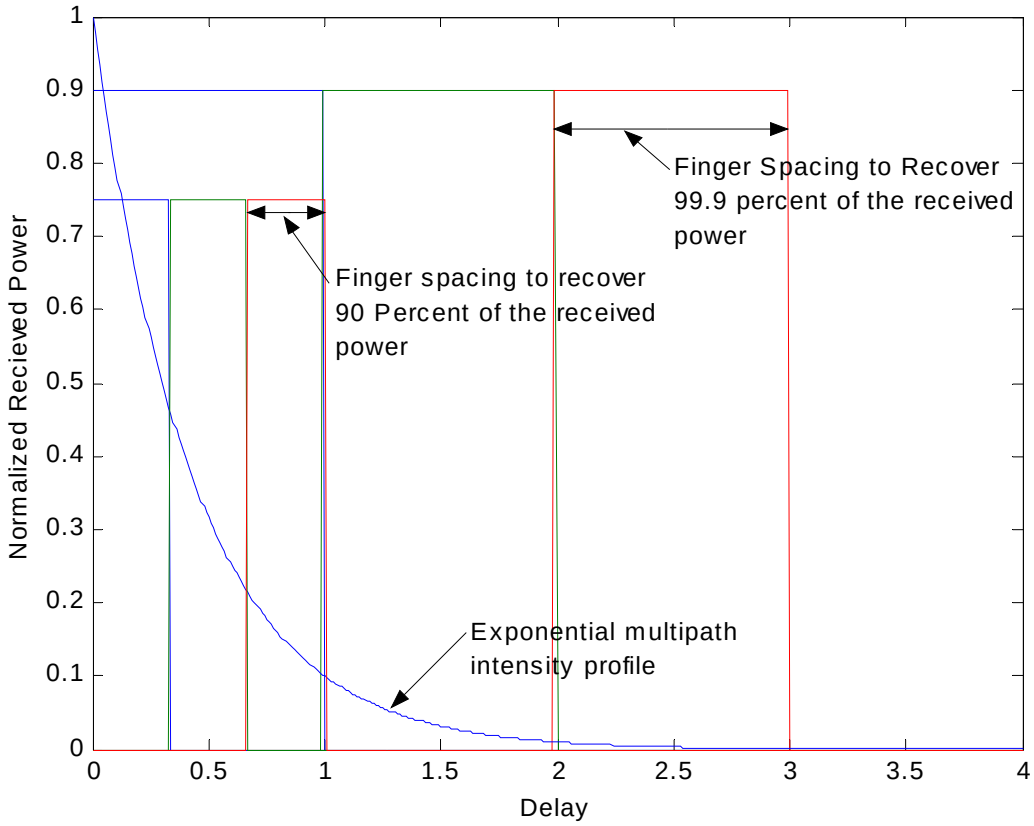

Figure 2.12 Multipath Intensity Profile with two Different *RAKE* Finger Spacings.

In order to find the optimal tradeoff between losing received signal power and getting better performance, we used hard decision Viterbi decoding and started with a *RAKE* receiver that recovered 99.9 percent of the received signal power and compared the results with a *RAKE* receiver that recovered one percent less power. We continued reducing the received signal power by one percent until the probability of bit error started to increase.

We found that, for a three finger *RAKE*, recovering 92 percent of the received signal power produces the lowest probability of bit error. In Figure 2.13 we show the results for a *RAKE* receiver that recovers 99.9 percent of the received power and a *RAKE* receiver that recovers 92 percent of the received power for hard decision Viterbi decoding where $E_b/N_0 = 15\,\text{dB}$, the pilot tone has a 20-dB loop SNR, a ratio of direct-to-diffuse power of

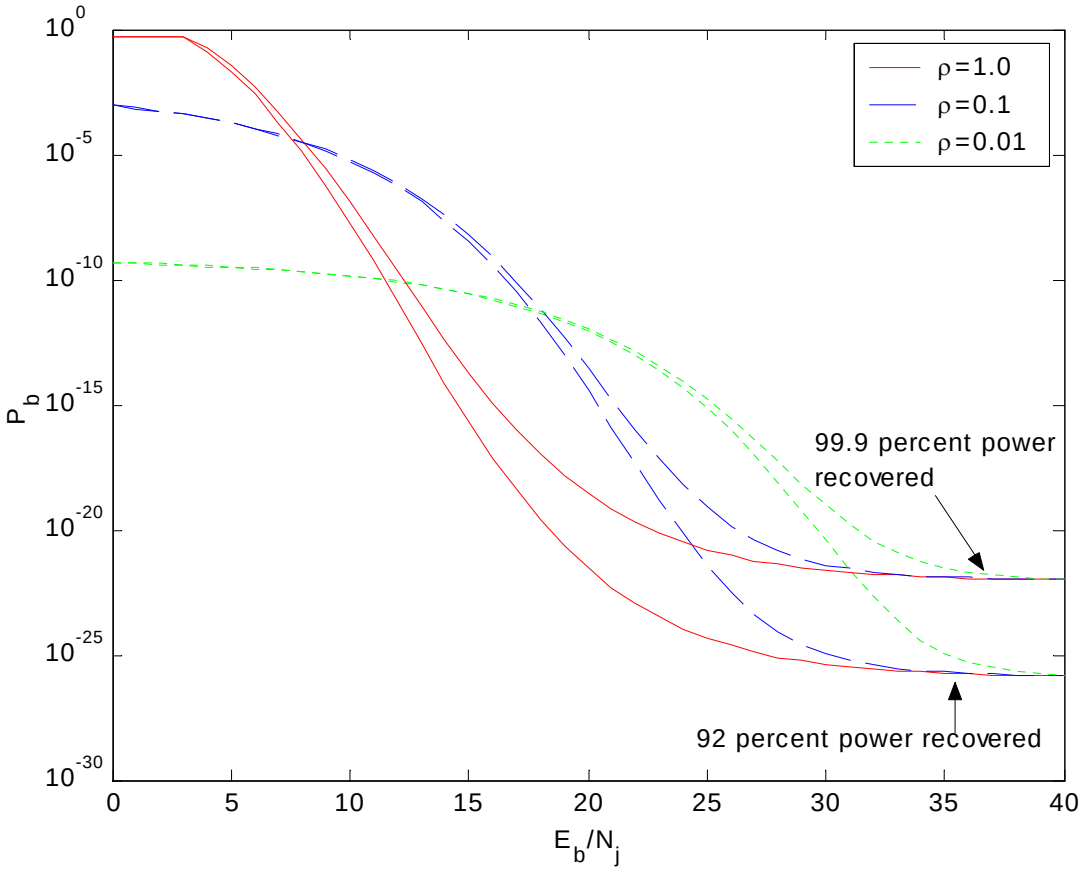

Figure 2.13 Two Different Finger Spacings with Hard Decision Viterbi Decoding.

10 dB, a interference signal that has a one percent duty cycle $(\rho = 0.01)$, ten percent duty cycle $(\rho = 0.1)$, and a 100 percent duty cycle $(\rho = 1.0)$. We see that for this E_b/N_0 there is very little improvement at low values of E_b/N_j, and the improvement at high values of E_b/N_j will probably not be noticed in a practical system. The hard decision

results, however, show that recovering 92 percent of the received power produces the lowest probability of bit error for large E_b/N_j.

Since the maximum-likelihood *RAKE* receiver for AWGN and pulse-noise interference with soft decision Viterbi decoding reduces the probability of bit error for pulse-noise interference down to the irreducible error floor caused by phase noise, we compare the performance of a finger spacing that recovers 99.9 percent of the received power against a finger spacing that recovers 92 percent of the received power with a interference signal that is on all the time. We make the same assumptions that we did for hard decision Viterbi decoding; however, with soft decision Viterbi decoding the error rate slightly increases when only 92% of the received power is recovered as shown in Figure 2.14.

It seems that when pulse-noise interference is present, performance with both hard and soft decision Viterbi decoding does not improve much when the *RAKE* finger spacing is decreased to provide better diversity performance. In fact, the soft decision performance was slightly worse. These results were obtained with $E_b/N_0 = 15\,\text{dB}$. The results might be different for larger or smaller E_b/N_0; however, based on the results obtained, we can conclude that it is not worth the extra system complexity to constantly measure the multipath intensity profile and adjust the finger spacing for large E_b/N_j.

6. Increased Phase Noise

The previous results have all been for a loop SNR of 15 dB. For a first order phase-locked loop, the loop SNR can be written

$$\text{Loop}_{\text{SNR}} = \frac{E_p}{\sigma^2 B_L}, \tag{2.78}$$

where E_p is the energy of the pilot tone, σ^2 is the loop noise power, which includes both thermal noise and interference noise, and B_L is the loop bandwidth. Decreasing the en-

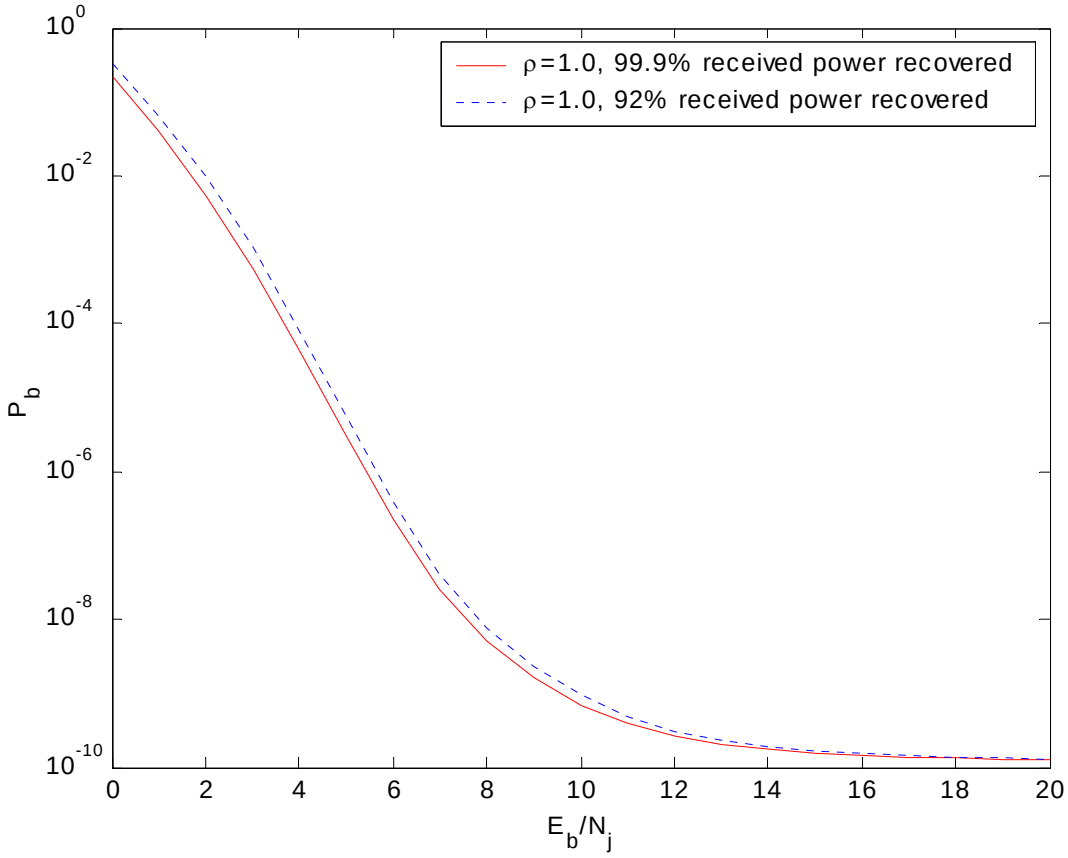

Figure 2.14 Two Different Finger Spacings with Soft Decision Viterbi Decoding.

ergy of the pilot tone or increasing either the loop bandwidth or noise power will decrease Loop_{SNR}. Figure 2.15 shows the significant error rate increase for a maximum-likelihood *RAKE* receiver designed for AWGN and pulse-noise interference with soft decision Viterbi decoding with a loop SNR of 10 dB, 15 dB and 20 dB when $E_b/N_0 = 15\,\text{dB}$, the ratio of direct-to-diffuse power is 10 dB, and the interference signal has a ten percent duty cycle. Monte-Carlo simulations performed using MATLAB show the error rate is 0.5 for a loop SNR of 10 dB, and is almost 10^{-2} at 15-dB loop SNR. Phase noise causes an irreducible error floor and problems with the union bound since $P_{12} \approx P_{14} \approx P_{16}$. The simulation results with 10-dB and 15-dB loop SNR have lower error rates than the results obtained analytically since the union bound used to obtain analytic results is very loose when phase noise dominates system performance. Still, the simulated

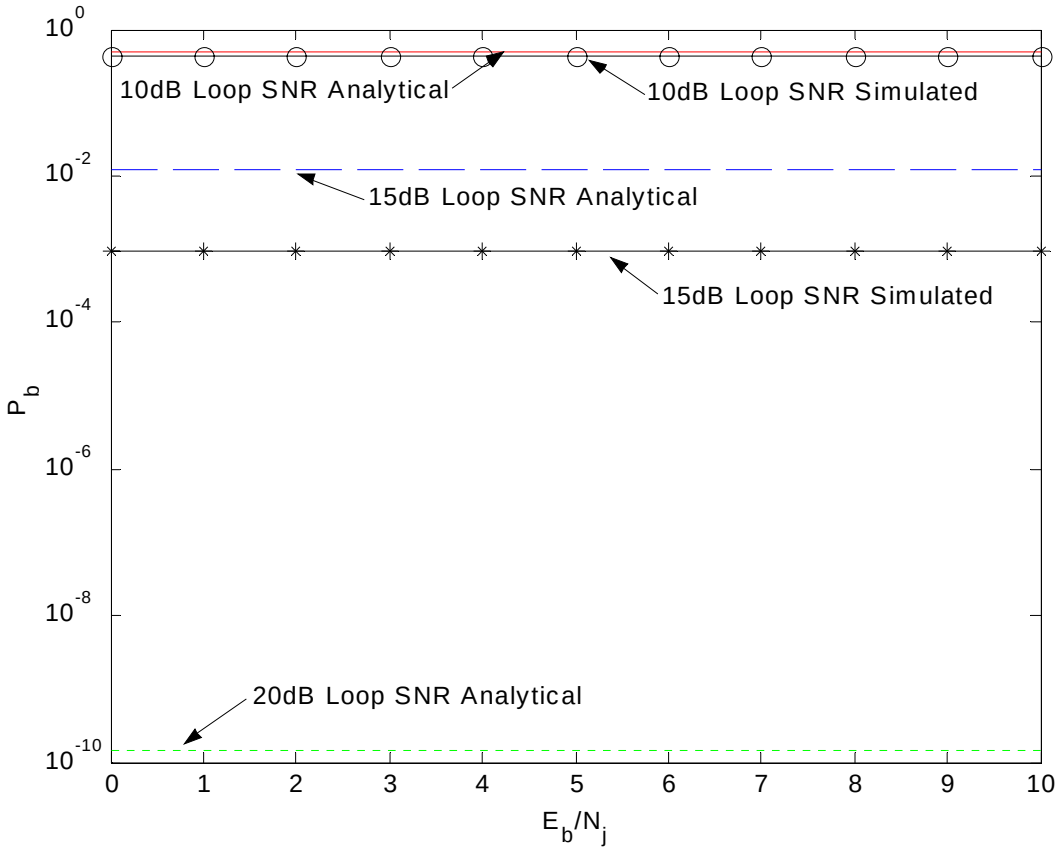

Figure 2.15 Soft Decision Viterbi Decoding with Various Loop SNR Values.

bit error ratio (BER) was extremely poor for a decoded signal. Since soft decision Viterbi decoding cannot provide reliable communication for a loop SNR of 15 dB or below, the classic interference strategy of interference the pilot tone is highly effective in this case.

Unlike soft decision Viterbi decoding, hard decision Viterbi decoding only uses the receiver estimate of what bit was transmitted without any estimate of the receiver confidence. While phase noise increases the bit error rate, a convolutional code can perform extremely well when the encoded error rate is less than 10^{-2}. Soft decision Viterbi decoding, however, uses an estimate of the receiver confidence, which is adversely affected by phase noise. Hence, it is expected that hard decision Viterbi decoding will perform better for 10-dB and 15-dB loop SNR. Figure 2.16 shows the performance for a maximum-likelihood *RAKE* receiver designed for AWGN and pulse-noise interference with hard decision Viterbi decoding, the direct-to-diffuse power is 10 dB, and the inter-

ference signal has a ten percent duty cycle. The results show that reliable communication is possible even with 10-dB loop SNR when hard decision Viterbi decoding is used. In fact, the performance for 10-dB and 15-dB loop SNR was better for hard decision Viterbi

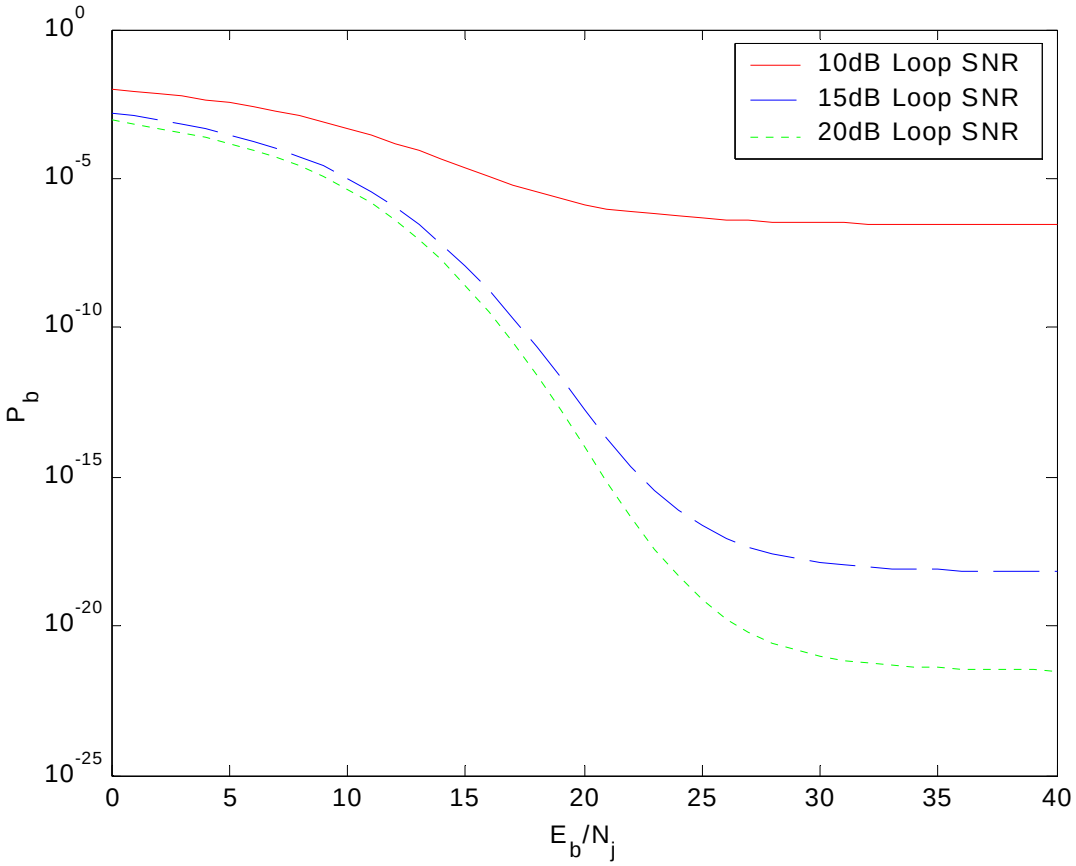

Figure 2.16 Hard Decision Viterbi Decoding with Various Loop SNR Values.

decoding for all E_b/N_j than for soft decision Viterbi decoding. When the loop SNR is equal to 20 dB, however, soft decision Viterbi decoding performs better than hard decision Viterbi decoding for small E_b/N_j. The soft decision Viterbi decoding used to obtain the results plotted in Figure 2.15 assumed a maximum-likelihood *RAKE* receiver for AWGN and pulse-noise interference. If a conventional *RAKE* receiver designed for AWGN only is used, then the performance for soft Viterbi decision decoding for small E_b/N_j is significantly worse than for hard decision for a 20-dB loop SNR. A decrease in the duty cycle of the pulse-noise interference signal causes problems for the *RAKE* re-

ceiver optimized for AWGN when soft decision Viterbi decoding is used; however, when hard decision Viterbi decoding is used, the performance for small E_b/N_j improves as the duty cycle decreases.

The maximum-likelihood *RAKE* receiver for pulse-noise interference was derived, and this detector improves the performance for soft decision Viterbi decoding down to the phase noise error floor. Unfortunately, soft decision Viterbi decoding performance cannot be improved below the phase noise error floor. Hard decision Viterbi decoding, on the other hand, performs much better than soft decision Viterbi decoding for low values of loop SNR since soft decision Viterbi decoding suffers more from the effects of imperfect phase synchronization. A plot of the phase error as a function of loop SNR was shown in Figure 2.3. As the loop SNR decreases, the phase error increases, which leads to performance degradation as a result of imperfect phase synchronization. Since soft decision Viterbi decoding makes bit decisions by combining a sequence of received bits, random losses due to imperfect phase synchronization affect the entire sequence of bits and are devastating when the pilot tone has a loop SNR of 15 dB or less. Hard decision Viterbi decoding makes decisions on a bit-by-bit basis and is only affected by phase noise if the imperfect phase synchronization loss is large enough to cause a bit error.

7. Varying the Value of K

The previous results were for a direct-to-diffuse power ratio of ten $(K=10)$. There are other important cases such as when $K \to \infty$ which represents no fading and $K=0$ which represents Rayleigh fading. The *RAKE* receiver is not optimal for channels without fading because all the signal power will be on the first finger and the other fingers will only add additional noise. Worst case fading occurs when there is no direct line of sight component $(K=0)$.

In Figure 2.17, we show the performance for a three finger *RAKE* receiver with soft decision Viterbi decoding where $E_b/N_0 = 15\,\text{dB}$, the pilot tone has a 20-dB loop SNR, the interference signal has a 100 percent duty cycle $(\rho = 1.0)$, and ratio of direct-to-diffuse power of 0, 10 and 100. The performance obtained for a direct-to-diffuse

power ratio of 100 approaches that obtained for $K \to \infty$, and performance is only slightly better than the $K = 10$ moderate fading case. Worst case fading $K = 0$ significantly increases the probability of bit error. Similar results are found when the interference signal is pulsed with a 10 percent duty cycle $\rho = 0.1$ as shown in Figure 2.18.

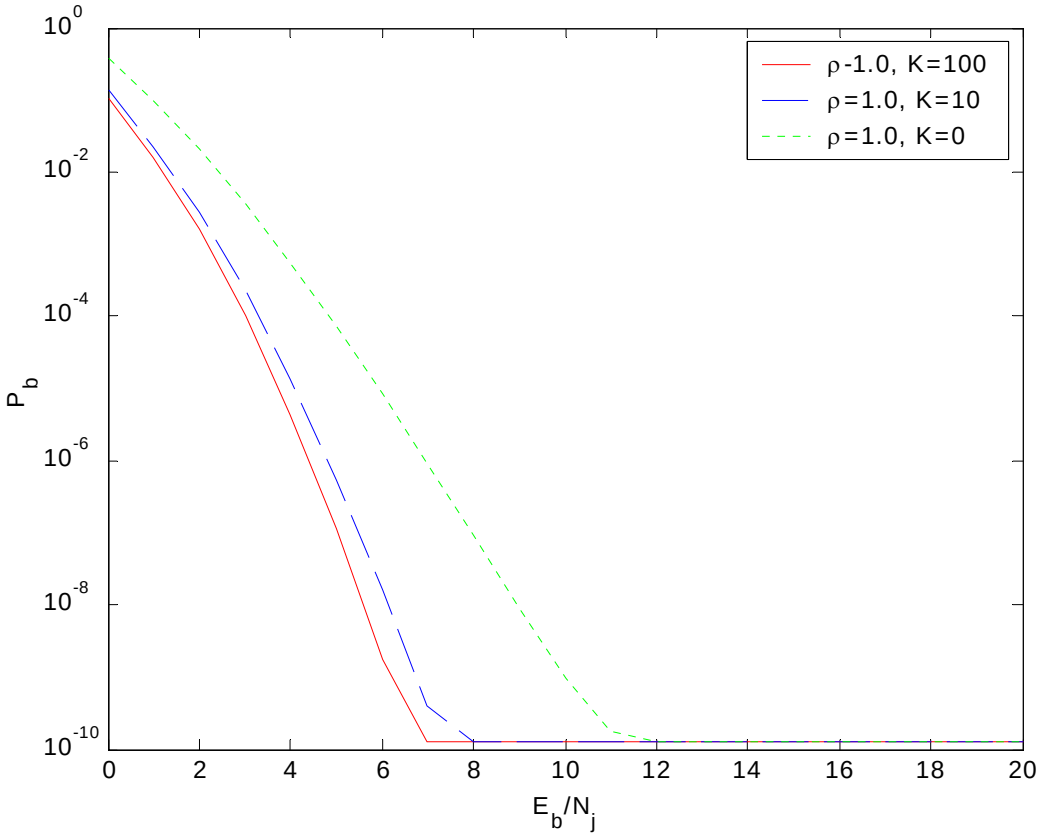

Figure 2.17 *RAKE* Receiver Performance for $\rho = 1.0$ and K=0,10, and 100.

Figures 2.17 and 2.18 show that there is a diminishing return gained when the value of K increases by a factor of 10 from 10 to 100. As the ratio of K increases, the power on the first finger increases and decreases on the second and third fingers. In order to compare the $K = 100$ with results from an AWGN only channel, we must convert the results as a function of E_b/N_j values into one of $E_b/\left(N_j + N_0\right)$. Since the calculations were performed for $E_b/N_0 = 15\,\text{dB}$, $E_b/N_j = 4$ dB converts to $E_b/\left(N_j + N_0\right) = 3.65$ dB.

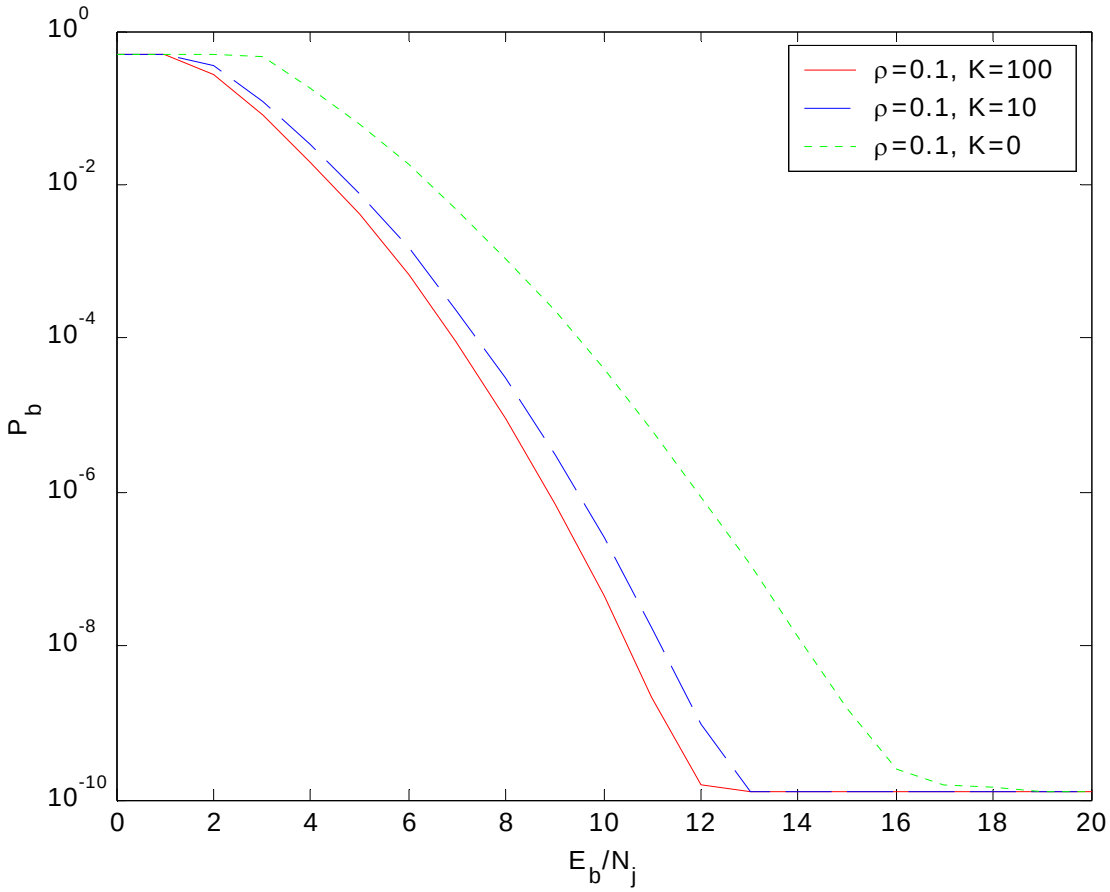

Figure 2.18 *RAKE* Receiver Performance for $\rho = 0.1$ and K=0,10 and 100.

The probability of bit error for $E_b/N_0 = 3.65$ dB AWGN only channel and a constraint length 9 convolutional code in [22] is slightly lower than the value shown at $E_b/N_j = 4$ dB in Figure 2.17. Since the *RAKE* receiver is not optimal for a nonfading AWGN channel and performance for $K = 100$ approaches performance for $K \to \infty$, the results presented in this dissertation show good agreement with previously published results.

THIS PAGE INTENTIONALLY LEFT BLANK

III. NONCOHERENT *RAKE* RECEIVER PERFORMANCE

The performance of a coherent *RAKE* receiver degrades when the pilot tone is received with a low SNR, so we now turn our attention to the noncoherent *RAKE* receiver which does not require any knowledge of the received signal phase. In this dissertation, only noncoherent BFSK is considered. The transmitted signal for a data bit "0" must be orthogonal to the transmitted signal for a data bit "1" just as for a conventional noncoherent signal. However, the transmitted signal must also be orthogonal to delayed versions of the transmitted signal when the delay is greater than the *RAKE* finger spacing for a noncoherent *RAKE* receiver.

For the noncoherent *RAKE* receiver, the transmitted signal for a bit "0" is defined as

$$a(t) = \sqrt{2}A_c c(t)\cos(\omega_0 t + \phi), \tag{3.1}$$

and the transmitted signal for a bit "1" is

$$a(t) = \sqrt{2}A_c c(t)\cos(\omega_1 t + \delta), \tag{3.2}$$

where $\sqrt{2}A_c$ is the unfaded carrier amplitude, $c(t)$ is the chipping waveform, which has an autocorrelation function defined in (2.5), and ϕ and δ are random starting phases. The transmitted frequencies ω_0 and ω_1 are chosen to be orthogonal over the bit duration T so that:

$$\int_0^T \cos(\omega_0 t)\cos(\omega_1 t)\,dt = 0. \tag{3.3}$$

When this signal is transmitted over the frequency-selective fading channel shown in Figure 1.4, the received signal can be expressed as

$$r(t) = \sum_{i=1}^{l} \sqrt{2}A_c \alpha_i c(t - iT_d)\cos\left[\omega_k (t - iT_d)\right]. \tag{3.4}$$

Each of the *l* components is modeled as a flat fading signal and can have a different fading coefficients α_i. When a bit "0" is transmitted $\omega_k = \omega_0$, and when a bit "1" is transmitted $\omega_k = \omega_1$. The received signal can be recovered by the noncoherent *RAKE* receiver shown in Figure 3.1

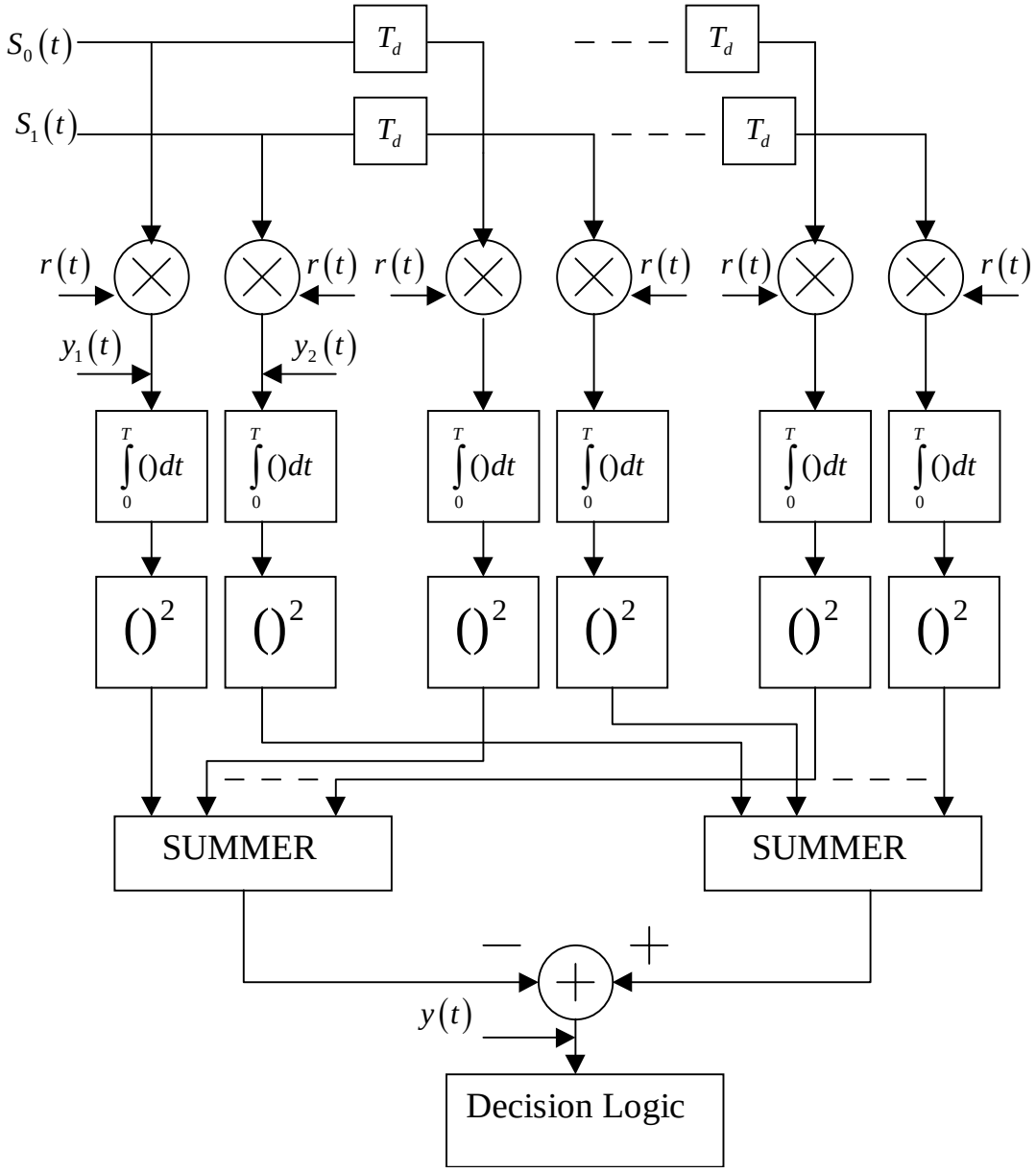

Figure 3.1 Noncoherent *RAKE* Receiver.

The locally generated signals are $S_0(t) = \sqrt{2}c(t)\cos(\omega_0 t)$ and $S_1(t) = \sqrt{2}c(t)\cos(\omega_1 t)$.

At the output of the mixer on the j^{th} finger we have

$$y_1(t) = \sum_{i=1}^{l} 2A_c\alpha_i c(t - iT_d)\cos\left[\omega_k(t - iT_d)\right]c(t - jT_d)\cos\left[\omega_0(t - jT_d)\right], \qquad (3.5)$$

for the received signal mixed with $S_0(t)$ and

$$y_2(t) = \sum_{i=1}^{l} 2A_c\alpha_i c(t - iT_d)\cos\left[\omega_k(t - iT_d)\right]c(t - jT_d)\cos\left[\omega_1(t - jT_d)\right], \qquad (3.6)$$

for the received signal mixed with $S_1(t)$. The integrator then integrates these signals, which will eliminate any delayed components of the received signal that do not have the same delay as the locally generated chipping waveform $c(t)$, since the chipping waveform has ideally zero correlation with delayed versions of itself as shown in (2.5). In reality, there are no PN sequences that give zero correlation with delayed versions of themselves, but practical PN sequences can be long enough that the correlation is zero for all practical purposes. The integrator also removes the double frequency term. Since the transmitted signal is orthogonal, in the absence of noise the output of the integrator on the signal branch will be $A_c\alpha_j$ and the non-signal branch integrator output will be zero. The integrator outputs are squared and combined. The results of the correlation of the received signal with $S_1(t)$ are then subtracted from the corresponding correlation with $S_0(t)$, and the receiver decides that a bit "0" was transmitted if the result is less than zero. Otherwise, the receiver decides a bit "1" was transmitted.

A. NONCOHERENT *RAKE* RECEIVER ANALYSIS WITH PULSE-NOISE INTERFERENCE AND RICEAN FADING

We will now derive the performance of a noncoherent *RAKE* receiver for a signal transmitted over a Ricean fading channel with pulse-noise interference. Both the *RAKE* receiver optimized for AWGN channels, analyzed in this section, and the maximum-likelihood *RAKE* receiver optimized for pulse-noise interference , analyzed in the next section, will be investigated. Convolutional coding with both hard and soft decision Viterbi decoding will also be considered.

We assume without loss of generality that the signal corresponding to bit "0" was transmitted. The conditional probability density function of the random variable X_{1k} at the output of the quadratic detector for the k^{th} finger of the signal branch given a signal amplitude $\sqrt{2}a_k$ is [17]

$$f_{X_{1k}}\left(x_{1k} \mid a_k\right) = \frac{1}{2\sigma_k^2}\exp\left(-\frac{x_{1k}+2a_k^2}{2\sigma_k^2}\right) I_0\left(\frac{a_k\sqrt{2x_{1k}}}{\sigma_k^2}\right), \tag{3.7}$$

where $I_0(\bullet)$ represents the modified Bessel function of the first kind and order zero. The average received power on the k^{th} finger is $\overline{a_k^2}$. The subscript $1k$ is used to identify the k^{th} finger of the signal branch, while the k^{th} finger of the noise only branch will be labeled with the subscript $2k$. The fading channel is modeled by assuming a_k to be a Ricean random variable. The probability density function of the Ricean random variable is [17]

$$f_{A_k}\left(a_k\right) = \frac{a_k}{\Omega_k^2}\exp\left(-\frac{a_k^2+\alpha_k^2}{2\Omega_k^2}\right) I_0\left(\frac{a_k\alpha_k}{\Omega_k^2}\right), \tag{3.8}$$

where α_k^2 is the average power of the direct signal component and $2\Omega_k^2$ is the average power of the diffuse signal component on the k^{th} finger. The total received power on the k^{th} finger is $\alpha_k^2 + 2\Omega_k^2$. The conditioning of X_{1k} on a_k is removed by integrating over the pdf for a_k:

$$f_{X_{1k}}\left(x_{1k}\right) = \int_0^\infty f_{X_{1k}}\left(x_{1k} \mid a_k\right) f_{A_k}\left(a_k\right) da_k. \tag{3.9}$$

Substituting (3.7) and (3.8) into (3.9), we obtain

$$\begin{aligned} f_{X_{1k}}\left(x_{1k}\right) = {} & \frac{1}{2\sigma_k^2\Omega_k^2}\exp\left(-\frac{x_{1k}\Omega_k^2+\alpha_k^2\sigma_k^2}{2\sigma_k^2\Omega_k^2}\right) \\ & \times \int_0^\infty a_k \exp\left(-\frac{2a_k^2\Omega_k^2+a_k^2\sigma_k^2}{2\sigma_k^2\Omega_k^2}\right) I_0\left(\frac{a_k\sqrt{2x_{1k}}}{\sigma_k^2}\right) I_0\left(\frac{a_k\alpha_k}{\Omega_k^2}\right) da_k. \end{aligned} \tag{3.10}$$

The above expression can be evaluated using the relationship

$$I_0\left(x\right) = J_0\left(jx\right), \tag{3.11}$$

where $j = \sqrt{-1}$, and (6.633.4) from [18], which gives

$$\int_0^\infty a_k \exp(-\alpha a_k) I_0(\beta a_k) J_0(\gamma a_k)\, da_k = \frac{1}{2\alpha}\exp\left(\frac{\beta^2-\gamma^2}{4\alpha}\right) J_0\left(\frac{\beta\gamma}{2\alpha}\right). \tag{3.12}$$

Evaluating (3.10) using (3.11) and (3.12), we get

$$f_{X_{1k}}(x_{1k}) = \frac{1}{2\Omega_k^2+\sigma_k^2}\exp\left(-\frac{2\alpha^2+x_{1k}}{2\left(2\Omega_k^2+\sigma_k^2\right)}\right) I_0\left(\frac{\alpha\sqrt{2x_{1k}}}{2\Omega_k^2+\sigma_k^2}\right). \tag{3.13}$$

The pdf at the output of the summer is then given by the convolution of the pdf from all the fingers of the *RAKE* receiver. In order to avoid doing these convolutions directly, the Laplace transforms of the pdf from each finger are multiplied together and the inverse transform of this product yields the pdf at the output of the summer. The Laplace transform of the pdf for X_{1k} is obtained from

$$F_{X_{1k}}(s) = \int_0^\infty f_{X_{1k}}(x_{1k}) \exp(-s x_{1k})\, dx_{1k}. \tag{3.14}$$

Substituting (3.13) into (3.14), we get

$$\begin{aligned} F_{X_{1k}}(s) = {} & \frac{1}{2\left(2\Omega_k^2+\sigma_k^2\right)}\exp\left(\frac{-\alpha^2}{2\left(2\Omega_k^2+\sigma_k^2\right)}\right) \\ & \times \int_0^\infty \exp\left(\frac{-x_{1k}}{2\left(2\Omega_k^2+\sigma_k^2\right)}\right)\exp(-s x_{1k})\, I_0\left(\frac{\alpha\sqrt{2x_{1k}}}{\left(2\Omega_k^2+\sigma_k^2\right)}\right). \end{aligned} \tag{3.15}$$

By making the change of variables

$$y = \sqrt{x_{1k}}, \tag{3.16}$$

then

$$dy = \frac{1}{2\sqrt{x_{1k}}}\, dx, \tag{3.17}$$

we can evaluate the integral in (3.15) using (6.631.4) from [18]:

$$\int_0^\infty x^{\nu+1}\exp\left(-\alpha x^2\right) J_\nu(\beta x)\, dx = \frac{\beta^\nu}{(2\alpha)^{\nu+1}}\exp\left(-\frac{\beta^2}{4\alpha}\right). \tag{3.18}$$

Hence, the Laplace transform of the pdf for the k^{th} finger of the signal branch can be written as

$$F_{X_{1k}}(s) = \frac{1}{1+2s\left(2\Omega_k^2+\sigma_k^2\right)} \exp\left(\frac{-2s\alpha^2}{\left(1+2s\left(2\Omega_k^2+\sigma_k^2\right)\right)}\right), \tag{3.19}$$

and the Laplace transform at the output of the summer for the signal branch is simply the product of the *k* signal branch fingers

$$F_{X_1}(s) = \prod_{k=1}^{L} F_{X_{1k}}(s). \tag{3.20}$$

The pdf for the noise only branch can be found from (3.19) by setting $\alpha_k^2 = \Omega_k^2 = 0$:

$$F_{X_{2k}}(x_{2k}) = \frac{1}{2\sigma_k^2} \exp\left(-\frac{x_{2k}}{2\sigma_k^2}\right). \tag{3.21}$$

As previously mentioned, the subscript $2k$ identifies the k^{th} finger on the noise only branch, i.e., $\sigma_k^2 = \sigma_0^2$ when only AWGN is present and $\sigma_k^2 = \sigma_0^2 + \sigma_j^2$ when pulse-noise interference is present. Using (3.14), we obtain the Laplace transform of (3.26) as

$$F_{2k}(s) = \frac{1}{2\sigma_k^2 s + 1}. \tag{3.22}$$

The pdf at the output of the summer on the noise only branch is the inverse Laplace transform of the product of all Laplace transforms for all the fingers at the input of the summer as

$$F_{X_2}(s) = \prod_{k=1}^{L} F_{X_{2k}}(s). \tag{3.23}$$

1. Soft Decision Viterbi Decoding

The probability of bit error for a system with convolutional coding is upper bounded by [9]

$$P_b < \sum_{d=d_{free}}^{\infty} B_d P_d, \tag{3.24}$$

where B_d is the total number of nonzero information bits in all weight *d* paths and P_d is the probability of selecting a code sequence that is a Hamming distance *d* away from the correct code sequence. The interleaver randomizes the order of the bits with interference at the decoder input, so P_d can be written [9] as

$$P_d = \sum_{i=0}^{d} \binom{d}{i} \rho^i (1-\rho)^{d-i} P_d(i), \tag{3.25}$$

where ρ is the duty cycle of the pulse noise interference, and $P_d(i)$ is the probability of selecting a code sequence a Hamming distance *d* from the correct code sequence given that *i* of the *d* receptions experience interference. For a rate ½, constraint length 9 convolutional code, the first three nonzero terms of the series are $33P_{12} + 281P_{14} + 2179P_{16}$, which are sufficient to accurately compute P_b when $P_b < 10^{-3}$. To calculate $P_d(i)$ when $d-i$ bits are received with only AWGN and *i* bits experience interference, we must evaluate

$$P_d(i) = 1 - \int_0^{\infty} f_{1X}(x_1) \left[\int_0^{x_1} f_{2X}(x_2) dx_2 \right] dx_1. \tag{3.26}$$

In order to evaluate (3.26), we obtain the required pdfs from

$$f_{X_1}(x_1) = \mathcal{L}^{-1}\left\{ F_{X_1}(s) \right\} \tag{3.27}$$

and

$$f_{X_2}(x_2) = \mathcal{L}^{-1}\left\{ F_{X_2}(s) \right\} \tag{3.28}$$

where

$$F_{X_1}(s) = \left(\prod_{k=1}^{L} F_{X_{1k}}\left(s \mid \sigma^2 = \sigma_0^2\right) \right)^{d-i} \left(\prod_{k=1}^{L} F_{X_{1k}}\left(s \mid \sigma^2 = \sigma_0^2 + \sigma_j^2\right) \right)^{i} \tag{3.29}$$

and

$$F_{X_2}(s) = \left(\prod_{k=1}^{L} F_{X_{2k}}\left(s \mid \sigma^2 = \sigma_0^2\right) \right)^{d-i} \left(\prod_{k=1}^{L} F_{X_{2k}}\left(s \mid \sigma^2 = \sigma_0^2 + \sigma_j^2\right) \right)^{i}. \tag{3.30}$$

The evaluation of (3.26) requires numerical inversion of (3.29) and (3.30), followed by numerical integration of (3.26). The inner integral does not have to be evaluated numerically since, as is well known [23],

$$L\left\{\int_0^{x_1} f\left(x_2\right)dx_2\right\} = \frac{F\left(s\right)}{s}. \tag{3.31}$$

The required inversions are done numerically using the method discussed in [24], which inverts the Laplace transform $\Phi\left(s\right)$ at any value of *x* from

$$f\left(x\right) = \frac{\exp(ax)}{2x}\left[\operatorname{Re}\Phi\left(a\right) + 2\sum_{n=1}^{\infty}\left(-1\right)^n \Phi\left(a + \frac{n\pi i}{x}\right)\right], \tag{3.32}$$

where *a* is a number greater than the real part of any singularity of $\Phi\left(s\right)$. The trapezoidal rule is then used to integrate the numerically inverted data points to obtain $P_d\left(i\right)$. These numerical inversions must be done $d + l$ times. For example, the P_{12} term includes the case where no soft decision outputs experience interference, where one experiences interference, where two experience interference, and so on to the case where all twelve outputs experience interference. These results are then substituted into (3.25) to obtain P_d.

Figure 3.2 shows the probability of bit error for a three finger *RAKE* optimized for the AWGN channel with rate ½, constraint length 9, Viterbi soft decision Viterbi decoding when $E_b/N_0 = 15\,\text{dB}$, the ratio of direct to diffuse power is 10 dB and the interference signal has a one percent duty cycle $\left(\rho = 0.01\right)$, ten percent duty cycle $\left(\rho = 0.1\right)$, and a interference signal that is on all the time $\left(\rho = 1.0\right)$. Results show that the probability of bit error increases when the interference duty cycle ρ is decreased. This is due to the fact that the interference power increases as the duty cycle decreases, since $\sigma_j^2 = N_j/rT_b$ where N_j is the interference noise power spectral density and T_b is the bit duration. Soft decision Viterbi decoding uses a sequence of soft decision receiver outputs to make a bit decision. If any of these soft decision receiver outputs have a large variance, then the probability of bit error will significantly increase.

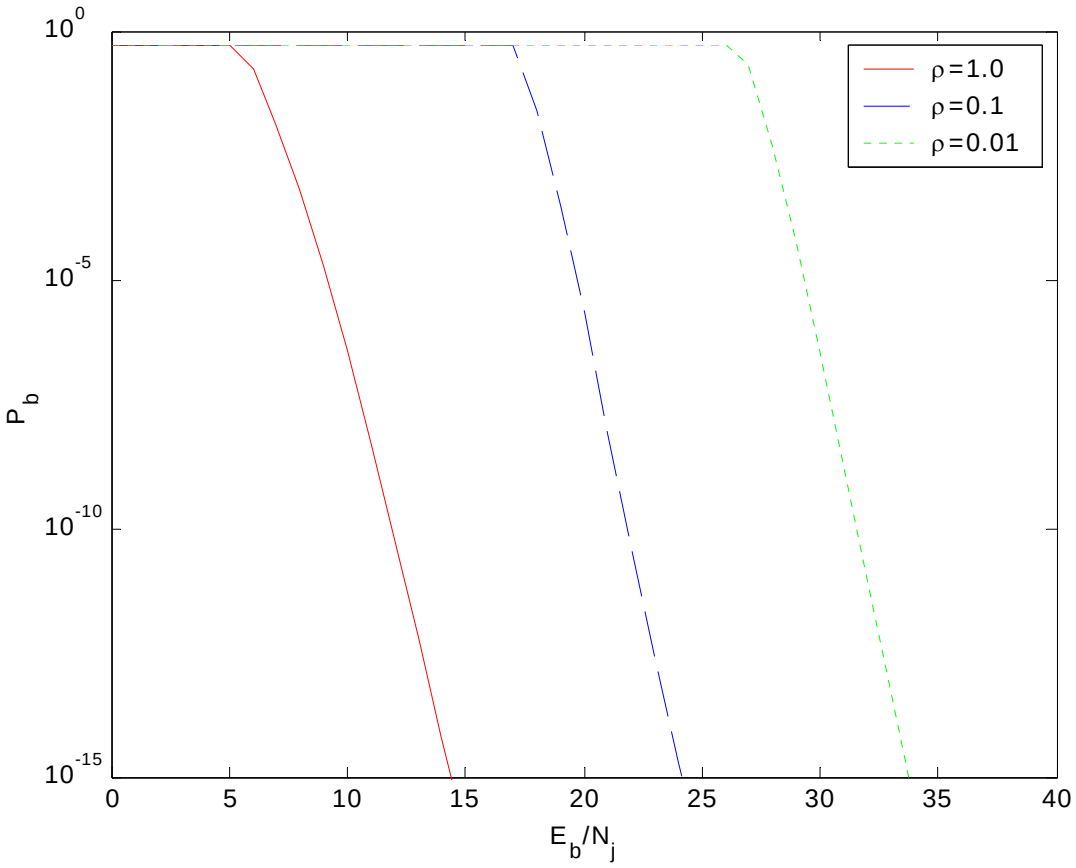

Figure 3.2 Noncoherent *RAKE* Receiver Optimized for the AWGN Channel Performance with Rate ½, Constraint Length 9, Viterbi Soft Decision Viterbi Decoding as a Function of Duty Cycle ρ.

The bits with interference will also affect future bit decisions, which will cause additional decoding errors. Comparing Figure 3.2 with Figure 2.10, shows that the coherent *RAKE* receiver performs better for low values of E_b/N_j but that the noncoherent *RAKE* receiver performs below the irreducible error floor caused by phase noise in the coherent *RAKE* receiver at high values of E_b/N_j. The noncoherent combining losses cause the noncoherent *RAKE* receiver to have catastrophic performance for E_b/N_j below 5 dB when the interference signal is on all the time and approximately for E_b/N_j below 26 dB when the interference signal had a one percent duty cycle $(\rho = 0.01)$. It should also be

noted that pulsing the interference signal increased the probability of bit error for both the coherent and noncoherent *RAKE* receivers designed for AWGN channels. Therefore, we can conclude that pulse-noise interference is a very effective interference strategy against a *RAKE* receiver designed for AWGN channels with soft decision Viterbi decoding. As a result, pulse-noise interference will be very effective against commercial systems since all commercial *RAKE* receivers are designed in this manner.

2. Hard Decision Decoding

If hard decision Viterbi decoding is utilized, P_d in (3.24) is [9]

$$P_d = \sum_{i=\frac{d+1}{2}}^{d} \binom{d}{i} \cdot p^i \cdot (1-p)^{d-i}, \tag{3.33}$$

when *d* is odd, and

$$\begin{aligned} P_d = \frac{1}{2} \cdot \binom{\frac{d}{2}}{\frac{d}{2}} \cdot p^{\frac{d}{2}} \cdot (1-p)^{\frac{d}{2}} \\ + \sum_{i=\frac{d}{2}+1}^{d} \binom{d}{i} \cdot p^i \cdot (1-p)^{d-i}, \end{aligned} \tag{3.34}$$

when *d* is even. In (3.33) and (3.34), the channel transition probability *p* is

$$p = \rho\left(P_b \mid \sigma^2 = \sigma_0^2 + \sigma_j^2\right) + (1-\rho)\left(P_b \mid \sigma^2 = \sigma_0^2\right), \tag{3.35}$$

where ρ is the duty cycle of the pulse-noise interference, $\left(P_b \mid \sigma^2 = \sigma_0^2 + \sigma_j^2\right)$ is the probability of bit error when a single bit experiences interference, and $\left(P_b \mid \sigma^2 = \sigma_0^2\right)$ is the probability of bit error when a single bit is transmitted with only AWGN present.

Figure 3.3 shows the probability of bit error for a three-finger *RAKE* with rate ½ constraint length 9 Viterbi hard decision decoding when $E_b/N_0 = 15\,\text{dB}$, the ratio of direct to diffuse power is 10 dB and the interference signal has a one percent duty cycle $(\rho = 0.01)$, ten percent duty cycle $(\rho = 0.1)$, and a interference signal that is on all the time $(\rho = 1.0)$. Soft decision Viterbi decoding uses a sequence of soft decision receiver

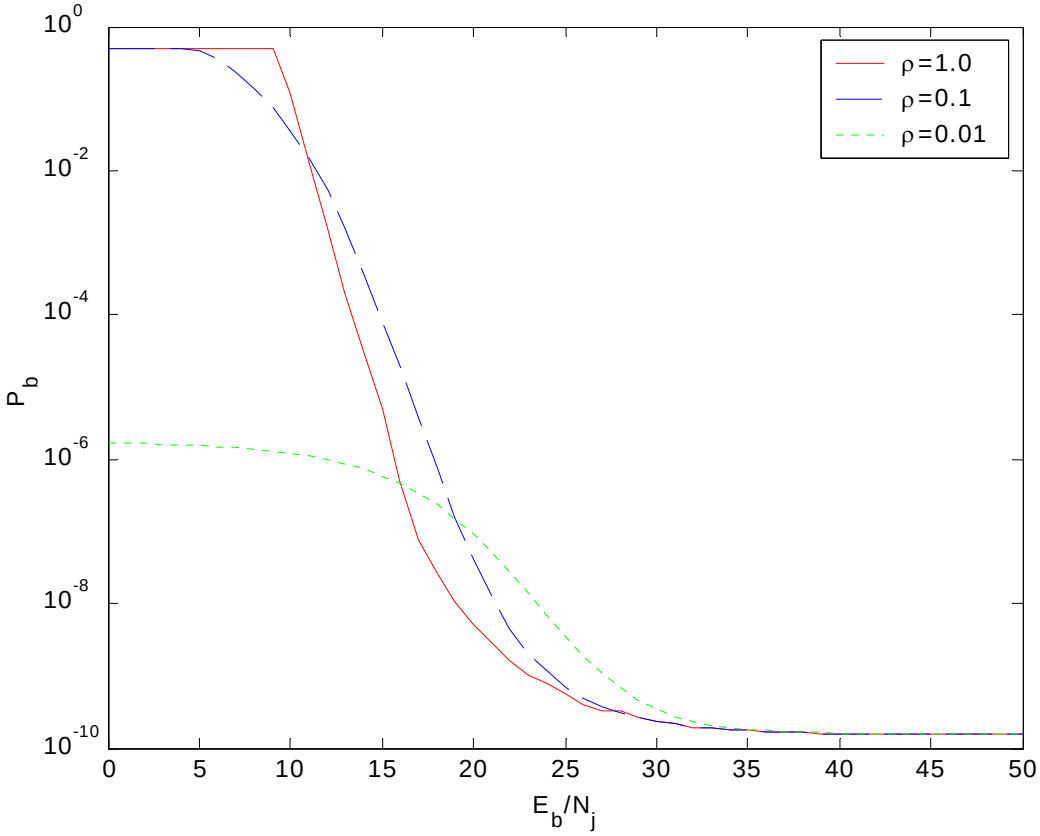

Figure 3.3 Noncoherent *RAKE* Receiver with Rate ½ Constraint Length 9 Viterbi Hard Decision Decoding.

outputs to make bit decisions. Note that interference one of these soft decision receiver outputs may cause the current bit decision to be incorrect as well as several of the following bits using a previous soft decision receiver output with interference. Hard decision Viterbi decoding makes hard decisions at the receiver and does not provide an estimate of the confidence in the bit decision. As a result, hard decision Viterbi decoding treats all bit errors equally and does not allow a single bit to with interference dominate the decoding decision. Further note that the hard decision receiver outputs have few errors when the pulse-noise interference duty cycle decreases. Hence, hard decision Viterbi decoding can provide bit error probabilities of 10^{-6} or lower when the pulse-noise interference duty cycle is one percent, which is a significant improvement over the soft decision Viterbi decoding that required $E_b/N_j \approx 30$ dB to achieve this bit error probability.

B. MAXIMUM-LIKELIHOOD RECEIVER FOR NONCOHERENT CHANNELS WITH GAUSSIAN NOISE, PULSE-NOISE INTERFERENCE, AND SOFT DECISION VITERBI DECODING

The maximum-likelihood receiver performance for a noncoherent *RAKE* receiver with AWGN, pulse-noise interference, and soft decision Viterbi decoding is derived in this section. Since P_d in (3.24) is equivalent to a d^{th} order diversity for soft decision Viterbi decoding [25], the analysis in this section can be applied to a wide range of systems that use diversity as well as error correction coding. The performance of the coherent *RAKE* receiver analyzed previously dramatically improved when it was designed for maximum-likelihood performance with AWGN and pulse-noise interference. As previously mentioned, the pulse-noise interference considered will have a duty cycle ρ and interference power spectral density N_j/ρ when the interference signal is on. Since the interference signal is modeled as additive Gaussian noise, the noise variance is equal to σ_0^2 when there is only AWGN present and $\sigma_0^2+\sigma_j^2$ when the interference is on. Assuming that the diversity receptions are independent, a reasonable assumption for a properly designed system, the joint density function is the product of the marginal density functions given in (3.7). We obtain the joint pdf for the "0" bit when i diversity receptions experience interference and $d-i$ diversity receptions have only Gaussian noise as

$$f_0(y)=\left(\frac{1}{2\sigma_0^2}\right)^{d-i}\exp\left[\frac{-1}{2\sigma_0^2}\sum_{m=1}^{d-i}y_{0_m}(t)+2\alpha_c^2\right]\times\prod_{m=1}^{d-i}I_0\left(\frac{\alpha_c\sqrt{2y_{0_m}(t)}}{\sigma_0^2}\right)$$
$$\times\left(\frac{1}{2\left(\sigma_0^2+\sigma_j^2\right)}\right)^{i}\exp\left[\frac{-1}{2\left(\sigma_0^2+\sigma_j^2\right)}\sum_{m=d-i+1}^{d}y_{0_m}(t)+2\alpha_c^2\right]\times\prod_{m=d-i+1}^{d}I_0\left(\frac{\alpha_c\sqrt{2y_{0_m}(t)}}{\sigma_0^2+\sigma_j^2}\right), \tag{3.36}$$

where $y_{0_m}(t)$ is a sequence of m diversity receptions of a bit "0" and α_c^2 is the average received power for the c^{th} *RAKE* finger. The joint pdf for a bit "1" is given by

$$f_1(y)=\left(\frac{1}{2\sigma_0^2}\right)^{d-i}\exp\left[\frac{-1}{2\sigma_0^2}\sum_{m=1}^{d-i}y_{1_m}(t)+2\alpha_c^2\right]\times\prod_{m=1}^{d-i}I_0\left(\frac{\alpha_c\sqrt{2y_{1_m}(t)}}{\sigma_0^2}\right)$$
$$\times\left(\frac{1}{2\left(\sigma_0^2+\sigma_j^2\right)}\right)^{i}\exp\left[\frac{-1}{2\left(\sigma_0^2+\sigma_j^2\right)}\sum_{m=d-i+1}^{d}y_{1_m}(t)+2\alpha_c^2\right]\times\prod_{m=d-i+1}^{d}I_0\left(\frac{\alpha_c\sqrt{2y_{1_m}(t)}}{\sigma_0^2+\sigma_j^2}\right), \tag{3.37}$$

where $y_{1_m}(t)$ is a sequence of m diversity receptions for a bit "1". The likelihood ratio is given by

$$\frac{f_1(y)}{f_0(y)} \underset{<}{\overset{s_1}{>}} 1. \tag{3.38}$$

Substituting (3.36) and (3.37) into (3.38), we get

$$\begin{aligned}
&\left(\frac{1}{2\sigma_0^2}\right)^{d-i} \exp\left[\frac{-1}{2\sigma_0^2}\sum_{m=1}^{d-i} y_{1_m}(t) + 2\alpha_c^2\right] \times \prod_{m-1}^{d-i} I_0\left(\frac{\alpha_c\sqrt{2y_{1_m}(t)}}{\sigma_0^2}\right) \\
&\times\left(\frac{1}{2\left(\sigma_0^2+\sigma_j^2\right)}\right)^{i} \exp\left[\frac{-1}{2\left(\sigma_0^2+\sigma_j^2\right)}\sum_{m=d-i+1}^{d} y_{1_m}(t) + 2\alpha_c^2\right] \times \prod_{m=d-i+1}^{d} I_0\left(\frac{\alpha_c\sqrt{2y_{1_m}(t)}}{\sigma_0^2+\sigma_j^2}\right) \\
&\underset{<}{\overset{s_1}{>}}\left(\frac{1}{2\sigma_0^2}\right)^{d-i} \exp\left[\frac{-1}{2\sigma_0^2}\sum_{m=1}^{d-i} y_{0_m}(t) + 2\alpha_c^2\right] \times \prod_{m=1}^{d-i} I_0\left(\frac{\alpha_c\sqrt{2y_{0_m}(t)}}{\sigma_0^2}\right) \\
&\times\left(\frac{1}{2\left(\sigma_0^2+\sigma_j^2\right)}\right)^{i} \exp\left[\frac{-1}{2\left(\sigma_0^2+\sigma_j^2\right)}\sum_{m=d-i+1}^{d} y_{0_m}(t) + 2\alpha_c^2\right] \times \prod_{m=d-i+1}^{d} I_0\left(\frac{\alpha_c\sqrt{2y_{0_m}(t)}}{\sigma_0^2+\sigma_j^2}\right).
\end{aligned} \tag{3.39}$$

Taking the natural log and rearranging terms, we get

$$\begin{aligned}
&\frac{1}{2\sigma_o^2}\sum_{m=1}^{d-i} y_{1_m}(t) + \sum_{m=1}^{d-i} \ln\left[I_0\left(\frac{\alpha_c\sqrt{2y_{1_m}(t)}}{\sigma_o^2}\right)\right] \\
&\quad + \frac{1}{2\left(\sigma_o^2+\sigma_j^2\right)}\sum_{m=d-i+1}^{d} y_{1_m}(t) + \sum_{m=d-i+1}^{d} \ln\left[I_0\left(\frac{\alpha_c\sqrt{2y_{1_m}(t)}}{\sigma_o^2+\sigma_j^2}\right)\right] \\
&\underset{<}{\overset{s_1}{>}} \frac{1}{2\sigma_o^2}\sum_{m=1}^{d-i} y_{0_m}(t) + \sum_{m=1}^{d-i} \ln\left[I_0\left(\frac{\alpha_c\sqrt{2y_{0_m}(t)}}{\sigma_o^2}\right)\right] \\
&\quad + \frac{1}{2\left(\sigma_o^2+\sigma_j^2\right)}\sum_{m=d-i+1}^{d} y_{0_m}(t) + \sum_{m=d-i+1}^{d} \ln\left[I_0\left(\frac{\alpha_c\sqrt{2y_{0_m}(t)}}{\sigma_o^2+\sigma_j^2}\right)\right].
\end{aligned} \tag{3.40}$$

Note that α_c on the $y_1(m)$ branch will be the same as α_c on the $y_0(m)$ branch since it was assumed that each *RAKE* finger will have flat fading. Hence, the $\ln\left[I_0(\bullet)\right]$ term

adds the same value on both sides of (3.40), and we can further simplify the maximum-likelihood receiver to

$$\frac{1}{\sigma_o^2}\sum_{m=1}^{d-i} y_{1_m}(t)+\frac{1}{\left(\sigma_o^2+\sigma_j^2\right)}\sum_{m=d-i+1}^{d} y_{1_m}(t)\underset{s_0}{\overset{s_1}{\gtrless}}\frac{1}{\sigma_o^2}\sum_{m=1}^{d-i} y_{0_m}(t)+\frac{1}{\left(\sigma_o^2+\sigma_j^2\right)}\sum_{m=d-i+1}^{d} y_{0_m}(t), \quad (3.41)$$

which shows that the output of each quadratic detector should be weighted by the inverse of the received bit variance $\sigma_0^2+\sigma_j^2$ or σ_0^2 depending on whether the bit experiences interference or not, respectively. A diagram of the maximum-likelihood combiner for AWGN and pulse- noise interference is shown in Figure 3.4, where $1/\sigma^2 = 1/\sigma_0^2$ when only AWGN is present and $1/\sigma^2 = 1/\left(\sigma_0^2+\sigma_j^2\right)$ when the received bit experiences interference. A maximum-likelihood noncoherent *RAKE* receiver designed for AWGN and

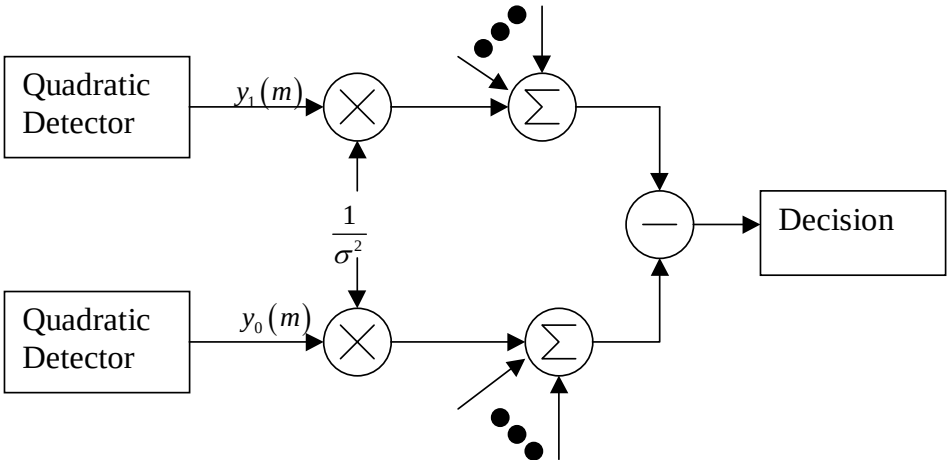

Figure 3.4 Maximum-Likelihood Combiner for AWGN and Pulse-Noise Interference.

pulse-noise interference is shown in Figure 3.5. Equation (3.41) shows that the maximum-likelihood noncoherent *RAKE* receiver scales the received bit by the inverse of the received bit variance $\sigma_0^2+\sigma_j^2$ or σ_0^2 depending on whether the bit experiences interference or not, respectively. We first examine the effect of this scaling on the signal branch in order to analyze the maximum-likelihood noncoherent *RAKE* receiver. We define $Z_{1k} = X_{1k}/\sigma^2$, which is the random variable on the k^{th} finger of the signal branch.

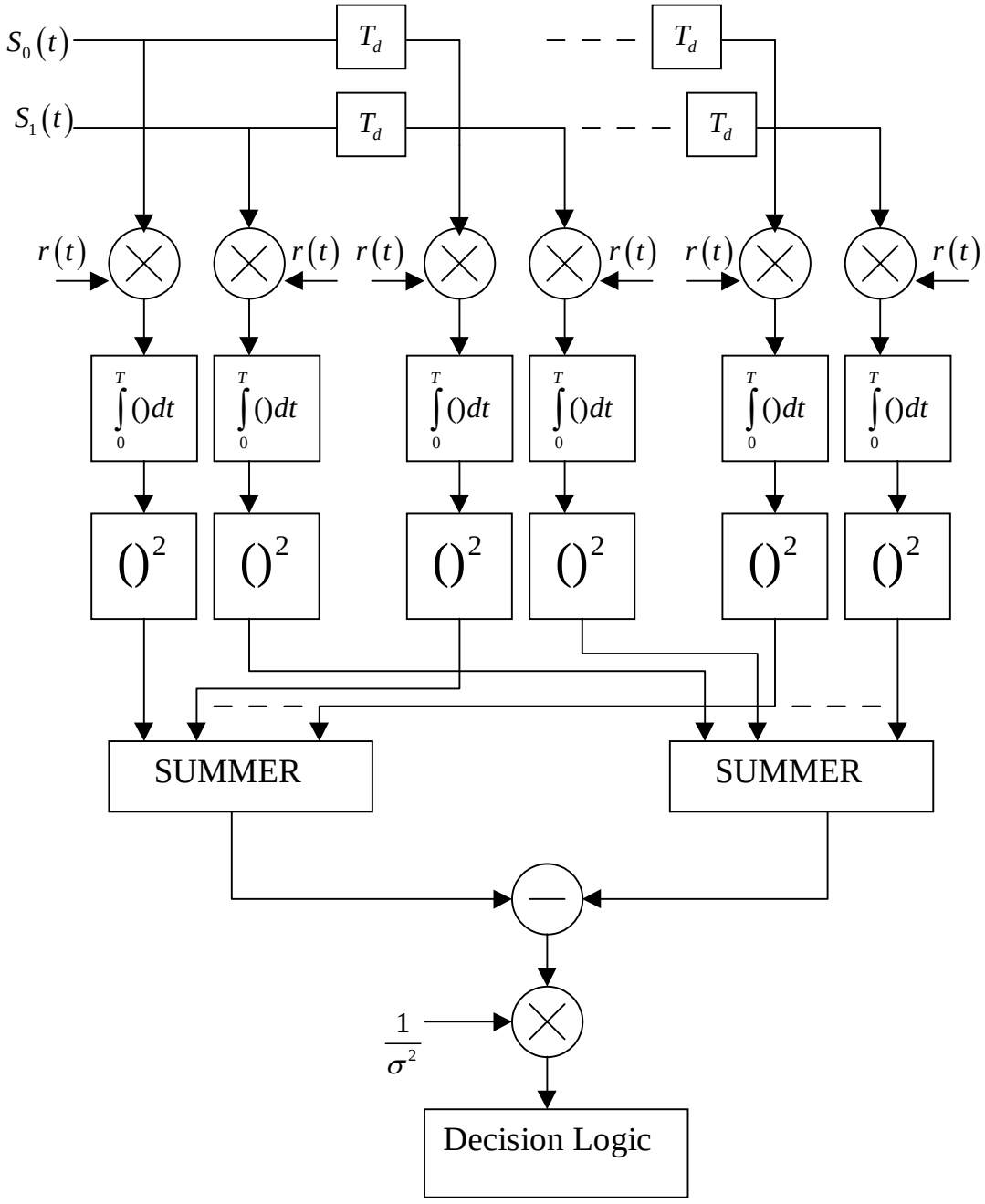

Figure 3.5 Maximum-Likelihood *RAKE* Receiver for AWGN and Pulse-Noise Interference.

To find the pdf for Z_{1k}, we make the transformation $Z_{1k} = X_{1k}/\sigma^2$, and from (3.7) we get

$$f_{Z_{1k}}\left(z_{1k} \mid a_k\right) = \frac{1}{2}\exp\left[-\left(\frac{\sigma_k^2 z_{1k} + 2a_k^2}{2\sigma_k^2}\right)\right] I_0\left(\frac{a_k\sqrt{2z_{1k}}}{\sigma_k}\right), \tag{3.42}$$

where $I_0(\bullet)$ represents the modified Bessel function of the first kind and order zero, a_k is assumed to be a Ricean random variable defined in (3.14), $\sigma_k^2 = \sigma_0^2$ when only AWGN is present and $\sigma_k^2 = \sigma_0^2 + \sigma_j^2$ when pulse-noise interference is present. We eliminate the dependence on a_k by substituting (3.42) and (3.9) into (3.10), leading to

$$\begin{aligned} f_{Z_{1k}}\left(z_{1k}\right) = {} & \frac{1}{2\Omega^2}\exp\left(-\frac{\Omega^2 z_{1k} + \alpha^2}{2\Omega^2}\right) \\ & \times \int_0^\infty a_k \exp\left(-\frac{2\Omega^2 a_k^2 + a_k^2\sigma_k^2}{2\Omega^2\sigma_k^2}\right) I_0\left(\frac{a_k\sqrt{2z_{1k}}}{\sigma_k}\right) I_0\left(\frac{a_k\alpha}{\Omega^2}\right) da_k. \end{aligned} \tag{3.43}$$

The integral can be evaluated using (3.11) and (6.633.4) from [23], which yields

$$f_{Z_{1k}}\left(z_{1k}\right) = \frac{\sigma_k^2}{2\left(2\Omega^2 + \sigma_k^2\right)}\exp\left[-\frac{2\alpha^2 + z_{1k}\sigma_k^2}{2\left(2\Omega^2 + \sigma_k^2\right)}\right] I_0\left(\frac{\alpha\sigma_k\sqrt{2z_{1k}}}{2\Omega^2 + \sigma_k^2}\right). \tag{3.44}$$

Making the substitutions $\rho_k = \frac{\alpha^2}{\sigma_k^2}$ and $\xi_k = \frac{2\Omega^2}{\sigma_k^2}$, we get

$$f_{Z_{1k}}\left(z_{1k}\right) = \frac{1}{2\left(1+\xi_k\right)}\exp\left[-\frac{1}{2}\left(\frac{z_{1k} + 2\rho_k}{1+\xi_k}\right)\right] I_0\left(\frac{\sqrt{2\rho_k z_{1k}}}{1+\xi_k}\right), \tag{3.45}$$

which is (5) in [26]. To calculate the Laplace transform of (3.45) we substitute (3.45) into (3.14) which yields

$$F_{Z_{1k}}\left(s\right) = \frac{1}{2\left(1+\xi_k\right)}\exp\left(-\frac{\rho_k}{1+\xi_k}\right)\int_0^\infty \exp\left[-z_{1k}\left(s + \frac{1}{2\left(1+\xi_k\right)}\right)\right] I_0\left(\frac{\sqrt{2\rho_k z_{1k}}}{1+\xi_k}\right) dz_{1k}. \tag{3.46}$$

By making the transformation of variables $u = \sqrt{z_{1k}}$ and $du = dz_{1k} \big/ 2\sqrt{z_{1k}}$, we get

$$F_{Z_{1k}}\left(s\right) = \frac{1}{2\left(1+\xi_k\right)}\exp\left(-\frac{\rho_k}{1+\xi_k}\right)\int_0^\infty u\exp\left[-\left(s + \frac{1}{2\left(1+\xi_k\right)}\right)u^2\right] I_0\left(\frac{\sqrt{2\rho_k}u}{1+\xi_k}\right) du, \tag{3.47}$$

which can be evaluated using (3.11) and (6.631.4) from [23] :

$$\int_0^\infty x^{v+1}\exp\left(-\alpha x^2\right)J_v\left(\beta x\right)dx=\frac{\beta^v}{\left(2\alpha\right)^{v+1}}\exp\left(-\frac{\beta^2}{4\alpha}\right). \tag{3.48}$$

Performing the integration and simplifying, we get

$$F_{Z_{1k}}\left(s\right)=\frac{1}{2s\left(1+\xi_k\right)+1}\exp\left[\frac{\alpha^2}{2s\left(1+\xi_k\right)}\right]. \tag{3.49}$$

The Laplace transform at the output of the signal branch summer is the product of the *L* signal branch fingers, so that

$$F_{X_1}\left(s\right)=\prod_{k=1}^{L}F_{X_{1k}}\left(s\right). \tag{3.50}$$

The pdf for the noise-only branch of the maximum-likelihood *RAKE* receiver can be found from (3.44) by setting the received direct signal power to zero $\left(\alpha^2=0\right)$ and the received diffuse signal power to zero $\left(2\Omega^2=0\right)$. Performing this substitution, we get

$$f_{Z_{2k}}\left(z_{2k}\right)=\frac{1}{2}\exp\left(-\frac{z_{2k}}{2}\right), \tag{3.51}$$

where z_{2k} represents the random variable on the k^{th} finger of the noise-only branch. The Laplace transform for the noise-only branch is calculated by substituting (3.51) into (3.14), which yields

$$F_{Z_{2k}}\left(s\right)=\frac{1}{2s+1}. \tag{3.52}$$

Since the maximum-likelihood *RAKE* receiver scales the received signal by the inverse of the variance $\sigma_0^2+\sigma_j^2$ or σ_0^2 depending on whether the bit experiences interference or not, respectively, the Laplace transform of the pdf for the noise-only *RAKE* fingers does not depend on the received signal variance $\left(\sigma_k^2\right)$. The Laplace transform of the pdf at the output of the summer is the product of the *L* noise-only fingers:

$$F_{X_2}(s) = \prod_{k=1}^{L} F_{X_{2k}}(s). \tag{3.53}$$

The Laplace transform at the output of the signal branch summer and the noise-only branch summer must be inverted and substituted into (3.26) to calculate the bit error probability. As an example, we use a three finger *RAKE* with $E_b/N_0 = 15\,\text{dB}$, and a 10-dB ratio of direct-to-diffuse power to calculate the performance of the maximum-likelihood noncoherent *RAKE* receiver against a interference signal with one percent duty cycle $(\rho = 0.01)$, ten percent duty cycle $(\rho = 0.1)$, and a interference signal that is on all the time $(\rho = 1.0)$. Results presented in Figure 3.6 show that the maximum-likelihood noncoherent *RAKE* receiver with rate ½, constraint length 9 soft decision Viterbi decoding improves performance when pulse-noise interference is present. In fact, the worst case interference at low SNR values was achieved when the interference was on all the time, which indicates that pulse-noise interference is not effective against a maximum-likelihood receiver designed for both AWGN and pulse-noise interference. The performance of the maximum-likelihood noncoherent *RAKE* receiver is significantly better than the performance of the standard noncoherent *RAKE* receiver, which has catastrophic performance for E_b/N_j below 25 dB when the interference signal has a one percent duty cycle. The maximum-likelihood noncoherent *RAKE* receiver has a probability of bit error at or below 10^{-20} for all values of E_b/N_j for this case. In summary, a noncoherent *RAKE* receiver designed for AWGN performs worse as the pulse-noise interference duty cycle decreases, whereas the opposite is true for the maximum-likelihood noncoherent *RAKE* receiver.

Comparing the maximum-likelihood coherent *RAKE* receiver performance shown in Figure 2.11 with that of the maximum-likelihood noncoherent *RAKE* receiver, we see that the noncoherent case does not have an irreducible phase noise error floor and is only limited by AWGN noise. When the interference signal is on all the time or has a ten percent duty cycle, the maximum-likelihood coherent *RAKE* receiver performs better for low

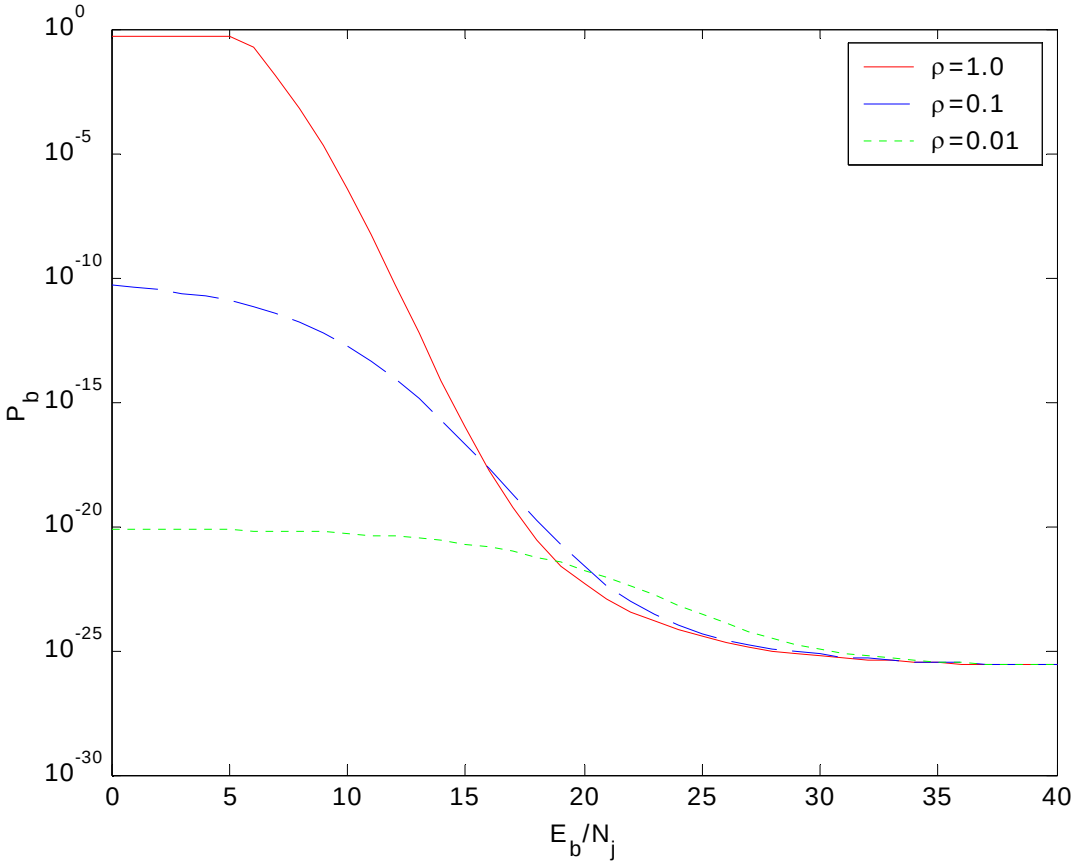

Figure 3.6 Maximum-Likelihood Noncoherent *RAKE* Receiver with Rate ½ Constraint Length 9 Viterbi Soft Decision Viterbi Decoding.

values of E_b/N_j ; however, when the interference signal has a one percent duty cycle the maximum-likelihood noncoherent *RAKE* receiver performs better for all values of E_b/N_j because the maximum-likelihood coherent *RAKE* receiver has an irreducible phase noise error floor. In both cases the worst performance occurs when the interference signal is on all the time. In conclusion, the maximum-likelihood *RAKE* designed for AWGN and pulse-noise interference provides dramatically better performance in the presence of pulse-noise interference than a commercial *RAKE* receiver designed for AWGN channels.

THIS PAGE INTENTIONALLY LEFT BLANK

IV. CONCLUSIONS

A. RESEARCH SUMMARY

The performance of a direct sequence spread spectrum (DSSS) signal transmitted over a Ricean frequency-selective, slowly fading channel with pule-noise interference, phase noise and AWGN has been analyzed. Both coherent and noncoherent modulation with an exponential multipath intensity profile were considered. These signals were compared using a direct to diffuse power ratio of ten $(K = 10)$, which represents moderate fading. The performance of conventional *RAKE* receiver optimized only for AWGN was compared with the maximum-likelihood *RAKE* receiver optimized for pulse-noise interference and AWGN. A rate ½ , constraint length 9 convolutional code was also considered with both hard and soft decision Viterbi decoding.

Analysis of the coherent *RAKE* receiver with soft decision Viterbi decoding demonstrated how critically important it is to have a strong pilot tone. In Figure 2.15 the performance for 10-dB loop SNR and 15-dB loop SNR does not provide reliable communication. In fact, the performance for 10-dB loop SNR produced a catastrophic 50 percent error rate and 15-dB loop SNR produced a 10^{-3} error rate. In order to avoid these disastrous error rates, commercial wireless systems dedicate as much as 20 percent of the total power to the pilot tone. The 20-dB loop SNR performance had an irreducible phase noise error floor slightly above 10^{-10}, which is more than sufficient for wireless communication systems. Fiber optic systems which operate at error rates of approximately 10^{-15} would require a loop SNR greater than 15 dB.

Commercial coherent *RAKE* receivers designed for AWGN with soft decision Viterbi decoding perform poorly in the presence of pulse-noise interference. Results presented in Figure 2.10 demonstrate that the commercial coherent *RAKE* receiver performs worse as the duty cycle of the pulse-noise interference signal decreases. A soft decision receiver provides estimates of whether the received signal is a bit”0” or a bit “1” and an estimate of the confidence in this decision. When a strong interference signal is present,

the soft decision receiver can produce a bit error with a high confidence of being the correct estimate. The convolutional decoder will produce a series of bit errors when the minimum weight path through the trellis includes a bit error with a high confidence estimate. Since the peak interference power increases as the pulse-noise interference duty cycle decreases, it is logical to expect the bit error rate to increase as the duty cycle of the pulse-noise interference duty cycle decreases. The maximum-likelihood coherent *RAKE* receiver optimized for pulse-noise interference and AWGN was derived and the analysis proved that measuring the variance of the received signal on a bit-by-bit basis and scaling each bit by the inverse of the variance is optimal according to the maximum-likelihood criteria. The efficacy of this receiver was demonstrated by the fact that it reduced the probability of bit error down to the irreducible phase noise error floor when pulse-noise interference was present. Results were derived analytically up to the point where no analytical solution to the required inverse Laplace transform existed, so numerical techniques were used both for inversion and integration to calculate the probability of bit error. Analytical results for the *RAKE* receiver designed only for AWGN were verified by simulation for the case when the interference signal was on all the time and the simulation results were within 1 dB of the analytical results. The maximum-likelihood coherent *RAKE* receiver designed for AWGN and pulse-noise interference was also simulated for 10-dB and 15-dB loop SNR. The simulated probability of bit error for 10-dB and 15-dB loop SNR were below the analytic values because the union bound is loose when phase noise dominates system performance.

Results showed that the *RAKE* receiver designed for AWGN only and hard decision Viterbi decoding performed better when the duty cycle of the interference signal was reduced. A hard decision receiver only provides an estimate of whether the received data is a bit “0” or a bit “1” and does not provide an estimate of the received bit decision confidence. As a result, a bit that experiences interference will not dominate the decoding decision since the decoder does not use estimates of the received bit confidence. Decreasing the duty cycle of the interference signal also decreases the number of bits that experience interference. With hard decision Viterbi decoding, fewer bits that experience interference at the input to the decoder produce fewer errors at the output of the decoder.

In Figure 2.9, when the duty cycle of the interference signal was one percent, the probability of bit error was approximately 10^{-10} or lower for all values of E_b/N_j. This is significantly lower than the probability of bit error for the same case with soft decision Viterbi decoding, which produced a catastrophic 50 percent error rate when E_b/N_j was less than 3 dB. From Figure 2.10, soft decision Viterbi decoding required $E_b/N_j = 15$ dB to reach a 10^{-10} probability of bit error. Hence, hard decision Viterbi decoding is a good method to limit the effect of pulse-noise interference.

In addition, hard decision Viterbi decoding also limits the effects of phase noise. The results showed that soft decision Viterbi decoding can not provide reliable communication for either 10-dB or 15-dB loop SNR. However, hard decision Viterbi decoding can reduce the probability of bit error to 10^{-6} for 25 dB or greater E_b/N_j with a loop SNR of 10 dB, and the 15-dB loop SNR case only required 11 dB E_b/N_j. This shows that interfering with the pilot tone would not cause a catastrophic error rate when the pilot tone and data are transmitted on different frequencies and hard decision convolutional coding is used.

Changing the *RAKE* finger spacing in order to improve the diversity performance by reducing the difference in the signal power on each finger was investigated. Since the analysis assumed a three-finger *RAKE*, when the finger spacing was reduced to decrease the difference in finger SNR, the total received power also decreased. Repeated analysis for hard decision Viterbi decoding demonstrated that recovering 92 percent of the received power produced the lowest probability of bit error. Decreasing the finger spacing further to provide better diversity performance did not fully compensate for the additional received signal power reduction. When soft decision Viterbi decoding was analyzed with a *RAKE* finger spacing that recovered 92 percent of the received signal power, the probability of bit error was approximately the same as the *RAKE* receiver that recovered 99.9 percent of the received signal power and each finger is 10 dB below the previous one. It should be noted that this analysis is specific to a three-finger *RAKE* receiver and it is possible that a *RAKE* receiver with four fingers or more could benefit by adapting the finger

spacing. Additionally, a 15-dB E_b/N_0 was assumed in the analysis. Adapting the *RAKE* finger spacing could be more effective for higher levels of AWGN.

Noncoherent *RAKE* receivers designed for AWGN with soft decision Viterbi decoding perform miserably in the presence of pulse-noise interference. Results presented in Figure 3.4 demonstrate that the noncoherent *RAKE* receiver performance degrades as the duty cycle of the pulse-noise interference signal decreases. When the pulse-noise interference signal uses a one percent duty cycle, the noncoherent *RAKE* receiver with soft decision Viterbi decoding has catastrophic performance for values of E_b/N_j below 26 dB. By comparison, at 26-dB E_b/N_j the coherent *RAKE* receiver designed for AWGN had a probability of bit error slightly above 10^{-10} for a interference duty cycle of one percent when the pilot tone was received with a 20-dB loop SNR. A strong pilot tone is critical for coherent systems. The noncoherent *RAKE* receiver performed better than the coherent *RAKE* receiver when the pilot tone was received with a 10-dB loop SNR, which had a 50 percent error rate for all values of E_b/N_j. Unlike the coherent *RAKE* receivers, the noncoherent *RAKE* receiver does not have an irreducible probability of bit error floor. Since noncoherent receivers demodulate the received bits without using a pilot tone, they are immune to random phase fluctuations that cause problems for coherent receivers.

Hard decision Viterbi decoding also limits the effect of pulse-noise interference on a noncoherent *RAKE* receiver designed for AWGN. When soft decision Viterbi decoding is used, the probability of bit error increases as the duty cycle of the interference signal decreases; however, the opposite is true for hard decision Viterbi decoding. Since a hard decision receiver does not provide an estimate of the confidence of the bit decision, the decoder will not have the problem of an erroneous bit decision with a high confidence estimate of being correct. The coherent *RAKE* receiver designed for AWGN with hard decision Viterbi decoding and 20-dB loop SNR performed better than the noncoherent *RAKE* receiver for all values of E_b/N_j. A strong received pilot tone is necessary for the coherent *RAKE* receiver to outperform the noncoherent *RAKE*.

The maximum-likelihood noncoherent *RAKE* receiver for pulse-noise interference and AWGN was also derived. Like the coherent case, measuring the variance of the received signal on a bit-by-bit basis and scaling each bit by the inverse of the variance is optimal according to the maximum-likelihood criteria. Our analysis demonstrated that, when the interference signal has a 10 percent duty cycle, this receiver has a probability of bit error below 10^{-10} for all values of E_b/N_j, and for a one percent duty cycle the probability of bit error was below 10^{-20} for all values of E_b/N_j. Since the maximum-likelihood noncoherent *RAKE* receiver for pulse-noise interference and AWGN effectively mitigates pulse-noise interference, the interference signal would have to transmit continuously; however, for values of E_b/N_j above 10 dB the probability of bit error is below 10^{-7}. Therefore, the maximum-likelihood noncoherent *RAKE* receiver for pulse-noise interference and AWGN is highly resistant to interference.

In summary, a *RAKE* receiver designed for AWGN does not perform well in the presence of pulse-noise interference. The maximum-likelihood *RAKE* receiver designed for AWGN and pulse noise interference mitigates the effect of pulse-noise interference for both coherent and noncoherent *RAKE* receivers. This demonstrates how important it is to design the receiver for the intended operational environment. It is also critically important for a coherent *RAKE* receiver to have a strong pilot tone. Random fluctuations of the pilot tone caused by high levels of AWGN have a devastating effect on soft decision Viterbi decoding. Hard decision Viterbi decoding can limit the impact of phase noise, but soft decision Viterbi decoding performs better than hard decision Viterbi decoding when the pilot tone is received with high SNR.

B. SUGGESTIONS FOR FURTHER RESEARCH

It was recently shown that the multipath amplitude distribution for indoor channels is well modeled by the Nakagami-m distribution [27]. Since direct sequence spread spectrum with binary phase-shift keying or quadrature phase-shift keying is often used

for indoor channels, it would be interesting to analyze the coherent and noncoherent *RAKE* receiver performance when the signal is transmitted over a Nakagami fading channel.

This dissertation assumed a rate ½ convolutional code that is one of two convolutional codes used in IS95 cellular communication systems. For a noisy reverse channel, IS95 systems use a rate 1/3 code, while the rate ½ convolutional code considered in this dissertation is specified for the forward channel. The interested reader can repeat this research for a rate 1/3, constraint length 9 convolutional code. The new 3G standards specify both a convolutional code and a turbo code. It would be very intriguing to compare coherent *RAKE* receivers with convolutional coding and turbo coding for an AWGN channel with pulse-noise interference.

The noncoherent *RAKE* receiver in this dissertation used binary frequency-shift keying (FSK). In [14] it was shown that a differential phase shift keyed (DPSK) signal can be represented as an orthogonal signal over a period of two bits. Thus DPSK typically has a 3-dB advantage over FSK for noncoherent communications. The noncoherent *RAKE* receiver, however, must be uncorrelated from finger to finger, and in [9] it is shown that a noncoherent *RAKE* receiver using DPSK modulation would require two chips between fingers instead of the one chip between fingers that FSK requires. It is not intuitively obvious that using DPSK modulation instead of FSK modulation would improve the performance of the noncoherent *RAKE* receiver, since the DPSK modulation would require the noncoherent *RAKE* receiver to operate at twice the chipping rate of the noncoherent *RAKE* receiver with FSK modulation for the same channel.

APPENDIX A

The Gauss-Chebyshev quadrature method given in (2.59) can be used as a quick iterative technique to calculate the Q function. Mathematically, the Q function can be expressed as $Q(x) = \int_{x}^{\infty} \left(\frac{1}{\sqrt{2\pi}} \right) \mathrm{e}^{-\frac{u^2}{2}} \, du.$ This integral of the Gaussian pdf is used to determine the probability of bit error for BPSK signals transmitted over an AWGN channel. While no closed form solution exists, the Q function has been tabulated for various values of *x*. We can calculate the value for Q(2) by substituting –2 for *m* and 1 for σ^2 in (2.46), which is the Laplace transform of the Gaussian pdf. The Gauss-Chebyshev quadrature method can now be used to invert the Laplace transform and integrate it from zero to infinity. Since we chose –2 for the mean value, the result should be the same as Q(2). The following MATLAB code implements the Gauss-Chebyshev quadrature method:

```
v=200;
i=sqrt(-1);
sum=0;
c=2.5;
for k=1:(v/2)
   tk=tan((((2*k)-1)*pi)/(2*v));
   sum=sum+real(LAP(c+(i*c*tk)))+(tk*imag(LAP(c+i*c*tk)));
end
res=sum/v;

function[y]=LAP(s)
y=exp(-2*s+(0.5*s^2));
```

When the code is run the result is 0.0228, which is the same value given for Q(2) in [14].

In this dissertation, the Laplace transforms that were inverted required choosing different values for *c* as the signal-to-noise ratio changed. In general, small values of *c*

were used for low signal-to-noise ratios and larger values were chosen for higher signal-to-noise ratios. The following MATLAB code was used for the coherent *RAKE* receiver optimized for AWGN with $\rho = 1$:

```
d=2*pi*besseli(0,31.623);
v=200;
i=sqrt(-1);
for p=1:41
   ebnj=(10^(.1*(p-1)));
   nj=1.585/ebnj;
   sum=0;
   for k=1:v/2
      tk=tan((2*k-1)*pi/(2*v));
      integ=0;
      for l=1:99
         c=.05;
          if p>2
             c=0.1;
          end
          if p>8
             c=0.5;
          end
          if p>25
            c=1.88;
         end

         a(l)=EX(c+(i*c*tk),((l*0.01*pi)-pi),nj);
      end
      for m=1:98
         g(m)=(a(m)+a(m+1))/2;
```

```
            n=cos((((m+m+1)/2)*0.01*pi)-pi);
            z(m)=0.02*pi*g(m)*(exp(31.623*n))/d;
            integ=integ+z(m);
        end
        sum=sum+real(integ)+tk*imag(integ);
    end
    res(p)=sum/v;
end

function[y]=F(s,p,ej)
No=.1;
Nj=.1+((2*ej)/1);
K=10;
g=1/22;
B=2*1.585*(cos(p)^2)*(1-((s/2)*No))*s;
B2=2*1.585*(cos(p)^2)*(1-((s/2)*Nj))*s;
y=((((exp(-2*K*0.9*B2*g/(1+2*0.9*B2*g)))/(1+2*g*0.9*B2))*((exp(-
2*K*0.09*B2*g/(1+2*0.09*B2*g)))/(1+2*g*0.09*B2))*((exp(-
2*K*0.009*B2*g/(1+2*0.009*B2*g)))/(1+2*0.009*B2*g)))^12)*((((exp(-
2*K*0.9*B*g/(1+2*0.9*B*g)))/(1+2*g*0.9*B))*((exp(-
2*K*0.09*B*g/(1+2*0.09*B*g)))/(1+2*g*0.09*B))*((exp(-
2*K*0.009*B*g/(1+2*0.009*B*g)))/(1+2*0.009*B*g)))^0);
```

This calculates the P_{12} term. To calculate P_{14} we change the function *F* as shown in the following:

```
function[y]=F(s,p,ej)
No=.1;
Nj=.1+((2*ej)/1);
K=10;
```

```
g=1/22;
B=2*1.585*(cos(p)^2)*(1-((s/2)*No))*s;
B2=2*1.585*(cos(p)^2)*(1-((s/2)*Nj))*s;
y=((((exp(-2*K*0.9*B2*g/(1+2*0.9*B2*g)))/(1+2*g*0.9*B2))*((exp(-
2*K*0.09*B2*g/(1+2*0.09*B2*g)))/(1+2*g*0.09*B2))*((exp(-
2*K*0.009*B2*g/(1+2*0.009*B2*g)))/(1+2*0.009*B2*g)))^14)*((((exp(-
2*K*0.9*B*g/(1+2*0.9*B*g)))/(1+2*g*0.9*B))*((exp(-
2*K*0.09*B*g/(1+2*0.09*B*g)))/(1+2*g*0.09*B))*((exp(-
2*K*0.009*B*g/(1+2*0.009*B*g)))/(1+2*0.009*B*g)))^0);
```

Next, P_{16} can be calculated using the following function *F*:

```
 function[y]=F(s,p,ej)
No=.1;
Nj=.1+((2*ej)/1);
K=10;
g=1/22;
B=2*1.585*(cos(p)^2)*(1-((s/2)*No))*s;
B2=2*1.585*(cos(p)^2)*(1-((s/2)*Nj))*s;
y=((((exp(-2*K*0.9*B2*g/(1+2*0.9*B2*g)))/(1+2*g*0.9*B2))*((exp(-
2*K*0.09*B2*g/(1+2*0.09*B2*g)))/(1+2*g*0.09*B2))*((exp(-
2*K*0.009*B2*g/(1+2*0.009*B2*g)))/(1+2*0.009*B2*g)))^16)*((((exp(-
2*K*0.9*B*g/(1+2*0.9*B*g)))/(1+2*g*0.9*B))*((exp(-
2*K*0.09*B*g/(1+2*0.09*B*g)))/(1+2*g*0.09*B))*((exp(-
2*K*0.009*B*g/(1+2*0.009*B*g)))/(1+2*0.009*B*g)))^0);
```

Finally, the probability of bit error can be calculated from
$P_b = \left(33P_{12}\right) + \left(281P_{14}\right) + \left(2179P_{16}\right)$.

APPENDIX B

The numerical Laplace transform inverse given in (3.32) can be implemented as shown below. This example inverts the Laplace transform $s/\left(s^2+1\right)^2$, which has a time domain inverse $\left(t/2\right)\sin\left(t\right)$. When $t=\pi/2$, the time domain function has a value of 0.2777, which is the same result we get using the following MATLAB code to invert the Laplace transform at the point $t=\pi/2$:

```
i=sqrt(-1);
v=1000;
t=pi/4;
a=7/t;
inside=0;
for k=1:v
   c=a+(k*pi*i/t);
   if rem(k,2) == 0
      inside=inside+(real(w(c)));
   else
      inside=inside+(real((-1)*(w(c))));
   end
end
tmp=real(w(a))+(2*inside);
tmp2=(exp(a*t)/(2*t));
tmp3=tmp2*tmp;

function[y]=w(s)
y=s/((s^2+1)^2);
```

The numerical Laplace transform inversions performed for this dissertation, required the constant *a* to be 11/*t* instead of 7/*t* as shown in the previous example. The following code

was used to invert the Laplace transforms for the noncoherent *RAKE* receiver designed for AWGN with rate ½, constraint length 9 convolutional coding and Viterbi soft decision decoding:

```
i=sqrt(-1);
v=2000;
for p=1:40
   ebnj=(10^(.1*(p-1)));
   nj=1+(31.623/(0.1*ebnj));
   for j=1:200
      t=j*6.0*(nj/31.623);
      a=11/t;
      inside=0;
      for k=1:v
         c=a+(k*pi*i/t);
         if rem(k,2)==0
            inside = inside+(real(w(c,nj)));
         else
            inside = inside+(real((-1)*w(c,nj)));
         end
      end
      tmp=real(w(a,nj))+(2*inside);
      tmp2=(exp(a*t)/(2*t));
      res(j)=tmp2*tmp;
   end;
   for zz=1:200
      if res(zz)<0;
         res(zz)=0;
      end
   end
   sum=0;
```

```
    for m=1:199
        int1=(res(m)+res(m+1))/2;
        int2=int1*6.0*(nj/31.623);
        sum=sum+int2;
    end
    endres(p)=sum;
end
```

For the $\rho = 1$ case, we can now use the following for the function w to calculate the P_{12} term:

```
function[y]=w(s,ej)
sig1=0.9*31.623*1/22;
sig2=0.09*31.623*1/22;
sig3=0.009*31.623*1/22;
alpha1=0.9*31.623*20/22;
alpha2=0.09*31.623*20/22;
alpha3=0.009*31.623*20/22;
A=(1./((2.*ej.*s)+1)).^12;
B=(1./((4.*s)+1)).^0;
C=((1./(2.*s.*(2.*sig1+ej))).*(exp((-
2.*s.*alpha1)./(1+(2.*s.*(2.*sig1+ej))))).*(1./(2.*s.*(2.*sig2+ej))).*(exp((-
2.*s.*alpha2)./(1+(2.*s.*(2.*sig2+ej))))).*(1./(2.*s.*(2.*sig3+ej))).*(exp((-
2.*s.*alpha3)./(1+(2.*s.*(2.*sig3+ej)))))).^0;
D=((1./(1+2.*s.*(2.*sig1+1))).*(exp((-
2.*s.*alpha1)./(1+(2.*s.*(2.*sig1+1))))).*(1./(2.*s.*(2.*sig2+1))).*(exp((-
2.*s.*alpha2)./(1+(2.*s.*(2.*sig2+1))))).*(1./(2.*s.*(2.*sig3+1))).*(exp((-
2.*s.*alpha3)./(1+(2.*s.*(2.*sig3+1)))))).^12;
y=(C.*D).*(1-((1./s).*(A.*B)));
```

The P_{14} value can now be calculated by using the following for the function *w*:

```
function[y]=w(s,ej)
```

```
sig1=0.9*31.623*1/22;
sig2=0.09*31.623*1/22;
sig3=0.009*31.623*1/22;
alpha1=0.9*31.623*20/22;
alpha2=0.09*31.623*20/22;
alpha3=0.009*31.623*20/22;
A=(1./((2.*ej.*s)+1)).^14;
B=(1./((4.*s)+1)).^0;
C=((1./(2.*s.*(2.*sig1+ej))).*(exp((-
2.*s.*alpha1)./(1+(2.*s.*(2.*sig1+ej))))).*(1./(2.*s.*(2.*sig2+ej))).*(exp((-
2.*s.*alpha2)./(1+(2.*s.*(2.*sig2+ej))))).*(1./(2.*s.*(2.*sig3+ej))).*(exp((-
2.*s.*alpha3)./(1+(2.*s.*(2.*sig3+ej)))))).^0;
D=((1./(1+2.*s.*(2.*sig1+1))).*(exp((-
2.*s.*alpha1)./(1+(2.*s.*(2.*sig1+1))))).*(1./(2.*s.*(2.*sig2+1))).*(exp((-
2.*s.*alpha2)./(1+(2.*s.*(2.*sig2+1))))).*(1./(2.*s.*(2.*sig3+1))).*(exp((-
2.*s.*alpha3)./(1+(2.*s.*(2.*sig3+1)))))).^14;
y=(C.*D).*(1-((1./s).*(A.*B)));
```

Finally, P_{16} can be obtained using:

```
function[y]=w(s,ej)
sig1=0.9*31.623*1/22;
sig2=0.09*31.623*1/22;
sig3=0.009*31.623*1/22;
alpha1=0.9*31.623*20/22;
alpha2=0.09*31.623*20/22;
alpha3=0.009*31.623*20/22;
A=(1./((2.*ej.*s)+1)).^16;
B=(1./((4.*s)+1)).^0;
C=((1./(2.*s.*(2.*sig1+ej))).*(exp((-
2.*s.*alpha1)./(1+(2.*s.*(2.*sig1+ej))))).*(1./(2.*s.*(2.*sig2+ej))).*(exp((-
```

```
2.*s.*alpha2)./(1+(2.*s.*(2.*sig2+ej))))).*(1./(2.*s.*(2.*sig3+ej))).*(exp((-
2.*s.*alpha3)./(1+(2.*s.*(2.*sig3+ej)))))).^0;
D=((1./(1+2.*s.*(2.*sig1+1))).*(exp((-
2.*s.*alpha1)./(1+(2.*s.*(2.*sig1+1))))).*(1./(2.*s.*(2.*sig2+1))).*(exp((-
2.*s.*alpha2)./(1+(2.*s.*(2.*sig2+1))))).*(1./(2.*s.*(2.*sig3+1))).*(exp((-
2.*s.*alpha3)./(1+(2.*s.*(2.*sig3+1)))))).^16;
y=(C.*D).*(1-((1./s).*(A.*B)));
```

Lastly, the probability of bit error can be calculated from

$$P_b = \left(33P_{12}\right) + \left(281P_{14}\right) + \left(2179P_{16}\right).$$

THIS PAGE INTENTIONALLY LEFT BLANK

LIST OF REFERENCES

1. Quirk, Kevin J. and Milstein, Laurence B., "The Effect of Low SNR in Phase Estimation in Wide-Band CDMA," *IEEE Journal on Selected Areas in Communications*, vol 19, no. 1, pp. 107-120, January 2001.

2. Quirk, Kevin J. and Milstein, Laurence B., "The Effects of Phase Estimation Errors on *RAKE* Receiver Performance," *IEEE Transactions on Information Theory*, vol. 48, no.3, pp. 669-682, March 2002.

3. Ziemer, Rodger E., Vojcic, Branimir R., Milstein, Laurence B., and Proakis, John G., "Effects of Carrier Tracking in *RAKE* Reception of Wide-Band DSSS in Rician Fading," *IEEE Transactions on Microwave Theory and Techniques*, vol 47, no. 6, pp. 681-686, June 1999.

4. Viterbi, Andrew J., *Principles of Coherent Communication*, McGraw-Hill, Inc., New York, NY,1966.

5. Simon, Marvin K. Omura, Jim K. Scholtz, Robert A. and Levit Barry K., *Spread Spectrum Communications Handbook*, McGraw Hill, Inc., New York, NY, 1994.

6. Lee, Jhong S., Miller, Leonard E., and Kim, Young K., "Probability of error Analyses of a BFSK Frequency-Hopping System with Diversity Under Partial-Band Interference Interference-Part II: Performance of Square-Law Nonlinear Combining Soft Decision Receivers," *IEEE Transactions on Communications*, vol 32, no. 12, pp. 1243-1250, December 1984.

7. Yoon, Yeomin, Lee, Kwangeog, Kim, Dosun, and Kim, Kiseon, "Performance Improvement of a Fast FH-FDMA System by the Clipped-Linear Combining Receiver," *Proceedings MILCOM*, vol 3, pp. 1014-1019, October 2001.

8. Proakis, John G., *Digital Communications*, 4^{th} ed., McGraw-Hill, Inc., New York, NY, 2001.

9. Eng, Thomas and Milstein, Laurence B., "Comparison of Hybrid FDMA/CDMA Systems in Frequency Selective Rayleigh Fading," *IEEE Journal on Selected Areas in Communications*, vol. 12, no. 5, pp. 938-951, June 1994.

10. Shamain, Prasard, and Milstein, Laurence B, "Detection With Spatial Diversity Using Noisy Channel Estimates in a Correlated Fading Channel," *Proceedings MILCOM*, vol. 1, pp.691-696, October 2002.

11. Chang, Ihn-Keil, and Stuber, Gordon, "Soft-Limiter *RAKE* Receivers For Coded DS/DPSK Over Pulse Jammed Multipath Fading Channels," *Proceedings MILCOM*, vol. 3, pp.1014-1019, October 1990.

12. Vojcic, Branimir, and Pickholtz, Raymond L., "Performance of Coded Direct Sequence Spread Spectrum in a Fading Dispersive Channel With Pulse Interference", *IEEE Journal on Selected Areas in Communications*, vol. 8, no.5, pp. 934-942, June 1990.

13. Peterson, Roger L., Zeimer, Rodger E. and Broth, David E., *Introduction to Spread Spectrum Communications*, Prentice Hall, Inc., Englewood Cliffs, NJ, 1995.

14. Sklar, Bernard, *Digital Communications Fundamentals and Applications*, Prentice Hall Inc., Englewood Cliffs, NJ, 1988.

15. Van Trees, Harry L., *Detection, Estimation and Modulation Theory*, John Wiley & Sons Inc., New York, NY, 1968.

16. Robertson, R. Clark, EC4560 Course Notes (unpublished).

17. Whalen, Anthony D., *Detection of Signals in Noise*, Academic, New York, NY, 1971.

18. Gradshteyn, I. S. and Ryzhik I. M., *Table of Integrals, Series and Products Corrected and Enlarged Edition Edited and Translated by Alan Jeffrey*, Academic Press, New York, 1980.

19. Biglieri, E., Caire, C., Taricco, G., and Ventura-Traveset, J., “Simple Method for Evaluating Error Probabilities,” *Electron. Lett.*, vol. 32, pp. 191-192, February 1996.

20. Lin, Shu and Costello, Daniel J., *Error Control Coding: Fundamentals and Applications*, Prentice Hall, Inc., Englewood Cliffs, NJ, 1983.

21. Viterbi, Andrew J., *CDMA Principles of Spread Spectrum Communication*, Addison-Wesley Longman, Inc., Reading, MA, 1995.

22. Benedetto, Sergio and Biglieri, Ezio, *Principles of Digital Transmission With Wireless Applications*, Plenum Publishers, New York, NY, 1999.

23. Tedesso, Thomas W., and Robertson, R. Clark, “Performance Analysis of a SFH/NCBPSK Communication System With Rate ½ Convolutional Coding in the Presence of Partial-Band Noise Interference”, *Proceedings MILCOM*, vol. 2, pp. 484-488, October 1998.

24. Simon, Richard M., Stroot, Michael T., and Weiss, George H., “Numerical Inversion of Laplace Transforms with Application to Percentage Labled Mitoses Experiments," *Computers and Biomedical Research*, vol. 5, pp. 596-607, 1972.

25. Clark Jr., George C., and Cain, J. Bibb, *Error-Correction Coding for Digital Communications*, Plenum Press, New York, NY, 1981.

26. Robertson, R. Clark, and Ha, Tri T., "Error Probabilities of Fast Frequency-Hopped MFSK with Noise-Normalization Combining in a Fading Channel with Partial-Band Interference," *IEEE Transactions on Communications*, vol. 40, no. 2, pp. 404-412, February 1992.

27. Cassioli, D., Win, Z. M., and Molisch, A. F., “The Ultra-Wide Bandwidth Indoor Channel: From Statistical Model to Simulations,” *IEEE Journal on Selected Areas in Communications*, vol. 20, no. 6, pp. 1247-1257, August 2002.

THIS PAGE INTENTIONALLY LEFT BLANK

INITIAL DISTRIBUTION LIST

1. Defense Technical Information Center
   Ft. Belvoir, Virginia

2. Dudley Knox Library
   Naval Postgraduate School
   Monterey, California

3. Chairman, Code EC/Po
   Department of Electrical and Computer Engineering
   Naval Postgraduate School
   Monterey, California

4. Professor Clark Robertson, Code EC/Rc
   Department of Electrical and Computer Engineering
   Naval Postgraduate School
   Monterey, California

5. Professor Tri T. Ha, Code EC/Ha
   Department of Electrical and Computer Engineering
   Naval Postgraduate School
   Monterey, California

6. Associate Professor Monique Fargues, Code EC/Fa
   Department of Electrical and Computer Engineering
   Naval Postgraduate School
   Monterey, California

7. Associate Professor Roberto Cristi, Code EC/Cx
   Department of Electrical and Computer Engineering
   Naval Postgraduate School
   Monterey, California

8. Research Associate Professor Wolfgang Baer, Code IS
   Department of Information Science
   Naval Postgraduate School
   Monterey, California

9. Kyle Kowalske
   Department of Defense
   Columbia, Maryland